University of Southampton

INFRARED SPECTROSCOPIC AND MASS SPECTROMETRIC STUDIES OF HIGH-TEMPERATURE MOLECULES RELEVANT TO SEVERE NUCLEAR REACTOR ACCIDENTS

A thesis submitted for Degree
of Doctor of Philosophy

by

Shirley Dickinson

Department of Chemistry
Southampton

January 1990

UNIVERSITY OF SOUTHAMPTON

ABSTRACT

FACULTY OF SCIENCE

CHEMISTRY

Doctor of Philosophy

INFRARED SPECTROSCOPIC AND MASS SPECTROMETRIC STUDIES OF HIGH-TEMPERATURE MOLECULES RELEVANT TO SEVERE NUCLEAR REACTOR ACCIDENTS

by Shirley Dickinson

This thesis describes the use of mass spectrometry and matrix isolation-infrared spectroscopy to characterise a number of high-temperature vapour species. The compounds studied were selected because of their possible roles in influencing the transport of fission products during a severe accident in a nuclear power reactor. The most important fission products, on the basis of abundance, volatility and radiobiological impact, are isotopes of iodine, caesium and tellurium, and some of the major uncertainties in severe accident analysis relate to the possible interactions between fission product vapours and other reactor materials. Three of the compounds studied, tin telluride, indium telluride and indium iodide, are possible products of such reactions. Caesium molybdate is postulated to form within the fuel, and may be important in determining the release and transport of both caesium and molybdenum isotopes.

Tin telluride, lead selenide and lead telluride vaporise mainly as MX molecules, together with small quantities of M_2X_2. The infrared spectra of the dimers have been interpreted on the basis of a planar ring structure. The tellurides and selenides of gallium and indium vaporise mainly as M_2X molecules. The infrared spectra of these molecules were consistent with non-linear structures, although considerable variation in the M-X-M angle was inferred. The low-frequency infrared-active vibrations of the caesium molybdate molecule have been established. These were interpreted in terms of a D_{2d} structure. Indium tri-iodide vaporises as the dimer at low temperatures, with increasing dissociation to InI_3 and eventually to InI and I_2 with increasing temperature. The infrared spectrum of matrix-isolated In_2I_6 was consistent with the established structure of this molecule in the solid and liquid phases. These studies also verified that the InI_3 molecule has a planar structure.

The infrared data have been used to estimate the non-infrared active frequencies (where appropriate) of the matrix-isolated molecules, and hence to calculate thermodynamic quantities for the vapour species over a wide range of temperatures.

ACKNOWLEDGEMENTS

Many thanks are due to the following:

Steve Ogden, for his expert tuition on the practical and theoretical aspects of the techniques used in this work, and for his enduring patience and enthusiasm over the past four years;

Brian Bowsher and Alan Nichols for their continual interest and encouragement, and for constructive criticism during the writing of this thesis;

All of those who helped me find my way around Southampton University, and in particular Alan Brisden and Nigel Young for their friendship and guidance;

Jenny Barker, Teresa Davis, Margaret Brown and Caroline Churchill for the excellent typing of this thesis;

The Winfrith Graphics Unit, and in particular Yvonne Elliot, Simone Weekes, Paul Clark and Dennis Burden, for producing the figures to such a high standard;

All of those, too numerous to mention, who have offered advice, help and encouragement, and a particular mention for Andy Beard for his work with the gas bottles!

Extra special thanks are due to Rod Jenkins, for his love, support and domestic skills during the last few months, without which the writing of this thesis would have been ten times more difficult.

"Mollycules is a very intricate theorem and can be worked out with algebra but you would want to take it by degrees with rulers and cosines and familiar other instruments and then at the wind-up not believe what you had proved at all ..."

Flann O'Brien, "The Dalkey Archive"

To my Parents
who gave me the aspiration

and Rod
who gave me the inspiration

CONTENTS

CHAPTER ONE

INTRODUCTION

1. HIGH-TEMPERATURE MOLECULES IN SEVERE REACTOR ACCIDENT ANALYSIS

The safety of nuclear power plants has become a subject of considerable public concern. Such concern centres particularly on the effects of any release of radioactive material on the surrounding population and environment. These issues have been brought into focus on two occasions in recent years, following the accidents at Three Mile Island (TMI-2) in 1979 and Chernobyl in 1986. These two events demonstrated that the consequences of major nuclear reactor accidents can vary widely - from the very small radioactivity release, and no significant offsite radiation dose, which resulted from the TMI-2 accident (1, 2), to the much more serious aftermath of the Chernobyl accident where a considerable amount of radioactive material was released, and which resulted in about 30 deaths from acute radiation syndrome in the two months after the accident (3). The reasons for these differences include the nature of the events which caused the accidents, many aspects of the design of the reactors involved, and the actions of the plant operators throughout the sequences of events. A detailed understanding of the role played by all these factors is important if the risk from nuclear reactor accidents is to be realistically assessed.

The estimation of risk to the public from reactor accidents is an important factor in the design, siting and licensing of nuclear power stations. The range of events considered in these analyses is very large, from normal operational transients to highly improbable scenarios involving the simultaneous failure of many independent systems. A distinction is made between design basis accidents, ie those in which any off-site radiation dose would be below the level at which measures to protect the public would be necessary, and accidents beyond the design basis which would require some such action (4). The term "severe

accident" is used to describe the most serious beyond-design-basis accidents, in which substantial degradation of the core occurs and/or the amount of radioactivity emitted results in significant risk to the public. It is this class of accident to which the work in this thesis is relevant.

There are two aspects to the quantification of risk: the probability that an event (or combination of events) will occur, and the consequences of such an occurrence. The likelihood of a given accident occurring can be computed from the probabilities of all the events and failures which are postulated to occur. For design basis accidents in the UK, detailed requirements are laid down at the design stage for the maximum permissible probabilities of event sequences resulting in specified off-site doses. In the case of beyond-design-basis accidents the UK licensing requirement is that the probabilities should be "as low as reasonably practicable" (5); in practice this is usually interpreted as less than one per million years of reactor operation.

The consequences of a reactor accident are defined in terms of the amount of radioactive material released from the reactor, and the resulting off-site radiation dose. The main source of radioactive material in the reactor is the nuclear fuel, and in particular the fission products, which are elements formed by the nuclear fission of the U-235 content of the uranium dioxide fuel. A fraction of the fission products are radioactive isotopes with significant half-lifes, and some of these could bring serious consequences if they were released to the environment. The accident consequences are thus determined by the extent to which these radiobiologically significant fission products escape from the fuel and travel through the reactor system to the environment, which in turn depends on many factors

relating to the design of the reactor involved and the nature of the accident. The diversity of reactor types worldwide (and even in the UK) means that these factors cannot be completely generalised; the processes occurring inside a liquid-metal-cooled fast reactor, for example, would differ substantially from those in a water- or gas-cooled system. The following discussion will therefore be restricted to pressurised water reactors (PWRs). This is the most widely-used reactor type in the world, and the first commercial power-generating PWR in the UK is currently under construction at Sizewell.

Efforts to predict the consequences of reactor accidents have been underway from the earliest days of the nuclear power industry. The first published analysis predicted that, in the most severe accidents considered, 50% of all the fission products would be released (6). Very high releases were also predicted in a 1962 study, the results of which were used in formulating the US Nuclear Regulatory Commission licensing regulations (7). Neither of these early studies analysed the physical processes by which fission products were transported from the core to the environment, and no assessment was made of specific accident sequences. The more sophisticated Reactor Safety Study (WASH-1400), published in 1975 (8), did attempt to model the physical transport processes and to consider different accident scenarios, but the lack of much relevant data meant that the study leant heavily on untested and conservative assumptions. The requirement to err on the pessimistic side resulted in considerable overestimation of the fission product release, such that the observed radioiodine release from Three Mile Island was about 100000 times smaller than predicted using this methodology (9).

Following the TMI accident, the radioactive releases from other accidents and experiments in which reactor fuel had been damaged by overheating were reassessed, and it became

apparent that the release of smaller-than-expected amounts of radioactivity was the rule rather than the exception (9). This prompted a number of experimental and theoretical studies, which have continued in many countries throughout the 1980s, aimed at developing a better understanding of the factors influencing the release of radioactive material from a reactor under accident conditions and hence allowing the consequences of such accidents to be more realistically predicted.

The great complexity of this problem necessitates the use of sophisticated computer codes to model the processes occurring throughout the reactor at all stages of the accident. Many different event sequences can be postulated, but the common "starting point" for all severe accidents can be considered to be the failure of the reactor coolant system to remove heat from the reactor core. Although any failure in the cooling system would automatically cause the reactor to "trip", stopping the nuclear reaction, the radioactive fission products which accumulate in the fuel during the reactor operation would continue to produce a considerable amount of heat. The remaining cooling water would boil off and, as the core temperature rose, the fuel cladding would begin to fail releasing the more volatile fission products into the primary coolant circuit. Less volatile fission products would initially be retained within the fuel, but could be released at later stages of the accident. The released fission products could be transported through a breach in the primary circuit to the reactor containment or, in certain scenarios, directly into the auxiliary buildings, and could eventually be released to the environment due to failure or leakage of the containment. The nature of this radioactive emission will depend on the quantities and identities of the fission products released from the fuel, their chemical and physical forms, and their interactions with the various materials encountered along the leakpath.

A number of severe accident assessments have identified the fission product nuclides which, on the basis of their abundance, volatility and radiobiological impact, would be predicted to dominate the consequences of a release (8). The most important of these are caesium, iodine and tellurium isotopes. These elements are very reactive and would be expected to combine with other materials within the reactor to form a variety of new compounds whose behaviour would then determine their transport and release to the environment. In a PWR, such materials could include the uranium dioxide fuel, other fission products, Zircaloy fuel cladding, steam from the evaporating coolant, hydrogen produced from the steam oxidation of metallic components, stainless steel primary circuit structures, Ag-In-Cd control rod alloy, boric acid (used as a soluble neutron absorber), Inconel fuel grids and steam generator tubing, and various paints, concrete and other surfaces within the containment building (10). Any reactions with these materials would be influenced by the surrounding atmosphere, which would vary from high temperature hydrogen-steam mixtures in the primary circuit to much cooler steam and air in the reactor containment. Furthermore, the reactants could be in the form of vapours (steam, fission products, boric acid), aerosols (control rod components, boron oxides), or surfaces (Zircaloy, steel, concrete etc), and this will influence the effect of a reaction on the fission product transport. For example, the interaction of a fission product vapour with a solid surface to form a less volatile product will, initially at least, retain the fission product in a part of the system from which the non-reacting vapour would have been released. If the temperature in this region increases, then the fission product could be revolatilised, possibly in a different chemical form, at a later stage in the accident. Reaction of the fission product vapour with airborne particulate material may also result in increased

attenuation due to deposition of the aerosol along the leakpath, and it is again possible that the deposited fission products could be revaporised in new chemical forms. Conversely, fission products associated with very fine aerosol particles could be carried further through the system than the volatility of the non-reacting vapour would have allowed, and the release may thus be enhanced. Such chemical and physical processes play an important role in influencing the amounts of radioactivity which could be released into the environment following a severe accident (11). A knowledge of the chemical identities and properties of the fission product vapour species is fundamental to the prediction of these reactions and therefore to the assessment of accident consequences.

One possible approach to the problem of characterising this complex chemical system is theoretical, involving the use of thermodynamic data to compute the equilibrium concentrations of the predicted species in different parts of the system under the relevant conditions of temperature, pressure and elemental composition. However, the accuracy of this approach depends entirely on a knowledge of all the species present, and the availability of thermodynamic data for all these species under the conditions of interest. Furthermore, the use of equilibrium thermodynamics may not be appropriate in all cases. For example, a reaction between a fission product vapour and a solid structural component may be important in attenuating the fission product release, and the extent to which such a reaction proceeds will be influenced by kinetic as well as thermodynamic considerations.

An alternative and complementary approach is to simulate experimentally the conditions of an accident, and determine the chemical composition of the system by in-situ analysis and examination of the final products. Such experiments can be used to test the results of theoretical

calculations, indicating any important species or effects which may have been neglected. A number of large-scale international experiments have been performed in recent years to address various aspects of fission product transport during a severe accident (12,13). However such experiments are generally very expensive to perform, and the data interpretation is often complicated. Furthermore, they do not give any direct information about the fission product vapour species involved.

The development of reliable theoretical models and the interpretation of complex data from large-scale "integral" experiments can be greatly assisted by small-scale studies. These allow selected parts of the overall system - for example, the release of fission products from the fuel, the reaction of a fission product vapour with a particular surface or aerosol, or the vaporisation behaviour of the product of such a reaction - to be studied under well-defined conditions, facilitating the identification of the reactions and products which are likely to be most significant. An approach which has been used in many studies involves vaporising simulant fission products, allowing the vapours to condense or interact on surfaces of interest, and analysing the condensed products (14, 15, 16). This method has the advantages of relative simplicity, good controllability of the reaction conditions, and accessibility of the reaction products for analysis by chemical or surface techniques. No direct identification of the vaporising or reacting species is made, although this can sometimes be inferred from the analysis of the products. However, the reaction products may undergo chemical or physical changes during the period between completion of the reaction and the analysis, particularly if samples are exposed to changes in atmosphere, and this will complicate the interpretation of the data. It is, therefore, advantageous to study the

vapour species in situ if the reaction mechanisms are to be established with confidence.

2. CHARACTERISATION OF HIGH-TEMPERATURE VAPOURS

The task of characterising high-temperature vapours can be divided into three areas: the production, detection and identification of the vapour species. The main problems associated with producing the high-temperature species lie in containing and heating the solid or liquid sample. The materials used must be both structurally stable and chemically inert at the high temperatures of interest, as well as being compatible with the analytical technique (for example, transparency to radiation in a certain region of the spectrum may be necessary).

A variety of techniques is available for characterising high-temperature species, including mass spectrometry, electron diffraction, microwave spectroscopy and vibrational (infrared and Raman) spectroscopies (17, 18). The first three of these techniques may be applied to molecular beams thereby avoiding problems associated with containing the vapour. The most direct method of identifying the vapour species is mass spectrometry. This gives information about the elemental composition of molecules in the vapour phase, and can also yield some thermodynamic information (19). However, mass spectrometry does not give any information about the structure of the molecules being studied. Another disadvantage of this technique is that it is not always possible to determine whether the ions detected reflect the neutral vapour species, or arise from fragmentation of larger molecules during the ionisation process.

The structure of gaseous molecules can be determined directly using electron diffraction or microwave spectroscopy. The latter technique is experimentally

difficult at high temperatures, and the complexity of the data interpretation limits both of these methods to the study of vapours containing a single vapour species. Structural information can also be obtained by gas-phase vibrational spectroscopy, and vibration frequencies can be used to calculate thermodynamic properties of the vapour species. Unfortunately, the low sensitivity of infrared and Raman spectroscopies preclude their application to molecular beams. This raises the problem of containing the vapour during the analysis, which is exacerbated by the need for the container materials to be transparent to infrared or visible radiation. The vibrational spectra obtained from gas-phase samples at high temperature are complicated by hot bands as well as rotational fine structure, and these features may cause difficulties particularly in interpreting the spectra of multi-component vapours. Many of the difficulties associated with gas-phase vibrational spectroscopy can be overcome using matrix isolation, and this technique has been applied to the study of high-temperature molecules in a wide variety of applications (20).

This thesis describes the application of mass spectrometry and matrix isolation-infrared spectroscopy to the analysis of vapour species produced from a number of systems relevant to severe reactor accident research. Details of the techniques used, and their operating principles, are given in Chapters Two and Three, and the theory underlying the interpretation and application of infrared spectroscopic data is outlined in Chapter Four. Chapters Five to Eight describe the experimental studies of four types of compound: tin telluride and lead selenide and telluride, the selenides and tellurides of gallium and indium, caesium molybdate and indium tri-iodide. In each experimental chapter, the general approach has been:

(i) identification of the important vapour species by a combination of mass spectrometry and matrix isolation-infrared spectroscopy,

(ii) detailed analysis of the infrared spectra of the matrix isolated species to establish the molecular structure and force field and hence estimate the frequencies of the non-infrared active vibrational modes, and

(iii) use of the vibrational and structural data to calculate the thermodynamic functions of the molecular species.

This work demonstrates the effectiveness of the combination of methods used, both in the identification of important vapour-phase species and in obtaining quantitative thermodynamic data for incorporation into computer codes used to model severe reactor accidents.

REFERENCES

1. Solon, L R, Ann Intern Med, 90, 424, 1979.

2. Phung, D L, Nucl Sci Eng, 90, 509, 1985.

3. Hill, M D, in "Chernobyl: A Technical Appraisal", British Nuclear Energy Society, London, 1987.

4. Bonell, P G, Caisley, J, Hayns, M R, Holloway, N J and McMillan, R N H, in "PWR Degraded Core Analysis", UKAEA Report ND-R-610(S) 49, 1982.

5. Tyror, J G and Taig, A R, IAEA Symposium on Severe Accidents in Nuclear Power Plants, Sorrento, March 1988, Volume 1, 198, IAEA Vienna, 1988.

6. "Theoretical Possibilities and Consequences of Major Accidents in Large Nuclear Plants", WASH-740, US Atomic Energy Commission, 1957.

7. Di Nunno, J J, "Calculation of Distance Factors for Power and Test Reactor Sites", TID-14844, 1982.

8. "Reactor Safety Study: An Assessment of Accident Risks in US Commercial Nuclear Power Plants", WASH-1400, (NUREG-75/014), US Atomic Energy Commission, 1975.

9. Loewenstein, W B and Vogel, R C, IAEA Symposium on Source Term Evaluation for Accident Conditions, Columbus, Ohio, 28 October - 1 November 1985, 21, IAEA Vienna, 1986.

10. Bowsher, B R, Prog Nucl Energy, 20, 199, 1987.

11. Levenson, M, Nucl Technol, 53, 97, 1981.

12. Osetek, D J and Sherry, J J, Proc ACS Symposium on Chemical Phenomena Associated with Radioactivity Releases During Severe Nuclear Plant Accidents, 9-12 September 1986, Anaheim, USA, NUREG/CP-0078, 4-85, 1987.

13. Berta, V T and Coryell, E W, "OECD LOFT Project Experimental Specification Document, Fission Product Experiment LP-FP-1", OECD/LOFT-T-3702, 1984.

14. Bowsher, B R and Dickinson, S, UKAEA Report AEEW-R 2102, 1986.

15. Johnson, I, Johnson, C E, Farahat, M, Settle, J L and Ritzman, R L, Proc ACS Symposium on Chemical Phenomena Associated with Radioactivity Releases During Severe Nuclear Plant Accidents, Anaheim, USA, 9-12 September 1986, NUREG/CP-0078, 3-53, 1987.

16. Collins, J L, Osborne, M F and Lorenz, R A, Workshop on Chemical Reactivity of Oxide Fuel and Fission Product Release, Berkeley, Glos, 7-9 April 1987, Volume 2, 425, 1988.

17. Beattie, I R, in "Vibrational Spectroscopy - Modern Trends", ed A J Barnes, Elsevier, Amsterdam, 1977.

18. Young, N A, PhD Thesis, University of Southampton, 1988.

19. Drowart, J, in "Advances in Mass Spectrometry", ed J F Todd, John Wiley and Sons, Chichester, 1986.

20. Ogden, J S, in "Matrix Isolation Spectroscopy", eds A J Barnes et al, NATO Advanced Study Institutes Series C76, 1981.

CHAPTER TWO

MASS SPECTROMETRY

1. INTRODUCTION

Mass spectrometry is the most direct method available for characterising species in the vapour phase. In addition to providing information about the elemental composition of vapour molecules, mass spectrometry has been widely used to investigate the thermodynamics of vapour phase and condensed phase-vapour phase equilibria (1). A recent review (2) indicates the scope of this technique in the study of high-temperature inorganic vapour species, and many examples are cited in the later chapters of this thesis.

The study of high-temperature vapours by mass spectrometry can be considered in four stages:

(i) vaporisation of the sample and its introduction to the mass spectrometer,

(ii) ionisation of the vapour species,

(iii) separation of the ions on the basis of their mass-to-charge ratios, and

(iv) detection and quantification of the separated ions.

These four stages are described in detail in the following sections, with particular reference to the techniques used in the present work.

2. THEORY AND PRACTICE

The experimental arrangement of the mass spectrometer used in this work is shown in Figure 1. The system is built around a VG SXP-600 Quadrupole Mass Spectrometer, which has a practical mass range of 1 to about 700 mass numbers. The

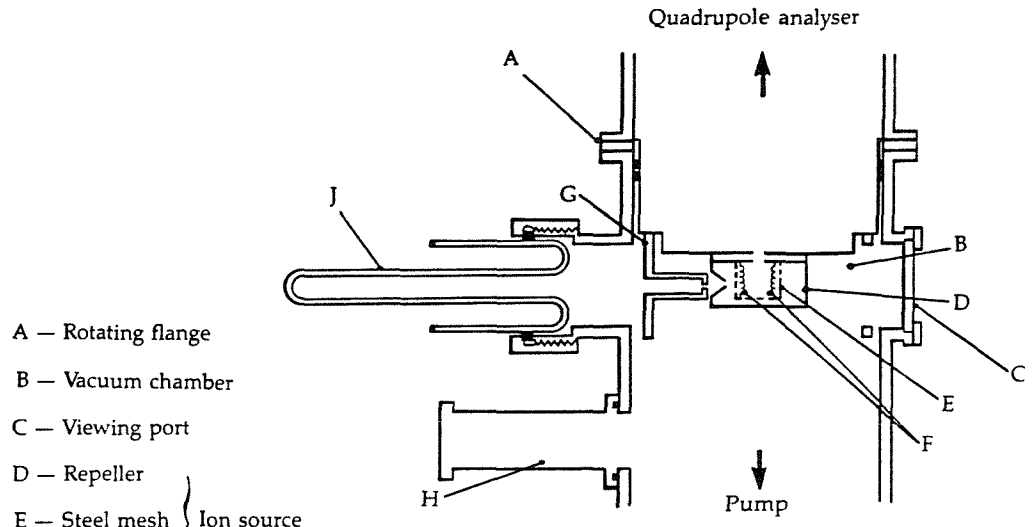

A — Rotating flange
B — Vacuum chamber
C — Viewing port
D — Repeller
E — Steel mesh } Ion source
F — Filaments
G — Radiation shield
H — Ion gauge
J — Sample holder
K — Additional sample port

a) **Vertical Section**

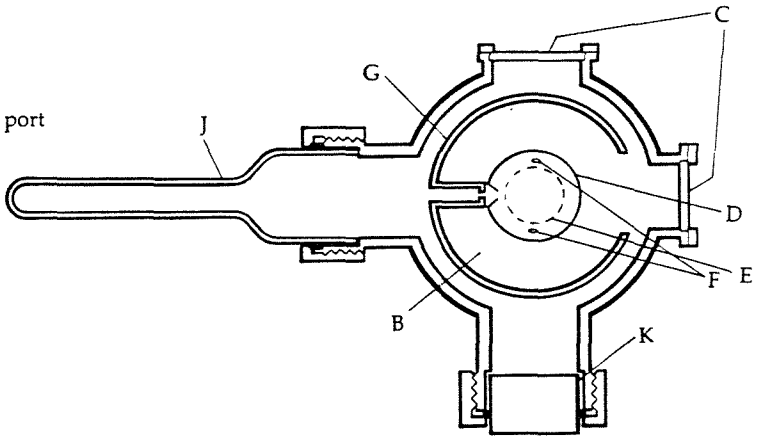

b) **Horizontal Section Showing Alternative Sample Holder**

L — Water-cooled jacket
M — Tantallum susceptor

Pyrometer line of sight

N — Alumina support tube
P — Sample holder
Q —'O' ring seal

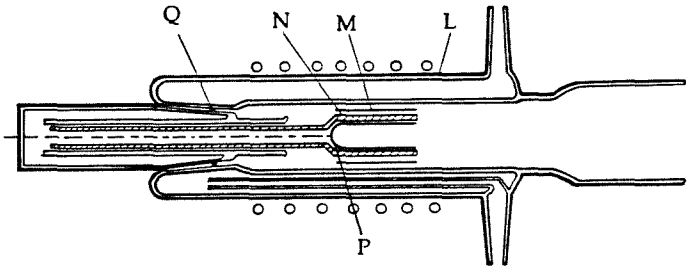

c) **Sample Holder for RF Heating**

Figure 1 Experimental Arrangement of Quadrupole Mass Spectrometer

analyser is seated on the vacuum chamber with a rotatable seal to allow alignment with either of the two sample inlet ports. The radiation shield surrounding the ion source protects the system from contamination by sample vapours. A pressure of about 2×10^{-7} mbar is maintained during operation by an oil diffusion pump and liquid nitrogen cryotrap backed by a rotary pump. The pressure within the chamber is monitored by a Penning gauge and an ion gauge, the latter being part of a protection system which trips the mass spectrometer if the pressure rises to a level which could cause damage to the instrument.

2.1 Sample Vaporisation

The design of the sample inlet system is determined by the volatility of the sample. The pressure inside the mass spectrometer during operation is maintained at about 10^{-6} - 10^{-7} mbar to minimise the possibility of ion collisions, and the pressure of the sample vapour entering the analyser must therefore be of this order. For gases or compounds which are very volatile at room temperature, a leak system is used to control the flow of gas or vapour into the spectrometer. This might consist of a glass sinter, a rubber membrane, one or more small orifices, or a needle valve.

In the present work, cold inlets have been used to admit argon gas and heptacosafluorotri-n-butylamine (PFTBA) for calibration purposes. An Edwards LV5 needle valve was used to control the argon flow, whereas the liquid PFTBA was contained in a glass tube and the vapour admitted via a PTFE/Pyrex tap.

None of the compounds studied in this work was volatile at room temperature, and sample heating in the range 150 to 1200°C was therefore required. This was achieved using the arrangements shown in Figure 1. For temperatures up to

about 850°C, the sample was placed in a silica holder (Figure 1a or 1b) and heated resistively using a nichrome-wound silica tube placed around the sample. The approximate temperature of the sample was monitored by a K-type thermocouple placed in contact with the sample holder. The sample holder shown in Figure 1a had the advantage of a shorter path length between the sample and the ion source, but the use of this holder was limited to temperatures below about 600°C due to overheating of the O-ring seal at higher temperatures.

Samples requiring higher temperatures for vaporisation were heated inductively using the arrangement shown in Figure 1c. The sample was placed in a recrystallised alumina tube which was surrounded by a close-fitting tantalum susceptor. The alumina tube was held in a Pyrex support tube and inserted into a Pyrex water-cooled jacket which was sealed onto the vacuum chamber. A resin-mounted induction coil was placed around the water-cooled jacket, and power was supplied by a Stanelco 3 kW induction furnace. The sample temperature was monitored either by a R-type thermocouple, which was sealed into the support tube and passed down the centre of the alumina sample holder, or by an Ircon two-colour pyrometer sighted through a quartz window at the end of the support tube and along the inside of the alumina tube.

2.2 Ionisation of the Vapour Species

A variety of ionisation methods have been used in mass spectrometry; Todd (3) identified 18 different techniques for application to volatile, involatile and dissolved samples. In many of these methods, particularly those applied to involatile materials or solutions, there is no separate vaporisation stage preceding the ionisation; samples are either volatilised within the ion source (eg the inductively coupled plasma method), or ions are

evaporated directly from the solid (eg thermal ionisation, secondary ion mass spectometry or fast atom bombardment). Since the intention of this work, however, was to study the vapour species produced by 'natural' evaporation, it was necessary to use a method suitable for application to volatile samples, preceded by vaporisation of the sample as described in the previous section.

The instrument used in these studies was equipped with an electron impact ion source as shown in Figure 1. This consisted of a fine cylindrical stainless steel wire mesh cage with two tungsten filaments mounted diametrically opposite to each other outside the cage. This assembly was surrounded by a circular repeller, and oriented coaxially with the quadrupole analyser. Electrons were produced by thermionic emission from one of the heated filaments, and accelerated across the ion chamber by a potential difference between the filament and the wire mesh cage. The sample molecules entered the ion source through a hole in the side of the repeller, and the positive ions produced by interaction with the electrons were accelerated through focussing plates at the top of the ion source into the mass analyser. The energy with which the positive ions left the ion source was determined by the potential of the mesh cage with respect to earth.

An electron accelerated through a voltage V into the ion chamber has energy zV, where z is the electronic charge, and a de Broglie wavelength of $\sqrt{(1.5/V)}$ nm. As the electron approaches a molecule, the electron wave and the electric field of the molecule are mutually distorted (4). The distorted electron wave can be considered to consist of many component waves, some of which will be of the correct frequency to interact with the molecular electrons. This may lead to electronic excitation of the molecule by promoting an electron from a lower to a higher orbital, or ejection of an electron from the molecule to leave a

positive ion. Attachment of the impacting electron is also possible, but the probability of producing a stable anion is low since the excess energy of the ion, arising from the translational energy of the electron, usually leads to re-emission of the electron or fragmentation of the ion. The possible electron-molecule reactions can be summarised thus:

$$\text{(i)} \quad M + e^- \rightarrow M^+ + 2e^-$$

$$\text{(ii)} \quad M + e^- \rightarrow M^* + e^-$$

$$\text{(iii)} \quad M + e^- \rightarrow M^-$$

In positive-ion mass spectrometry only reaction (i) is of interest, although probably fewer than 1% of the sample molecules undergo this conversion, the majority passing unchanged through the ion source. Any negative ions are discharged at the repeller and pumped away together with neutral species.

In order for reaction (i) above to occur, the energy of the ionising electron must be greater than the ionisation potential of the neutral species M. The conventional value for the electron energy in mass spectrometry is 70 eV, although lower energies (15 - 25 eV) were generally used in the present studies. First ionisation potentials for atoms are of the order of 5 to 15 eV (5), and reported molecular ionisation potentials have similar values (2, 6). The ions produced by electron impact are therefore likely to possess excess internal energy, and this may lead to fragmentation of molecular ions. For example, consider the ionisation of a diatomic molecule AB. The potential energies of the molecule and the ion AB^+ can be represented by Morse functions, as shown in Figure 2. At moderate temperatures the molecule is almost certain to be in the ground vibrational state. However, if the ionisation process is

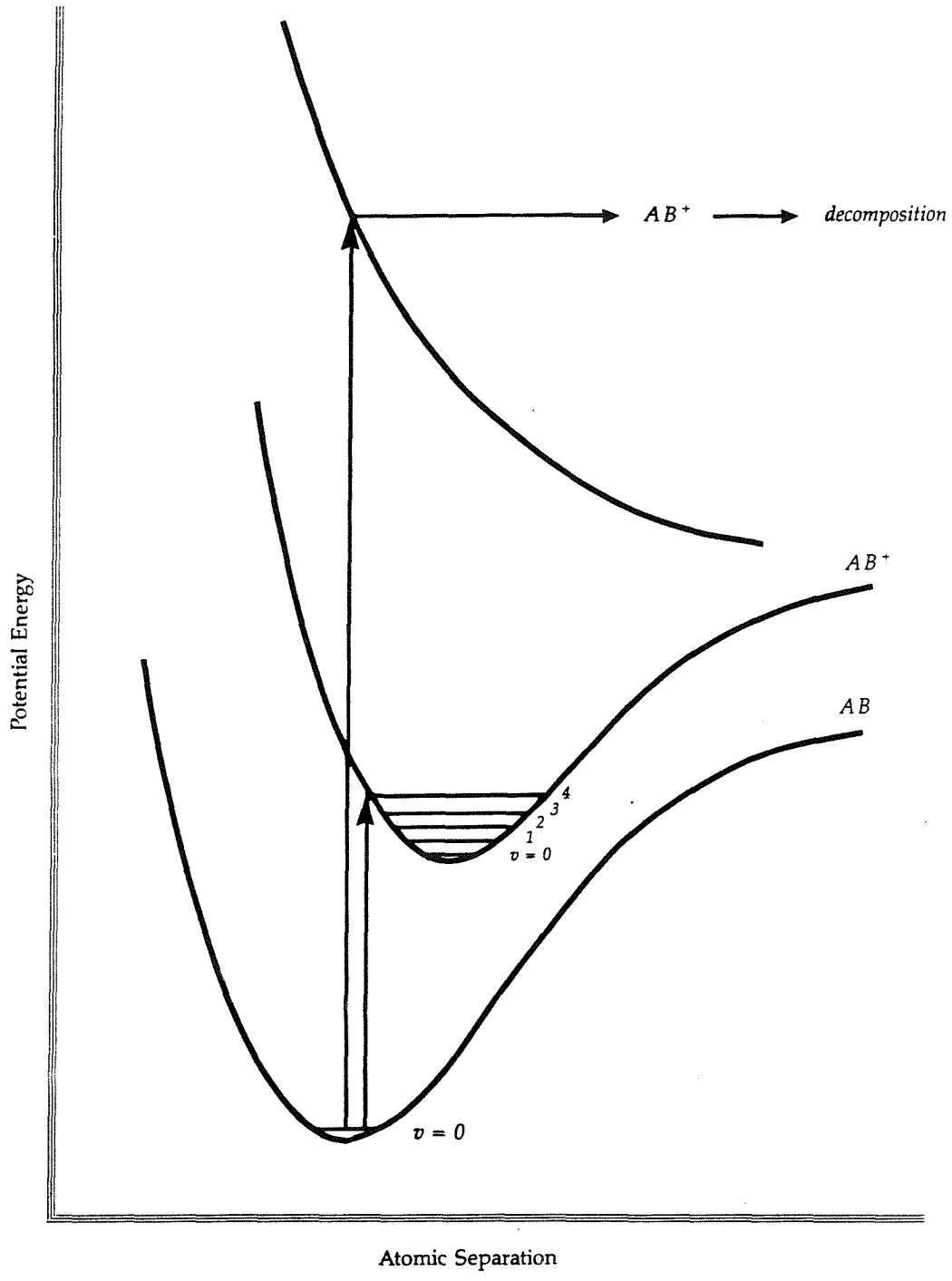

Figure 2 Morse Curves for a Diatomic Molecule Showing Vertical Ionisations to a Dissociative or Non-Dissociative Ground-State Ion

rapid compared to the vibration frequency, there will be a vertical transition from AB to AB^* and, as the potential energy minima of the molecule and the ion are not likely to coincide, AB^* will be in an excited vibrational state. It should be noted that electron impact ionisation does not produce strictly vertical ionisation translations, since the molecule is distorted by the approach of the electron. If the transition occurs to a vibrational level above the dissociation limit of AB^*, then the ion will fragment as soon as it begins to vibrate. Alternately, the ground state of AB^* may be completely dissociative so that the ion will decompose immediately on formation. Similar arguments apply to polyatomic molecules, where the Morse curves are replaced by potential energy surfaces for each vibrational mode.

If the ionising electrons are sufficiently energetic, electrons can be removed from lower orbitals of the molecule to give electronically excited ions. Such excited ions may dissipate their excess energy by internal electron redistribution accompanied by radiation emission to give a ground state ion, or by radiationless potential surface crossings by which the electronic energy of the excited state ion is transformed into vibrational energy in the ground-state ion. However, decomposition may occur from any excited state with sufficient vibrational energy.

2.2.1 Ionisation Efficiencies and Appearance Potentials

From the above discussion, it is apparent that the ions observed in the mass spectrum of a given vapour will depend to some extent on the ionising electron energy. The effect of varying this parameter can be seen by studying the ionisation efficiency (IE) curves of the ions of interest. The IE curve is obtained by tuning the mass spectrometer to collect only ions of a given m/e value, and measuring the ion current as a function of the ionising electron energy.

The resulting curve is characteristic of the particular ion and the mechanism by which it is formed (parent or fragment ion), but the general shape is the same for all ions (6), as shown in Figure 3. The main features of the curve are a threshold electron voltage, below which the ion current is zero, a curved 'tail' section over the first few eV above the threshold, a linear portion, a broad peak, and a gradual decrease in ion intensity at higher electron energies. The shape of the curve can give quantitative information about the origin of the ion; a molecular ion or fragment formed by a single bond-rupture process tends to give a curve with a shorter tail and more steeply-sloping linear section than an ion formed by a more complicated process (6). A more quantitative measurement which can be obtained is the appearance potential (AP) of the ion. This is defined as the minimum energy required to produce an ion in its ground vibrational state from the original atom or molecule, also in its ground vibrational state. The appearance potential of a parent ion is therefore equal to the first ionisation potential of its precursor atom or molecule.

It is apparent that:

(i) the AP of a fragment ion will always be greater than that of the parent ion formed from the same precursor, and

(ii) the AP of a given ion formed by fragmentation will be larger than that of the same ion formed as a parent species, the difference being equal to the appropriate bond dissociation energy term involved in the fragmentation plus the excess excitation and kinetic energies of the particles produced.

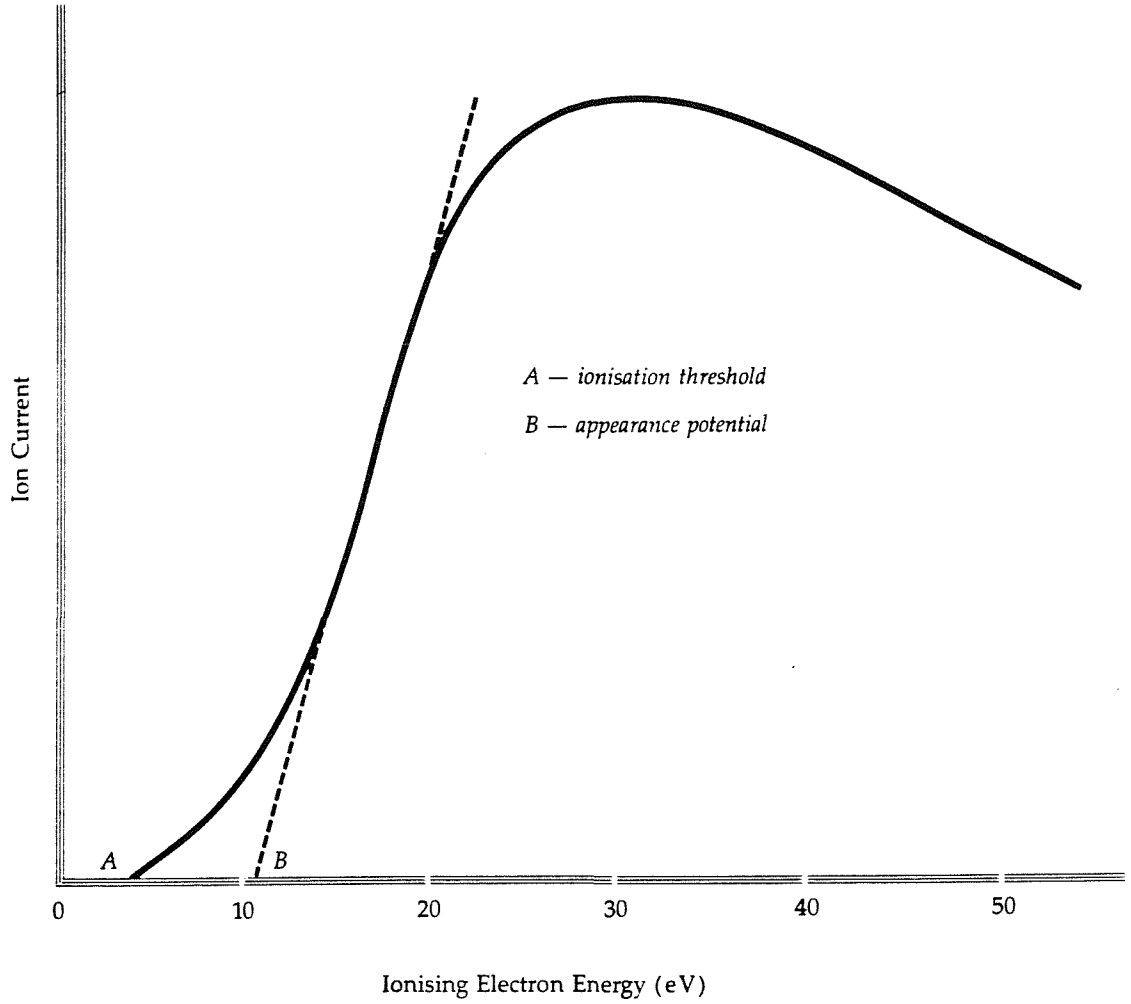

Figure 3 Typical Ionisation Efficiency Curve

In this work, these observations have been applied to discriminate, where possible, between parent and fragment ions. However, appearance potential measurements have been widely used elsewhere to estimate bond dissociation energies (2), although the assumption that kinetic and excitation energy terms can be neglected may lead to overestimations.

The accuracy with which appearance potentials can be determined is limited by the energy distribution of the bombarding elecrons in a normal electron-impact source. This effect can be corrected for by referring the measured appearance potential to that obtained for an ion of known ionisation potential. For very accurate work, however, a monoenergetic beam of electrons is required. A further complicating factor, discussed in the previous section, is that ions are likely to be produced in a number of excited vibrational and electronic states, since the energy differences between these states may be less than the energy-spread of the ionising electrons. The measured appearance potential will therefore not conform strictly to the above definition, and is likely to be an overestimate of the true value.

Several methods exist for determining appearance potentials from ionisation efficiency curves (6), the basic aim being to pinpoint the energy at which the onset of ionisation occurs. In this work, the linear part of the ionisation efficiency curve was extrapolated back to zero ion intensity, and the intercept taken as the appearance potential (Figure 3). This method is not completely accurate, but does allow comparisons to be made between ions obtained from different sources.

2.3 Mass Analysis

The analysis of ions according to their mass-to-charge ratios (m/z) can be achieved by magnetic or electric fields, either alone or combined. Several mass analysis techniques are available, falling broadly into two types (3):

(1) Ion transport methods, in which ions are separated by their transport behaviour under the influence of the applied field(s). Quadrupole, time-of-flight and sector instruments fall into this category.

(2) Ion storage methods, in which the ions are trapped within the field(s), imparting a motion which is in some way characteristic of the m/z ratio. An example of this type is Fourier transform ion cyclotron resonance (FT-ICR or FTMS).

In these studies, a quadrupole mass filter (QMF) was used. This consists of four parallel electrodes arranged in a square array, as shown in Figure 4. Each electrode is electrically connected to the one diagonally opposite, and an oscillating radiofrequency potential is applied between the pairs. A dc voltage is also applied to the electrodes, one pair having a positive and the other pair a negative bias. The overall potential is therefore

$$\Phi(t) = \pm (U + V \cos(\omega t)) \qquad [1]$$

where U is the dc voltage, V is the peak amplitude of the rf voltage of frequency f, and

$$\omega = 2\pi f$$

The ions enter the analyser in the direction of the central axis, and the rf and dc fields perpendicular to this axis

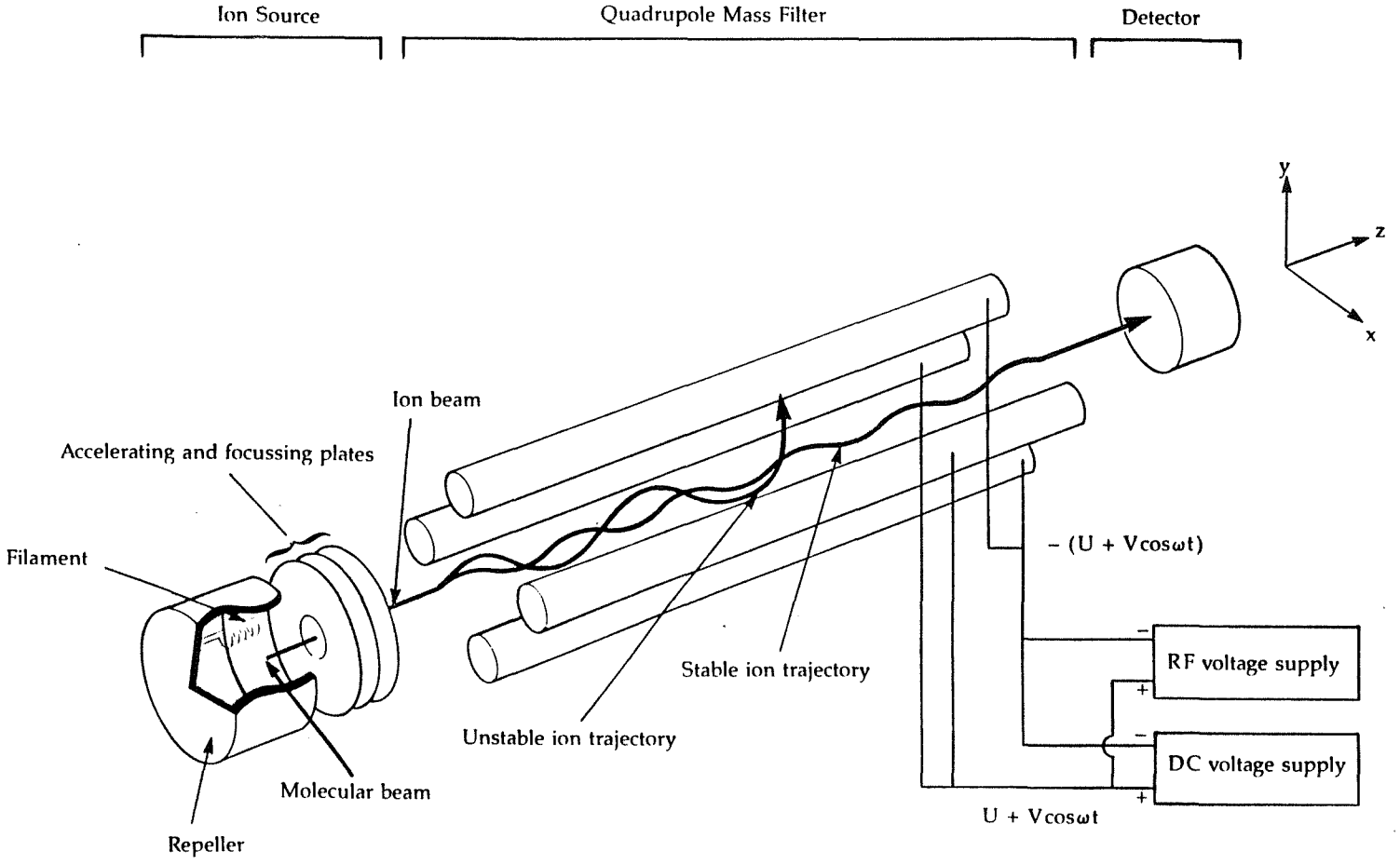

Figure 4 Schematic View of Quadrupole Mass Spectrometer

impart a complex trajectory on the ions. This motion can be described by deriving the field equation for the QMF by the strong-focussing effect (7, 8).

The potential at any point in an ideal quadrupole field can be considered as the sum of the potentials in the x, y and z directions:

$$\Phi(x,y,z) = \Phi(x) + \Phi(y) + \Phi(z) \qquad [2]$$

The strong-focussing effect requires that the force on a particle is proportional to its distance from the origin. Defining the axis of the QMF as the z axis, the origin of the x-y plane can be chosen as the zero of potential.

Considering the force in the x direction:

$$F_x \alpha x \qquad \text{and} \qquad F_x = zE_x$$

where z is the ionic charge and E_x is the electric field in the x direction, which is given by

$$E_x = - \frac{\partial \Phi(x,y,z)}{\partial x} = - \frac{\partial \Phi(x)}{\partial x} \qquad [3]$$

combining these equations with the condition that $\Phi(0) = 0$ gives

$$\Phi(x) = ax^2 \qquad [4]$$

where a is a constant. A similar treatment for the y and z axes gives

$$\Phi(x,y,z) = ax^2 + by^2 + cz^2 \qquad [5]$$

However, since there is no applied potential in the z direction,

$$\Phi(x,y,z) = ax^2 + by^2 \qquad [6]$$

Applying Laplace's equation

$$\frac{\partial^2\Phi}{\partial x^2} + \frac{\partial^2\Phi}{\partial y^2} + \frac{\partial^2\Phi}{\partial z^2} = \nabla^2\Phi = 0$$

gives

$$\nabla^2\Phi(x,y) = 2a + 2b = 0 \qquad [7]$$

and therefore

$$a = -b$$

If r_o is the radius of the inscribed circle at the closest approach of the rods, then at the surface of one of the electrodes lying in the yz plane ($x = r_o$, $y = 0$):

$$\Phi(r_o,0) = \Phi_o = ar_o^2$$

where Φ_o is the potential applied to the electrodes. This gives

$$a = \frac{\Phi_o}{r_o^2} \quad \text{and similarly} \quad b = -\frac{\Phi_o}{r_o^2} \qquad [8]$$

substituting into [6]

$$\Phi(x,y) = \Phi_o(x^2 - y^2)/r_o^2 = \Phi_o(\sigma x^2 + \lambda y^2) \qquad [9]$$

where $\sigma = -\lambda = \dfrac{1}{r_o^2}$

The electrode voltage for the QMF is given by

$$\Phi_o = U + V\cos(\omega t)$$

and so

$$\Phi(x,y) = (U + V\cos(\omega t))\ (x^2 - y^2)/r^2 \qquad [10]$$

and the electric fields are

$$E_x = \frac{\partial\Phi(x,y)}{\partial x} = \frac{-2}{r^2}(U + V\cos(\omega t))x$$

$$E_y = \frac{\partial\Phi(x,y)}{\partial y} = \frac{2}{r^2}(U + V\cos(\omega t))y \qquad [11]$$

$$E_z = 0$$

Now, since

$$F = zE = ma$$

the equations of motion can be derived:

$$\frac{d^2x}{dt^2} + \frac{2z}{mr^2}(U + V\cos(\omega t))x = 0$$

$$\frac{d^2y}{dt^2} - \frac{2z}{mr^2}(U + V\cos(\omega t))y = 0 \qquad [12]$$

$$\frac{d^2z}{dt^2} = 0$$

The motions of the particle in each direction can therefore be considered separately. If a quantity ϵ is defined as

$$\epsilon = \frac{\omega t}{2}$$

it can be shown that

$$\frac{d^2}{dt^2} = \frac{\omega^2}{4} \cdot \frac{d^2}{d\epsilon^2}$$

and the equations of motion then become

$$\frac{d^2\mu}{d\epsilon^2} + (a_\mu + 2q_\mu \cos 2\epsilon)\mu = 0 \qquad [13]$$

where

$$a_\mu = \frac{8zU\gamma}{m\omega^2} \quad \text{and} \quad q_\mu = \frac{4zV\gamma}{m\omega^2} \qquad [14]$$

in which μ is either x or y, and γ is associated with x or y in place of λ and σ in equation [9] (ie $\gamma = \pm {}^1/_{r_o{}^2}$).

Equation [13] is a special type of linear second-order differential equation known as the Mathieu equation, to which there are two types of solution:

(i) x or y continue to increase with t giving non-bounded, unstable trajectories,

(ii) x or y is periodic with t giving stable trajectories provided that the maximum excursion from the z axis is less than r_o.

For a given ion, the form of the solution depends on the values of a and q. The boundaries between stable and unstable solutions can be plotted on an 'a-q diagram', and pairs of values giving stable solutions lie within distinct areas between these boundaries. For the QMF, two sets of a-q diagrams (U, V positive and U, V negative) are superimposed, and the regions of stability are given by the overlap of the stable regions of the separate diagrams. There are a number of possible overlap regions but only that corresponding to the lowest values of a and q is of practical interest, and this is illustrated in Figure 5. If a straight line of slope a/q is drawn on the a-q diagram, then the portion of the line lying within the stability envelope will give the range of stable a and q values. The masses corresponding to these ranges of values for a given analyser will depend on the values of U, V, r_o and ω, and can be calculated from equations [14] above. The limits of mass ranges which are stable in a and q will not be identical, and the actual range of stable masses will be those which lie in the overlap between the two mass ranges. Increasing the a/q ratio narrows the stability ranges and therefore corresponds to increased resolution.

From equation [14], it can be seen that a/q is equal to 2U/V, and the instrument resolution is therefore determined by the U/V ratio. To generate a mass spectrum, the

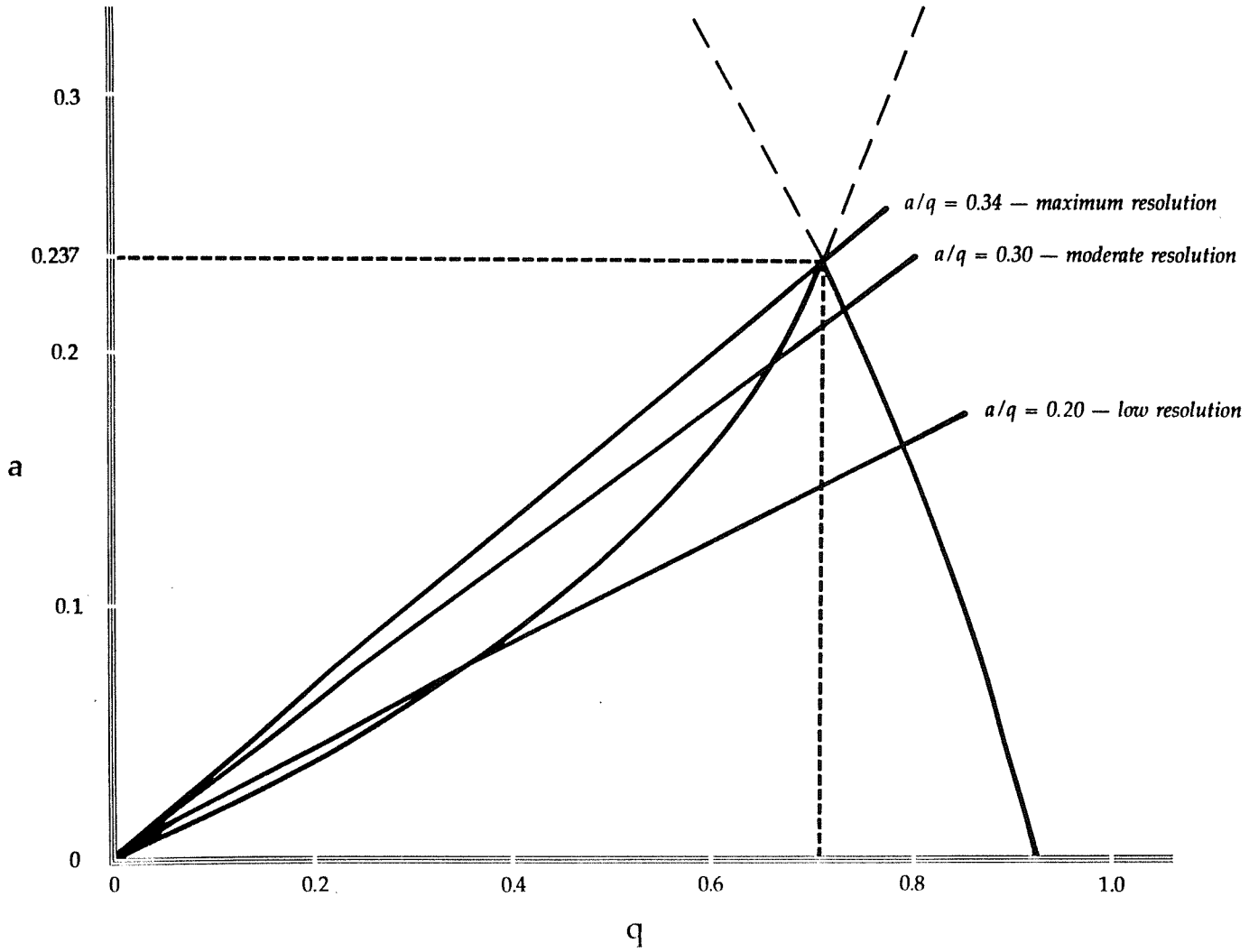

Figure 5 a—q Stability Diagram for Quadrupole Mass Filter

appropriate parameters must be swept whilst keeping this ratio constant. This can be achieved either by sweeping U and V at constant ω, or sweeping ω at fixed U and V. In practice the first method is normally used because a linear voltage scan produces a linear mass scale.

Although the theoretical resolution of the QMF can be calculated from the U/V ratio as discussed above, the practical resolution is also affected by aspects of the instrument design (8). The ideal quadrupole field assumed in the derivation of the field equation can only be achieved if the electrodes have hyperbolic cross-sections. Most commercially-available instruments, however, have electrodes of circular cross-section, due to the technical difficulties in manufacturing hyperbolic rods. The cost of this compromise is a reduction in resolution by a factor of two or three. Another factor affecting the resolution is the residence time of the ions in the quadrupole field. This arises because the resolution is related to the number of rf oscillations to which the ion is subjected, and hence to the entrance velocity of the ion in the z direction. An important result of this is that, for a given ion energy, heavier ions will have lower z velocities and so experience more rf oscillations. This means that the resolution increases with mass, with a corresponding decrease in sensitivity. The maximum resolution which can be obtained, although theoretically infinite, is limited by the accuracy with which the various parameters are controlled, and variations in the trajectories of the ions entering the filter. In practice, the maximum resolution is about 2000.

2.4 Ion Detection and Measurement

In the simplest form of ion detector, ions are collected on a metal plate connected to earth through a resistor. The resulting neutralisation of the charge on the ions produces

a current through the resistor which gives a measure of the number of ions arriving at the detector. A more efficient form of this is the Faraday cup detector. The emission of secondary electrons must be suppressed to avoid a false indication of the ion current, and this is usually achieved by placing a negative electrode close to the collector surface. The disadvantage of the Faraday plate or cup is its low sensitivity. The arrival of one ion per second at the collector produces a current of 1.6×10^{-19} A, and the lowest current generally detectable with conventional amplifiers is 10^{-15} A. The detection limit for direct measurement of the ion current is therefore about 6000 ions per second. For higher sensitivity, an electron multiplier is used. The channel electron multiplier used in this work consists of a curved glass tube with a resistive coating on the inner surface. The entrance to the detector is at a high negative potential, which drops to earth along the length of the tube. An ion entering the detector strikes the inner wall and liberates a number of electrons which flow down the potential gradient towards a collector. The electrons repeatedly collide with the resistive surface resulting in a cascade of electrons which finally reach the collector, where the electron current is transmitted to the amplifier. The gain of the channel electron multiplier is of the order of 10^5, offering a considerable increase in sensitivity over the Faraday plate.

The amplified signal from the electron multiplier can be recorded using a chart recorder or, more commonly, converted into digital form and collected by computer. The data collection system used in this work was a DEC VT-103 computer. The software used was developed at Winfrith Technology Centre.

3. ACQUISITION AND INTERPRETATION OF MASS SPECTROMETRIC DATA

3.1 Experimental Procedure

The same general procedure was followed for all the systems studied, although minor variations were necessary to take account of the differing natures of the substances under investigation. A suitable sample holder was selected, based on the expected volatility of the sample, and loaded with about 100 mg of sample. The holder was mounted onto one of the inlet ports, and the system evacuated to about 2×10^{-7} mbar. The sample was then heated gradually whilst repeatedly scanning the mass spectrum over a suitable mass range. The sensitivity of the instrument was varied by changing the resolution of the mass filter and the electron multiplier gain. Ionising electron energies of 15 to 25 eV were used to favour parent ion production.

Although it was possible to cover the whole mass range in a single scan, this was not done since the changing sensitivity across the mass range meant that a given set of scan conditions would only be optimised for a limited part of the mass range. The spectrum was typically scanned in 30 to 100 mass number sections.

During the early stages of heating, the spectrum was scanned over the region where atomic fragment ions were expected to occur. Once these ions were observed, other mass ranges were examined for parent ions, polyatomic fragments and higher-mass polymeric species.

Different scan rates varying from 0.1 to 1000 sec/scan could be selected; scan times of 3 to 30 seconds were most frequently used. The data collection system allowed for co-addition of repeated scans to improve the signal-to-noise ratio, and this option was most frequently used for

low-intensity, high-mass ions, or to eliminate random interference from the rf generator during induction heating.

3.2 Data Interpretation

There are two aspects to the interpretation of mass spectrometric data: the identification of the observed ions, and their classification as either parent or fragment species. Identification of the ions was relatively straightforward in these studies, where the identity of the starting material was known and only two or three elements were involved in each system. The m/z values of the observed ions could therefore be compared with those calculated for the relatively small number of possible ion species arising from combination of the elements concerned. In many cases, unambiguous identification was aided by the presence of several isotopes giving a characteristic pattern of peaks, rather than a single peak, for these ions. The calculation of expected isotope patterns, although straightforward, is tedious for ions containing more than one polyisotopic ion, and a routine for performing such calculations was therefore included in the software package.

Ionisation efficiency curves were plotted by tuning the mass spectrometer to the most abundant m/z value of the ion of interest, and measuring the ion current as a function of the ionising electron energy. The ion current data were collected and plotted on the computer, and the linear part of the curve was selected interactively and extrapolated to zero current to determine the ion appearance potential.

3.3 Calibration

The calibration of the mass scale was verified by the experimental spectra of a number of known vapour species,

including iodine (I^+, HI^+ and I_2^+ ions) and tellurium (Te^+, Te_2^+, Te_3^+ and Te_4^+ ions), and was found to be accurate to better than 0.5 mass numbers. Routine calibration checks were performed using heptacosafluorotri-n-butylamine (PFTBA) which gives a well-characterised fragmentation pattern producing ions over the whole mass range of the spectrometer. The ionising electron energy scale was calibrated by comparing measured appearance potentials with literature values for several ions including H_2O^+ and Ar^+. Traces of water vapour were always present in the system, and argon was introduced via a needle valve as discussed in Section 2.1. These measurements revealed that the electron energy values indicated by the instrument were about 15% high. This error was attributed to space-charging effects within the ion source (9), and the potentiometer used to select the electron energy was adjusted to give readings which were consistent with reference values.

REFERENCES

1. Grimley, R T, in "The Characterisation of High-Temperature Vapors", ed J L Margrave, John Wiley and Sons, New York, 1967.

2. Drowart, J, in "Advances in Mass Spectrometry", ed J F J Todd, Volume 1, John Wiley and Sons, Chichester, 1986.

3. Todd, J F J, in "Advances in Mass Spectrometry", ed J F J Todd, Volume 1, John Wiley and Sons, Chichester, 1986.

4. Rose, M E, Johnstone, R A W, "Mass Spectrometry for Chemists and Biochemists", Cambridge University Press, 1982.

5. CRC Handbook of Chemistry and Physics, 64th Edition, CRC Press, Boca Raton, 1984.

6. Litzow, M R and Spalding, T R, "Mass Spectrometry of Inorganic and Organometallic Compounds", Elsevier, Amsterdam, 1973.

7. Campana, J E, Int J Mass Spec Ion Phys, 33, 101, 1980.

8. Lawson, G and Todd, J F J, Chem Br, 8, 373, 1972.

9. Batey, J H and Grant, R B, VG Quadrupoles Ltd, Private Communications, 1987.

CHAPTER THREE

MATRIX ISOLATION AND FOURIER TRANSFORM INFRARED SPECTROSCOPY

1. INTRODUCTION

The technique of matrix isolation allows spectroscopic studies to be made of molecular species whose chemical and physical properties make analysis in the gas phase experimentally difficult. The principle of the method is to simulate the gaseous phase by co-condensing the molecular species of interest with a large excess of inert gas onto a cryogenically-cooled support. This results in the trapping of sample molecules within the solid, inert matrix, which can then be studied by a variety of spectroscopic methods.

Matrix isolation was originally developed for application to free radicals and other unstable species (1), whose low concentrations and short lifetimes hindered analysis by existing techniques, and the logical extension of the technique to the study of high-temperature vapours was made a few years later (2). The wide range of studies of high-temperature or reactive species to which matrix isolation has since been applied can be seen in the extensive reviews and bibliographies (3-7), and its success and popularity in these fields can be ascribed to two important general features of the technique:

(i) The production of the sample vapour is spatially separated (albeit only by a few centimetres) from the site of analysis. This means that well-established Knudsen vaporisation or molecular beam techniques can be used to produce the vapour, and only the elements of the furnace need to be capable of withstanding the high temperatures which may be required. The problems of reconciling high-temperature vapour containment with the required spectroscopic properties, which would be necessary for direct study of the vapour species, therefore do not arise.

(ii) The use of a large excess of the matrix gas ensures that the trapped species are well-isolated from each other, and the low temperatures used, typically 4 to 30 K, prevent diffusion within the matrix. The probability of bimolecular reactions or polymerisation within the matrix is therefore minimised. Furthermore, at these low temperatures, only reactions with very low activation energies can occur, and so the possibility of unimolecular decomposition is also minimised. The lifetimes of unstable species can be extended almost indefinitely, greatly increasing the scope of the analysis. The formation of interaction or polymerisation products within the matrix can be studied, if required, either by altering the matrix-to-solute ratio, or by allowing the matrix to warm up slowly, and observing changes in the spectrum.

The species of interest may either be condensed together with the matrix gas, or generated in situ by photolysis of an appropriate matrix-isolated precursor (1). Alternatively, reactive gases may be used as, or included in, the matrix gas to allow the study of new species formed on condensation (8). Once the matrix has been prepared, a wide variety of techniques can be used to characterise the trapped species, ranging from the radiofrequency (n.m.r) to the γ-ray (Mössbauer) region of the spectrum (6). In practice, however, the most commonly-used techniques are infrared, UV-visible and e.s.r. spectroscopy.

In this work, high-temperature vapour molecules have been isolated in inert (argon or nitrogen) matrices, and the trapped species characterised by Fourier transform infrared spectroscopy. In the following sections, particular features of matrix isolation-infrared spectroscopy are discussed, and the equipment used is described in detail.

2. INFRARED SPECTROSCOPY OF MATRIX-ISOLATED MOLECULES

Infrared spectroscopy is the most frequently applied of the many techniques that have been used to study matrix-isolated molecules. The usefulness of vibrational spectroscopy in identifying new molecules, together with the comparative ease with which infrared spectra can be obtained, readily account for the popularity of this analytical method. In addition to the general features noted in the previous section, matrix isolation-infrared spectroscopy has a number of advantages over gas-phase spectroscopy, particularly when applied to high-temperature or unstable species:

(i) The trapping of the sample molecules in the rigid matrix prevents rotational motion of all but a few small molecules. The elimination of rotational fine structure leads to much sharper vibrational bands, which allows very accurate frequency measurements to be made. Furthermore, the narrowing of the vibrational bandwidth means that it is often possible to resolve very closely-spaced bands such as may arise from different isotopomers or conformational isomers (9).

(ii) The thermal population of vibrational states other than the ground state is negligible at the low temperature of the matrix (~ 12K), so transitions originating from vibrationally excited states cannot occur. This allows greatly simplified spectra to be obtained for high-temperature species, for which gas-phase spectra would be complicated by the appearance of hot bands.

(iii) The cumulative nature of the matrix preparation allows comparatively large amounts of sample to be studied by the use of long deposition times. This facilitates the observation of weakly-absorbing or low-concentration species.

Inevitably, there are also disadvantages in the use of matrix isolation, which need to be weighed against the above advantages. The elimination of rotational motion noted in (i) is a double-edged sword, since this will also mean the loss of any structural information which might be obtained from the rotational fine structure. However, this loss might be at least partially compensated for by the additional information provided by isotopic structure. The most serious shortcomings of the matrix isolation technique arise from the possibility that the trapping of a molecule in a rigid matrix may introduce significant perturbations in the measured parameters. This is, of course, only a problem insofar as matrix isolation is being used to provide pseudo-gas-phase information; the origins of such perturbations are a rich field of study in their own right (10).

The interactions between a molecule and its matrix environment may affect both the number and frequencies of the observed vibrational bands. These effects are considered below.

2.1 Matrix Shifts

The vibrational frequencies of matrix-isolated molecules are generally shifted from the gas-phase values by less than 1%, although considerably larger shifts are observed for highly polar molecules (9). Attempts to rationalise the observed shifts (10, 11, 12) have been based on models of solvent-solute interactions in the liquid phase. The interactions between solute and matrix molecules are made up of electrostatic, inductive, dispersive and repulsive

contributions, and the resulting frequency shifts are therefore functions of the dipoles and polarisabilities of the molecules, as well as the nature of the matrix site. The nature of these contributions for diatomic molecules is discussed in detail by Barnes (13). However, the agreement between observed and calculated frequency shifts is semi-quantitative at best, and particularly poor for polar matrices with non-spherical sites.

A qualitative model has also been developed (10) for frequency shifts in polyatomic molecules, involving the reduced mass and force constants of the molecule, as well as the potential function describing the solute-matrix interaction and the sensitivity of this function to the vibration coordinate. The frequency shift then depends on the separations between the solute and the matrix molecules relative to an equilibrium value, with large separations ("loose cage" case) resulting in shifts to lower frequencies, and vice-versa. This model was in qualitative agreement with observed data, which indicated that stretching vibrations tended to be shifted to lower frequencies whereas bending vibrations moved to higher frequencies; the rationale being that as the molecule is distorted to fit into the matrix site, distortion will be greater along low-force-constant (bending) coordinates, and the matrix site will therefore be a "tight cage" with respect to these vibrational modes. Whilst this quantitative model is not always consistent with more recent data (14), a more coherent model has yet to be developed for polyatomic species.

2.2 Band Splitting

Another effect of matrix-solute interactions is the possibility that unexpected bands may be observed. Multiple bands can occur if molecules are trapped in different types of matrix site, or in different orientations within the site (3), or if isolated solute

molecules are close enough together for interaction between them to occur. In all of these cases, the splitting arises from variations in the matrix-solute interaction resulting in slightly different frequency shifts. Band-splitting may also occur if the symmetry of the trapped molecule is sufficiently perturbed by the matrix site to cause vibrational degeneracies to be lifted. Taken to the extreme, such perturbations could alter the shape of the trapped molecule to such an extent that the spectrum could not be interpreted in terms of the gas-phase molecular geometry (15).

2.3 Properties of Matrix Materials

The quality of the prepared matrix is determined by the nature of the matrix gas, the deposition rate and concentration of the matrix, and the deposition temperature. The most frequently-used matrix gases are argon and nitrogen, although other types of gases such as simple hydrocarbons have also found some application. The matrix-to-solute ratio should be large enough to give good isolation, and is usually of the order of 500 to 1000. Deposition temperatures are typically in the range 5 to 25 K. In optimising the conditions for matrix preparation, the properties of the matrix gas need to be considered in detail (16):

(i) Purity. Because of the low solute concentrations used to give good isolation, small quantities of impurities in the matrix gas may build up in comparable quantities to the species being studied, giving rise to spurious bands in the spectrum. For this reason, it is also important to maintain a high vacuum in the system.

(ii) Transparency. The absence of strong absorptions in the spectral region of interest is an obvious requirement. Scattering may also be a problem,

and glassy matrices are preferable to crystalline since the latter give higher reflection losses. Slow deposition rates tend to give smoother, more transparent matrices, and the temperature at which measurements are made may also be important.

(iii) Inertness. Interaction between the matrix and the solute is generally undesirable, although reactive gases can be used to study specific reactions within the matrix.

(iv) Melting point. This determines the rigidity of the matrix, which is important in preventing solute diffusion. The melting point of the matrix material (in K) should be at least twice the temperature of the matrix.

(v) Volatility. For ease of use, the matrix material should be a gas or highly volatile liquid at room temperature. It should also have a low vapour pressure at the matrix temperature to prevent evaporation under the vacuum conditions.

(vi) Latent heat of fusion. This determines the amount of heat which needs to be removed in order to solidify the gas. Since the rate of heat removal will be limited by the performance of the cooling system, a high latent heat of fusion may limit the matrix deposition rate.

(vii) Lattice energy. The lattice energy is related to the energy required for molecular diffusion within the lattice.

(viii) Thermal conductivity. As gas molecules are deposited on the surface of the matrix, the excess heat must be removed as quickly as

possible to avoid local heating of the matrix, which may result in opacity and solute diffusion. The thermal conductivity of a material may place limits on the thickness of the matrix.

(ix) Electrical properties. Factors such as the dielectric constant, polarisibility, ionisation potential and electric multipole moments of the matrix gas will influence the matrix-solvent interactions described above.

(x) Crystal structure. The crystal properties of the matrix material will determine the type of site(s) which the solute molecules can occupy, and hence influence the observed matrix effects. The noble gases crystallise in a close-packed arrangement, producing tetrahedral and octahedral interstitial sites. Solute molecules can also occupy substitutional sites, replacing one or more matrix molecules. The different geometries of the various types of site will influence the perturbation of the trapped molecules. Occupation of interstitial sites is limited by their comparatively small sizes, so most molecules will occupy substitutional sites. The rapid condensation of the matrix gas produces a high concentration of defects in the crystal lattice, and these can act as additional trapping sites or diffusion pathways. Lattice dislocations can sometimes be removed by gently annealing the matrix.

Some of the above properties for argon and nitrogen matrices are summarised in Table 1. Argon crystallises in

TABLE 1

SELECTED CRYSTAL PROPERTIES FOR ARGON AND NITROGEN (16)

Property	Argon	Nitrogen
Melting Point (K)	83.3	63.2
Diffusion Temperature (K)	35	30
Boiling Point (K)	87.3	77.4
Temperature (K) for vapour pressure of 10^{-3} torr	39	34
Latent heat of fusion (J mol^{-1})	1190	721
Lattice energy at 0 K (J mol^{-1})	7724	6904
Thermal Conductivity (W m^{-1} K^{-1})	1.3	0.4
Average Polarisibility (A)	1.641	1.767
Refractive index	1.29	1.25
Site diameters (Å)	3.76 (s) 1.56 (o) 0.85 (t)	4.00
Vibration Frequencies (cm^{-1})	73,64,42	69,49

s = subtitutional site

o = octahedral interstitial site

t = tetrahedral interstitial site

a cubic close-packed structure, but the presence of impurities stabilises the metastable hexagonal close-packed form, particularly at higher temperatures. Nitrogen adopts a slightly distorted face-centred cubic structure at low temperatures, but undergoes a phase change at 35.6 K to a hexagonal close-packed structure. This higher-temperature phase allows free rotation of the nitrogen molecules, and is opaque to infrared radiation. Argon and nitrogen have no infrared-active vibrations, but the presence of impurities can activate low-frequency lattice modes, giving rise to the bands shown in Table 1.

3. FOURIER TRANSFORM INFRARED SPECTROSCOPY

There are two basic methods by which an infrared spectrum can be measured. The first is that used by conventional grating instruments, in which a light beam is shone through the sample and the transmitted radiation passes through an entrance slit into a monochromator. The beam is dispersed, and an exit slit allows only the small frequency element of interest into the detector. The spectrum is therefore scanned by measuring the intensity of the transmitted radiation in each resolution unit across the spectrum. The main disadvantage with this system is that only a very small proportion of the total radiation from the source reaches the detector at any instant; for example, in a spectrometer scanning between 4000 and 400 cm^{-1} with 8 cm^{-1} resolution the proportion of energy reaching the detector is only about 0.2%, and this decreases to about 0.03% at 1 cm^{-1} resolution. The consequence of this is that long measurement times are required to obtain spectra with acceptable signal-to-noise ratios, particularly at high resolution or in the far-infrared region where sources are less intense.

The second technique is that of Fourier transform infrared (FT-IR) spectroscopy. The FT-IR spectrometer has no slits or grating; its central feature is the interferometer. A schematic diagram of the interferometer of the Bruker IFS-113V spectrometer used in these studies is shown in Figure 1. This design differs slightly from the Michelson interferometer used in many FT-IR spectrometers, but the operating principle is the same. Infrared radiation enters the spectrometer through an aperture and is focussed onto the beamsplitter, where half the radiation is transmitted and half reflected. The two beams are reflected via two mirrors onto the two faces of a double-sided moving mirror, before being reflected back and recombined at the beamsplitter. Half of the recombined beam returns to the source chamber, and half passes into the sample chamber.

If the moving mirror M_m (Figure 1) is exactly equidistant from the two mirrors M_a and M_B, then the path lengths travelled by the two beams A and B between their separation and recombination at the beamsplitter will be identical. All of the component frequencies of the beams will therefore be in phase when the beams recombine, and constructive interference will occur at all frequencies. However, if the moving mirror is moved a distance of $\delta/4$ towards mirror M_a, then the path length of beam A will be δ shorter than that of B, and the quality δ is termed the retardation. In this case, only those frequencies where $\delta = n\lambda$ ($n = 1,2,3 \ldots$) will recombine in phase to give constructive interference at the beamsplitter. Frequencies where $\delta = (n + 0.5)\lambda$ will be recombined with a phase difference of 180°, ie complete destructive interference occurs. All other frequencies will be partially out of phase. If the intensity of a frequency $\bar{\nu}$ ($\bar{\nu} = \frac{1}{\lambda}$) of the source is $I(\bar{\nu})$, then the intensity of $\bar{\nu}$ at the detector for a given retardation ($I'(\delta)$) is given by

Ma, Mb	Fixed mirrors
Mm	Double-sided moving mirror
BMS	Beamsplitter
OPF	Optical filter

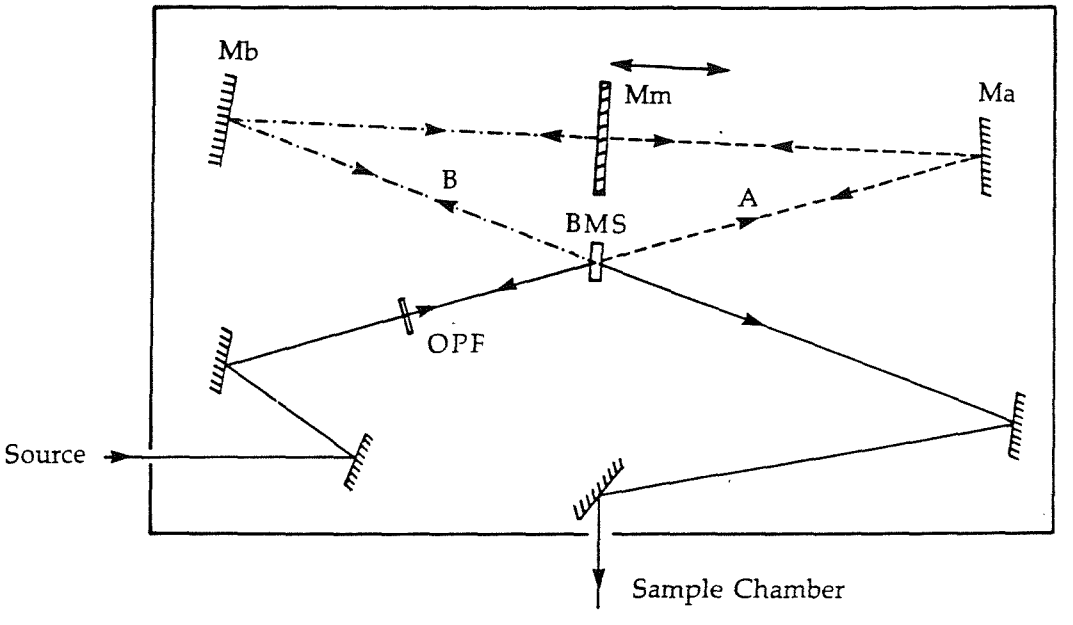

Figure 1 Interferometer Optics in Bruker IFS-113V FT-IR Spectrometer

$$I'(\delta) = \tfrac{1}{2}I(\bar{\nu})\{1 + \cos(2\pi\delta\bar{\nu})\} \quad [1]$$

In practice the signal intensity will be affected by other factors such as the beamsplitter efficiency, detector response, and amplifier characteristics. These effects may be combined into a single frequency-dependent correction factor $H(\bar{\nu})$ to give

$$I(\delta) = B(\bar{\nu})\cos(2\pi\bar{\nu}\delta) \quad [2]$$

where $B(\bar{\nu}) = \tfrac{1}{2}I(\bar{\nu})H(\bar{\nu})$.

$I(\delta)$ is defined mathematically as the cosine Fourier transform of $B(\bar{\nu})$.

The total intensity measured at the detector will be the sum of the $I(\delta)$ for all the component frequencies of the source:

$$I(\delta) = \int_0^\infty B(\bar{\nu})\cos(2\pi\bar{\nu}\delta)\, d\bar{\nu} \quad [3]$$

This integral is one half of a cosine Fourier transform pair, the other being

$$B(\bar{\nu}) = 2\int_0^\infty I(\delta)\cos(2\pi\bar{\nu}\delta)\, d\delta \quad [4]$$

These relationships imply that if the signal intensity at the detector is measured as a function of δ, then the contribution of each frequency $\bar{\nu}$ can be calculated. This is the basis of the Fourier transform method.

Fourier transform infrared spectroscopy offers potential advantages over the dispersive technique in both signal-to-noise ratios and frequency accuracy over a wide frequency range (17, 18). The main improvement in

signal-to-noise ratio arises from the fact that all the radiation passing through the sample is measured throughout the whole measurement time. For example, if a spectrum of range 4000 to 400 cm is recorded with 1 cm^{-1} resolution on a dispersive instrument, then the measurement time per resolution unit is T/3600, where T is the total measurement time. On a FT instrument, since all frequencies are measured simultaneously, the equivalent measurement time is T. Since the signal-to-noise ratio varies as the square root of the measurement time, it can be seen that in this example the FT method gives a factor of 60 improvement in either measurement time or signal-to-noise ratio. This is known as the multiplex or Fellgett advantage. Further improvements in signal-to-noise ratio can be achieved as a result of the greater optical throughput of an FT-IR instrument arising from the absence of slits. This is known as Jacquinot's advantage, but is generally of less importance than the multiplex advantage in chemical spectroscopy, since the practical throughput is often limited by the sample geometry or detector size.

The potential advantage in frequency accuracy arises from the fact that the FT-IR spectrometer determines frequencies from mirror displacement, which is accurately measured by a He-Ne laser. The importance of this laser reference or Connes advantage rather depends on the required application of the data (18); in many matrix isolation studies, high precision measurement of frequency differences between isotopomers is more important than absolute frequency accuracy.

There are, inevitably, certain disadvantages to the use of FT-IR which may partially offset the advantages discussed above, and an excellent discussion on the relative merits of FT-IR can be found in Reference 18. The negative aspects arise largely from the lack of directness of the Fourier transform method; the fact that the spectrum is constructed mathematically from the interferogram

introduces a number of artefacts for which compensation needs to be made.

The integral in [4] implies that $I(\delta)$ is known for infinitely small increments of δ. In practice, however, the interferogram is digitised by sampling the detector signal at finite values of the retardation. This means that if the retardation increment between data points is $\Delta\delta$, then the maximum frequency, $\bar{\nu}_{max}$, which can be present in the computed spectrum is $1/(2\Delta\delta)$. If the "real" spectrum contains radiation of higher frequency than this maximum, then the effect of digitisation will be to make the higher frequency components appear as lower frequencies ie a spectral feature which actually occurs at $(\bar{\nu}_{max} + k)$ will appear in the Fourier transformed spectrum at $(\bar{\nu}_{max} - k)$. This effect, known as spectral folding, necessitates the use of filters to ensure that no frequencies above $\bar{\nu}_{max}$ are present in the interferogram.

Another implication of [4] is that δ varies from zero to infinity, whereas in practice δ is limited by the finite displacement of the moving mirror. This has the effect of limiting the spectral resolution such that if the maximum retardation is δ_{max}, then the resolution $\Delta\bar{\nu}$ is approximately equal to $1/\delta_{max}$. A further consequence of the truncation of the interferogram at a finite retardation is that the computed lineshape of a peak is distorted by the appearance of 'ripples' on either side at the base of the peak. These artefacts can be removed by applying a weighting function to the interferogram before transformation, the most common being a triangular function in which the weighting increases linearly from 0 at δ_{max} to 1 at $\delta=0$. This is known as apodisation, since the effect is to remove the 'feet' of the peak.

The way in which a Fourier transform spectrometer operates means that it cannot be used as a double-beam instrument in the same way as a dispersive machine, in which the beam is

chopped and passed through the sample and reference cells in rapid alternation to allow background absorbances to be subtracted. Instead, a reference spectrum has to be recorded at the beginning of the experiment, and subsequent sample spectra are compared with this. Care must therefore be taken to ensure that changes in the background absorbancies are kept to a minimum during the experiments. This was achieved in the spectrometer used in this work by evacuating the optical bench to a pressure of about 1 mbar.

4. EXPERIMENTAL DETAILS

The matrix isolation-infrared spectroscopy apparatus is shown schematically in Figure 2. The sample is vaporised from a platinum or ceramic holder inside the furnace, which consists of an alumina tube wound with either nichrome or platinum-rhodium wire. The temperature of the sample is monitored by a thermocouple (K or R-type) located in the furnace insulation. Sample temperatures of up to 1700°C can be achieved using the Pt-Rh furnace.

The furnace assembly is located within a stainless steel water-cooled jacket which is sealed to the vacuum housing of the cryostat. It is necessary for experiments to be performed under vacuum to avoid condensation of atmospheric gases on the cold window, and the system is pumped to 10^{-6} mbar by an oil diffusion pump and cryotrap backed by a rotary pump. The windows of the vacuum housing are made of either caesium iodide, which is transparent down to about 200 cm^{-1}, or polythene, which is transparent below 700 cm^{-1}. The matrix gas enters via a needle valve which allows the deposition rate to be controlled. Argon (99.995%) and oxygen-free nitrogen (99.9%) have been used as matrix gases.

The cryostat assembly, which consists of the expander module of the refrigeration unit, the radiation shield and the cooled window, is mounted on top of the vacuum housing

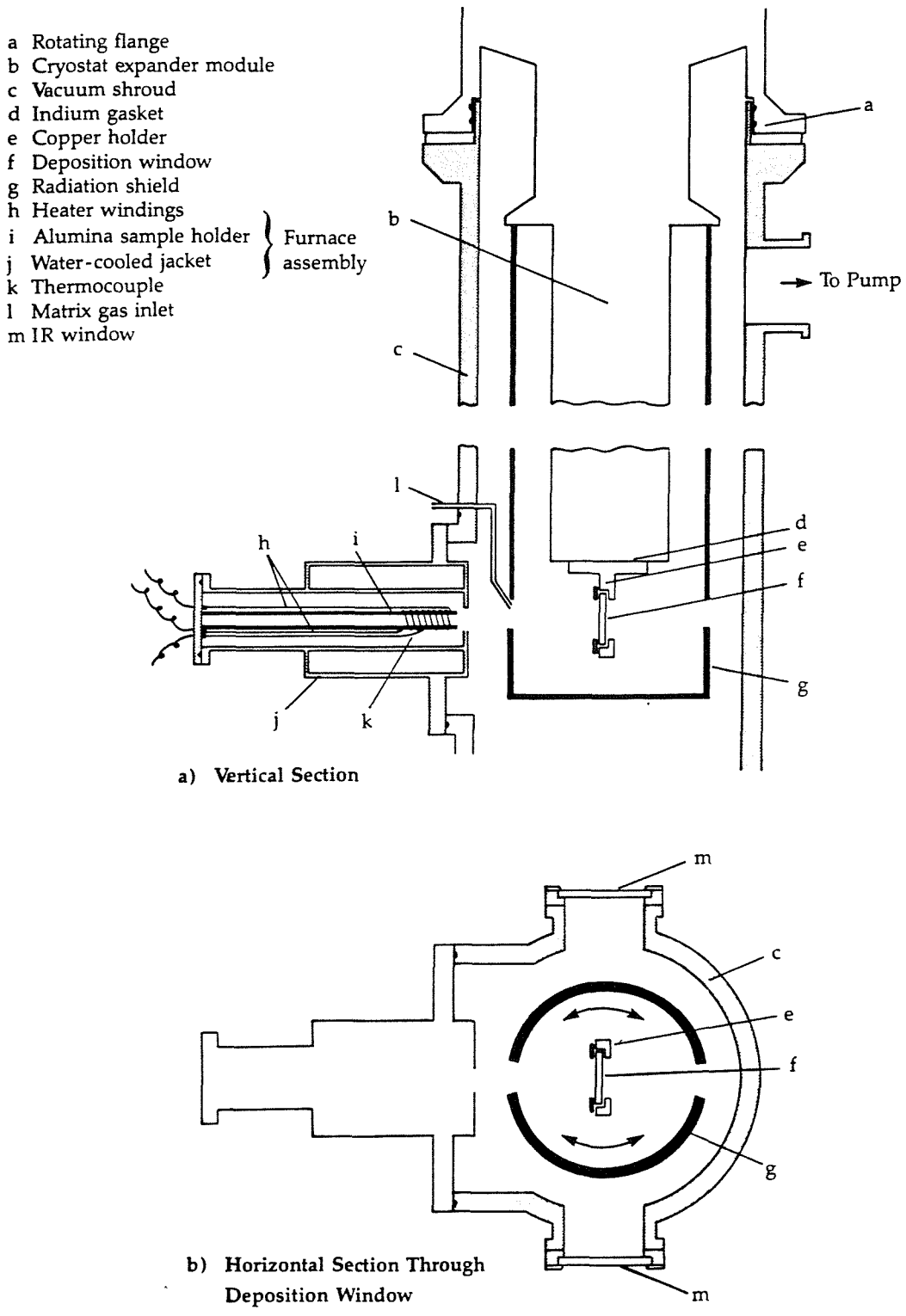

Figure 2 Matrix Isolation-Infrared Experimental Arrangement

via a rotating seal. The assembly is cooled by a Heraeus closed-cycle cryostat using helium as the working fluid. The helium is compressed at room temperature and passed to the expander module where it expands against a piston, becoming cooler as a result. The piston then moves the gas back to the compressor unit. The expansion takes place in two stages, the first producing a temperature of ca. 40K and the second producing the working temperature of ca. 10K. The temperature at the cold tip is monitored by a temperature controller, which also allows heating of the cold tip. The cold window is held in a copper holder mounted onto the bottom of the cold tip. Caesium iodide and single-crystal silicon windows are used for mid-infrared and far-infrared experiments respectively, and indium gaskets are used in mounting the windows to ensure good thermal contact. The radiation shield ensures that the minimum temperatures are attained and also protects the expander from contamination by the sample.

The vacuum shroud and cryostat assembly are suspended in one of the sample chambers of the Bruker IFS-113V infrared spectrometer. This is an evacuable Fourier transform instrument with a spectral range of 5000 to 10 cm^{-1}. This wide range is achieved by the use of a number of sources, beamsplitters and detectors. For mid-infrared measurements (4000 to 400 cm^{-1}), a globar source, a KBr beamsplitter and a mercury-cadmium telluride (MCT) detector are used. In the far-infrared (700 to 10 cm^{-1}), either a globar source (down to 100 cm^{-1}) or a mercury discharge lamp (below 100 cm^{-1}) are used together with a Mylar beamsplitter and a deuterated triglycine sulphate (DTGS) detector. Five different thicknesses of Mylar beamsplitter, from 3.5 μm to 50 μm, are available to optimise the far-infrared region of interest.

The spectrometer has two independent sample chambers with removable top and side panels. This allows the matrix

isolation facility to be permanently mounted in one chamber whilst retaining the capability for conventional infrared spectroscopy with demountable attachments for transmission or reflectance measurements in the other chamber.

It was originally planned to mount the matrix isolation assembly directly onto the spectrometer, with the vacuum shroud and furnace assembly being incorporated into modified top and side panels respectively (see Figure 3a). However, it was found that the vibration produced by the operating cryostat destabilised the interferometer resulting in very noisy spectra.

A sample well was therefore designed and constructed to remove any mechanical contact between the matrix isolation assembly and the spectrometer. This consisted essentially of a stainless steel box placed in the sample chamber with openings at the top and at one side which were sealed to corresponding openings of the spectrometer, and ports to allow the infrared beam to pass through. The cryostat vacuum shroud was suspended in the well, and the furnace assembly mounted through the side opening (Figure 3b). Initially, infrared-transparent windows were mounted in the beam ports, to allow the spectrometer to be used in the evacuated mode. The well was purged with dry nitrogen to minimise absorptions from atmospheric gases in the gap between the spectrometer and cryostat windows (Figure 4a). This arrangement was later modified by removing the outer set of windows and sealing the beam ports to the cryostat windows with large-bore flexible rubber connecting tubes (Figure 4b). This arrangement was found to transmit minimal vibration to the spectrometer, and the removal of the outer set of windows increased the throughput of the assembly and removed the need for a purge gas. A further advantage of the modified arrangement was that the cryostat

a Cryostat assembly
b Sample chamber wall
c Evacuated region
d Sample well

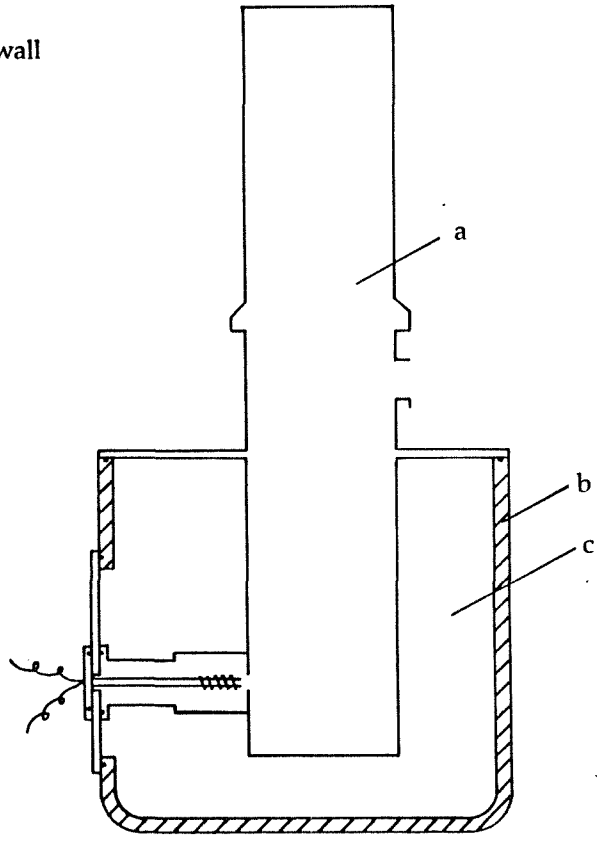

a) Proposed Design

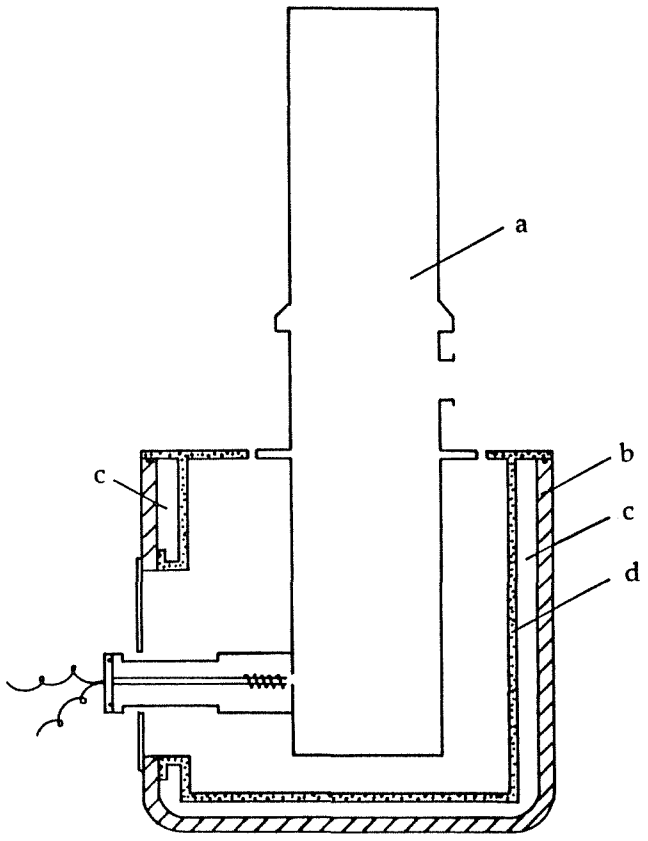

b) Modified Design to Isolate Spectrometer from Cryostat Vibration

Figure 3 Cryostat Mounting in IR Sample Chamber

A Inner window
B Outer window
C Flexible rubber connector

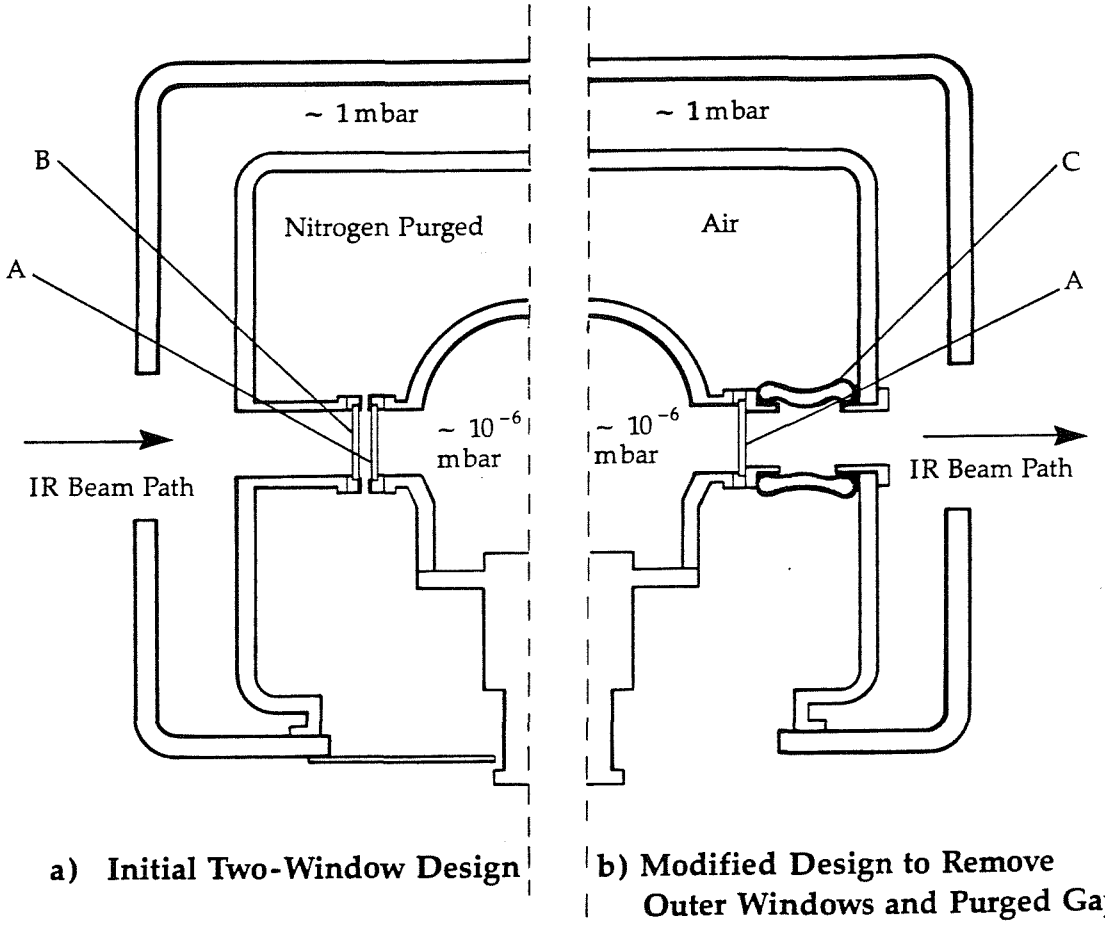

a) Initial Two-Window Design

b) Modified Design to Remove Outer Windows and Purged Gap

Figure 4 Horizontal Cross-Section Through Sample Well

windows could be removed for cleaning or replacement without removing the whole cryostat assembly.

The general technique used for the matrix isolation experiments was as follows. The sample was loaded and the system evacuated to 2 x 10^{-6} mbar. During the initial evacuation period the sample was degassed by heating to a temperature below its vaporisation temperature. The cryostat unit was switched on and the system cooled to about 10 K, which took about 30 minutes. The cryostat assembly was rotated into the measurement position, and a background spectrum recorded at the highest resolution required, after which the head was rotated into the matrix deposition position (see Figure 2b). The matrix gas flow was started and controlled so that the system pressure and the pressure at the gas inlet were about 2 x 10^{-6} and 1 mbar respectively. The furnace was brought up to a temperature which was selected on the basis of previous mass spectrometric experiments or literature vapour pressure data on the sample. After about 20 minutes the cryohead was rotated into the measurement position and the spectrum recorded at low resolution (4 cm^{-1}). If no change in the spectrum was observed, the sample temperature was increased and deposition continued for a further 20 minutes. This process of deposition and measurement was repeated until a sample spectrum was observed, and deposition was then continued at this temperature for 2 to 6 hours, with spectra being taken at hourly intervals. The final spectra were recorded at higher resolution (usually 1 or 2 cm^{-1}) with a larger number of scans (512 or 1024) to give good signal-to-noise ratios.

REFERENCES

1. Whittle, E, Dows, D A and Pimentel, G C, J Chem Phys, 22, 1943, 1954.

2. Linevsky, M J, J Chem Phys, 34, 587, 1961.

3. Downs, A J and Peake, S C, Mol Spec, 1, 523, 1973.

4. Chadwick, B M, Mol Spec, 3, 281, 1975.

5. Chadwick, B M, Mol Spec, 6, 72, 1979.

6. Almond, M J and Downs, A J, "Spectroscopy of Matrix Isolated Species", John Wiley and Sons, Chichester, 1989.

7. Ball, D W, Kafafi, Z H, Fredin, L, Hauge, R H and Margrave, J L, "A Bibligraphy of Matrix Isolation Spectroscopy, 1954-1985", Rice University, Houston, 1988.

8. See for example:

   Andrews, L, Appl Spectrosc, 33, 199, 1979;

   Long, S R, Lee, Y-P, Krogh, O D and Pimental, G C, J Chem Phys, 77, 226, 1982;

   Hauge, R H, Kauffman, J W and Margrave, J L, J Am Chem Soc, 102, 6005, 1980.

9. Barnes, A J, Rev Anal Chem, 1, 193, 1972.

10. Pimentel, G C and Charles, S W, Pure Appl Chem, 7, 111, 1963.

11. Hallam, H E, Mol Spec Proc Conf 4th, 329, 1968.

12. Barnes, A J and Hallam, H E, Quarterly Rev Chem Soc, 23, 392, 1969.

13. Barnes, A J in "Vibrational Spectroscopy of Trapped Species", ed H E Hallam, John Wiley and Sons, London, 1973.

14. Swanson, B I and Jones, L H, in "Vibrational Spectra and Structure", ed J R Durig, Vol 12, Elsevier, Amsterdam, 1983.

15. Beattie, I R, Jones, P J, Millington, K R and Wilson, A D, J Chem Soc Dalton Trans, 11, 2759, 1988.

16. Hallam, H E and Scrimshaw, G F, in "Vibrational Spectroscopy of Trapped Species", ed H E Hallam, John Wiley and Sons, London, 1973.

17. Griffiths, P R, "Chemical Infrared Fourier Transform Spectroscopy", John Wiley and Sons, New York, 1975.

18. Green, D W and Reedy, G T, in "Fourier Transform Infrared Spectroscopy", Volume 1, ed J R Ferraro and L J Basile, Academic Press, London, 1978.

CHAPTER FOUR

VIBRATIONAL SPECTROSCOPY

1. INTRODUCTION

The study of infrared spectra can yield important information about molecular structure and the nature of the forces acting between the atoms in a molecule. In this chapter, the principles underlying the interpretation of vibrational spectroscopic data are outlined, and a brief description is given of the computation methods used in later chapters. The vibrational data obtained can also be used to calculate the thermodynamic properties of the gaseous molecule, and this aspect is discussed in Section 6.

The information given by vibrational spectroscopy concerns the absorption of energy by a molecule as it is excited from a lower to a higher vibrational state. At normal temperatures, most molecules occupy the ground vibrational level [v=0], so that the only significant transition will be from this ground level to the first excited vibrational state [v=1]. However, changes in the rotational energy level may also occur, with a change in the rotational quantum number J of ± 1, so that for a molecule in its ground vibrational, nth rotational state [v=0, J=n] there are three allowed transitions to [v=1, J=n+1], [v=1, J=n-1] (provided n>0), and [v=1, J=n], although the last of these is not allowed for most diatomic molecules or for some vibrations of linear polyatomics. As the energy separation of the rotational states is much smaller than that of the vibrational levels, several rotational levels will be occupied even at low temperatures, giving rise to a number of possible rotational-vibrational transitions each with a defined energy. Such rotational changes appear as fine structure on the vibrational spectrum, and can give structural information about the molecule. However, this rotational structure is usually absent from the spectra of matrix isolation molecules, as discussed in the previous

chapter, so the following discussion is restricted to vibrational changes.

Infrared data can be applied to the identification and analysis of unknown molecules in a number of different ways.

(i) Fingerprinting. The spectrum of an unknown substance can be compared with spectra of known compounds to find the closest 'match'. This is widely used in the case of organic compounds where spectra are too complicated to assign all the peaks.

(ii) 'Functional Group' analysis. The positions of individual peaks on the spectrum of the unknown can be compared with observed or reported frequencies for vibrations involving particular combinations of atoms. This gives an indication of the type of groups present, and again is widely used in the analysis of organic compounds.

(iii) Structural and vibrational analysis. A proposed structure for an unknown compound can be tested by comparing the observed spectrum with that predicted for the model. At a simple level this involves verifying that the number of infrared-active bands, their relative positions and intensities and any isotopic effects are consistent with the proposed molecular shape. Once this has been achieved the model may be refined by calculation of bond angles and force constants based on observed frequencies, and this model may then be used in estimating the frequencies of non-infrared active modes.

The application of vibrational spectroscopy to the molecules studied in this work lies mainly in the third of

these areas. Details of the theory used in defining the relationships between the observed vibration frequencies and the structure and forces of a molecule are given elsewhere (1, 2), and selected aspects are outlined in the following sections.

2. MOLECULAR VIBRATIONS

The atoms in a molecule, even near the absolute zero of temperature, continuously oscillate about their equilibrium positions. The motions of the molecule as a whole can be described by the x, y and z components of the movements of its constituent atoms, so an N-atomic molecule has 3N degrees of freedom. Of these, three will correspond to the movement of all the atoms along the x, y or z axis (translations) and a further three (two in the case of a linear molecule) will correspond to rotation of the whole molecule about these axes. The remaining 3N-6 (3N-5 for a linear molecule) degrees of freedom correspond to the molecular vibrations (3).

The oscillation frequency is a function of the potential and kinetic energy changes which occur in the vibrating molecule. In a diatomic molecule, the only possible mode of vibration is the oscillation of both atoms along the molecular axis. In the simple harmonic oscillator approximation, the potential and kinetic energies are given by

$$2V = kq^2 \quad \text{and} \quad 2T = \mu\dot{q}^2 \qquad [1]$$

where q is the variation of the bond length from its equilibrium value, k is the force constant and μ the reduced mass of the molecule. The oscillation frequency can be shown classically to be

$$\nu = \frac{1}{2\pi}\sqrt{\frac{k}{\mu}} \qquad [2]$$

and the vibrational energy levels, from the Schrödinger equation, are

$$E_v = h\nu(v + \tfrac{1}{2}) \qquad [3]$$

where v is the vibrational quantum number.

The motion of the atoms in a polyatomic molecule is more complicated, but can be considered as arising from the superimposition of 3N-6 (3N-5 for a linear molecule) different vibrational modes. In each of these so-called normal modes of vibration, the atoms oscillate with different amplitudes but at the same frequency (the "normal frequency"), and all pass through their equilibrium positions simultaneously. Each normal mode has associated with it a normal coordinate, Q, which expresses the amplitudes of vibration of each of the 3N cartesian displacement coordinates of the atoms in the molecule.

The potential and kinetic energies expressed in terms of the normal coordinates are

$$2T = \sum_{i}^{3N} \dot{Q}^2 \quad \text{and} \quad 2V = \sum_{i}^{3N} \lambda_i Q_i^2 \qquad [4]$$

It can then be shown classically that

$$Q_i = K_i \cos(\lambda_i^{\frac{1}{2}} t + e_i) \qquad [5]$$

in which λ is related to the vibration frequency $\bar{\nu}$ by

$$\lambda = 4\pi^2 c^2 \bar{\nu}^2 \qquad [6]$$

and K_i and e_i are constants relating to the amplitude and phase of the vibration.

The values of λ can be calculated from the force constants and structure of the molecule using the GF matrix method (1,2). This involves expressing the kinetic and potential energies of the molecule in terms of a set of internal coordinates such as changes in bond lengths or angles:

$$2V = \tilde{\underline{R}}\ \underline{F}\ \underline{R} \quad \text{and} \quad 2T = \dot{\tilde{\underline{R}}}\ \underline{G}^{-1}\ \dot{\underline{R}} \qquad [7]$$

where $\underline{R}$ is a column matrix whose components are the internal coordinates, $\tilde{\underline{R}}$ is the transpose of $\underline{R}$, $\underline{F}$ is a matrix of force constants and $\underline{G}$ is constructed from the masses and geometrical arrangement of the atoms within the molecule (4). The normal frequencies can then be obtained by solving the determinantal equation

$$\left|\underline{G}\ \underline{F} - \underline{E}\lambda\right| = 0 \qquad [8]$$

This is a polynomial in λ, the order of which is equal to the number of internal coordinates used which must be at least 3N-6. The solution can be greatly simplified by using symmetrised $\underline{F}$ and $\underline{G}$ matrices which has the effect of factoring the secular equation into a number of lower-order polynomials.

A worked example of the GF analysis of a cyclic M_2X_2 molecule is given in Appendix 2. However, the calculation is cumbersome and time-consuming, particularly for large molecules or those with low symmetry. In such cases, the problem is best tackled by computer, and the SOTONVIB program (5) has been used for many of the molecules studied in this thesis. This program takes as input the masses and approximate cartesian coordinates of the atoms together with a set of internal coordinates, and these are

used to compute the G matrix. The equation $|\underline{G}\ \underline{F} = \underline{E}\lambda|$ is then solved iteratively by adjusting a set of estimated force constants until agreement with observed frequencies is obtained.

3. SYMMETRY CONSIDERATIONS

Molecular symmetry considerations can be used to determine the degeneracies and infrared and Raman activities of the normal vibrations (1, 2, 6), as well as simplifying the solution of the secular equation.

3.1 Determining the Symmetry of the Normal Coordinates

If the symmetry species of the normal coordinates are known, then the degeneracies and infrared and Raman activities of the corresponding vibrations can be ascertained. Briefly, the method consists of first establishing the point group of the molecule from its symmetry elements, and then generating a reducible representation based on either cartesian or internal coordinates. This is done by adding up the number of coordinates which are transformed into themselves by each symmetry operation of the point group, multiplied by -1 if the operation changes the sign of the coordinate.

The representation can then be reduced using the formula

$$n^{(\gamma)} = \frac{1}{g} \sum_{j} g_j \chi_j^{(\gamma)} * \chi_j \qquad [9]$$

where $n^{(\gamma)}$ is the number of times the irreducible representation $\Gamma^{(\gamma)}$ appears in the reduced representation, g is the number of symmetry operations in the group, g_j is the number of symmetry operations in the jth class, and χ_j

and $\chi_j^{(\gamma)}$, are the characters of the jth class in the reducible representation and the irreducible representation ($\Gamma^{(\gamma)}$) respectively.

Since the transformations of the displacement coordinates are a representation of the point group of the molecule, then the normal coordinates, which to a first approximation are linear combinations of the displacement coordinates, must also be a representation of the group. The normal coordinates corresponding to non-degenerate frequencies are not mixed by symmetry operations, and therefore form the basis of one dimensional irreducible representations of the group. If n normal coordinates are degenerate, they will form the basis of a n-dimensional irreducible representation. Reduction of the representation formed from the displacement coordinates therefore gives the number of normal coordinates of each symmetry species. This reduced representation will include coordinates representing the rotation and translation of the molecule. The symmetries of the translations and rotations are the same for all molecules in the same point group, and are indicated in character tables, so that the removal of these coordinates from the reduced representation is easily achieved.

The normal coordinates are also linear combinations of the internal coordinates, and so the representation formed by 3N-6 internal coordinates must be the same as that formed from the normal coordinates. However, if internal coordinates are used as the basis of the reducible representation, then the translational and rotational species are automatically excluded from the reduced representation. Furthermore, since the symmetry operations will only interchange internal coordinates which are symmetrically equivalent, a reducible representation can be generated and reduced for each set of equivalent

coordinates, the representation of the whole molecule being the sum of these individual representations.

In many cases, the internal coordinates which make up a symmetrically equivalent set are not all independent, and it is necessary to use more than 3N-6 coordinates to generate the representation. This gives rise to redundant species in the reduced representation, which can usually be identified by observation or comparison with the representation based on cartesian coordinates. If there are redundant conditions in the internal coordinate set used for the GF analysis, these will give rise to zero roots in the secular equation.

3.2 Vibrational Selection Rules and Intensities

The intensity of an IR absorption is determined by the probability of the corresponding transition. For a normal vibration whose normal coordinate is Q_a, this probability depends on the integral

$$[\mu]_{v'v''} = \int \Psi_{v'}(Q_a)\mu\Psi_{v''}(Q_a)\ dQ_a \qquad [10]$$

where μ is the molecular dipole moment in the electronic ground state and v' and v" are the vibrational quantum numbers before and after the transition. This integral can be resolved into x,y and z components, and if any of these are non-zero then the vibration will be infrared active.

The integral of a product of two functions is non-zero only if the integrand, or some term in it, is invariant to all the symmetry operations of the molecular point group, and this only occurs if the two functions belong to the same representation (6). In order for the product of three functions to be non-zero, therefore, the representation of the direct product of two of the functions must be, or contain, the representation of the third.

For a fundamental vibration (v'=0, v"=1), the vibrational wave functions are (6),

$$\Psi_{0,}(Q_a) = N_{0,}\ e^{-\frac{1}{2}\gamma_a Q_a^2}$$

$$\Psi_{1,}(Q_a) = 2(\gamma_a^{\frac{1}{2}} Q_a) N_{1,}\ e^{-\frac{1}{2}\gamma_a Q_a^2} \qquad [11]$$

in which N_n is a normalising factor, and

$$\gamma_a = \frac{4\pi^2 \nu_a}{h}$$

Since all symmetry operations transform Q_a to $\pm Q_a$, then Q_a^2, and hence $\Psi_0(Q_a)$ will be invariant to all symmetry operations. In order for the integral [10] to be non-zero, the direct product of the representations of μ and $\Psi_1(Q_a)$ must be or contain the totally symmetric representation, ie μ and $\Psi_1(Q_a)$ must belong to the same representation. The symmetry of $\Psi_1(Q_a)$, however, is the same as that of Q_a, and so in order for a vibration to be infrared active, the normal coordinate must have the same symmetry as one component of the dipole moment. A similar argument applies for the Raman activity, except that in this case the normal coordinate must have the same symmetry as a component of the polarisability tensor. The symmetry species of the dipole moment and polarisability tensor components are given in character tables, and so the infrared or Raman activity of a normal mode of known symmetry is easily ascertained.

It must be noted, however, that the fact that a particular mode is predicted to be infrared active on symmetry grounds does not guarantee that a corresponding band will be observed in the spectrum since its intensity may be very

low. The intensity of the infrared absorption band due to the ith normal vibration is given by

$$I_i = K\left[\left(\frac{\partial \mu_x}{\partial Q_i}\right)_o^2 + \left(\frac{\partial \mu_y}{\partial Q_i}\right)_o^2 + \left(\frac{\partial \mu_z}{\partial Q_i}\right)_o^2\right] \qquad [12]$$

where K is constant for a fixed path length and concentration. If the molecule possesses sufficient symmetry, only one of the three derivatives will be non-zero.

The $\frac{\partial \mu}{\partial Q}$ terms can be expressed in terms of cartesian or internal coordinates by

$$\frac{\partial \mu_g}{\partial Q_i} = \sum_t \frac{\partial \mu_g}{\partial R_t} \cdot \frac{\partial R_t}{\partial Q_i} \qquad [13]$$

The derivative of the molecular dipole with respect to internal coordinates is evaluated by assuming that the molecular moment with respect to the g axis is equal to the sum of the g-direction components of all the bond moments. If the magnitude of each bond dipole is regarded only as a function of the bond length, then the effect of a particular bond stretching or bending coordinate on the g-component of the associated bond dipole(s) can be quite easily visualised.

The $\frac{\partial R}{\partial Q}$ term in equation [13] expresses the amplitudes of oscillation of each internal coordinate within the normal coordinate. The relationship between internal and normal coordinates can also be written in the form

$$\underline{R} = \underline{L}\ \underline{Q} \qquad [14]$$

The L matrix satisfies the relationship

$$\underline{G}\ \underline{F}\ \underline{L} = \underline{L}\ \underline{\Lambda} \qquad [15]$$

where $\underline{\Lambda}$ is a diagonal matrix of the λ values. This allows the ratios of the L elements associated with each normal coordinate to be obtained, and the absolute L values can then be determined from the normalisation condition (1):

$$\underline{L}\ \tilde{\underline{L}} = \underline{G} \qquad [16]$$

An alternative to this bond dipole approach is the point charge model, which is used in the SOTONVIB program. In this model, an effective charge is assigned to each atom and assumed to move with this atom during the vibration. The overall dipole change during the vibration is therefore obtained by summation of the cartesian displacements of all the charges. The amplitudes of the displacements in terms of cartesian coordinates are expressed by

$$\underline{R}_X = \underline{L}_X\ \underline{Q} \qquad [17]$$

and the $\underline{L}_X$ matrix can be obtained in terms of the $\underline{L}$ matrix from the relationship between the cartesian and internal coordinates.

4. ISOTOPIC EFFECTS

If an atom of a molecule is replaced by a different isotope of the same element, the potential energy function and configuration of the molecule are effectively unchanged, but the vibration frequencies may be significantly altered by the change in mass. If an atom involved in a vibration is polyisotopic, therefore, the spectrum will show a number

of peaks whose intensities reflect the abundances of the different isotopes. If more than one polyisotopic atom is involved, the pattern will be a more complicated superimposition of the frequency shifts due to all combinations of the isotopes. Such frequency shifts are proportionally larger for vibrations in which the polyisotopic atom(s) oscillates with a relatively large amplitude, and therefore depend on the geometry of the molecule and the form of the normal coordinate. Isotopic fine structure - arising from either natural isotopic variations or deliberate isotopic substitution of selected atoms within the molecule - can thus be used to gain structural information, or to provide additional frequency values for use in force constant calculations. These applications are of particular relevance in matrix isolation studies since the sharpness of the vibrational bands make it possible to resolve very small isotopic shifts.

If the vibrational analysis is carried out by hand, expressions are obtained relating the vibration frequency to the relevant bond angles, atomic masses and force constants. The expressions for two or more molecules of different isotopic compositions can therefore be solved simultaneously to give bond angle and/or force constant data. The SOTONVIB program does not use isotopic data in the evaluation of these variables, but calculates isotopic frequencies on the basis of a pre-determined force field and structure. These isotopic data can then be compared with experimental values, and the input parameters adjusted to give the best agreement.

5. APPLICATIONS

Solution of the secular equation, as outlined in Section 2, relates the fundamental frequencies of a molecule to its geometry and the magnitude of the various molecular force

constants. In theory, therefore, it is possible given the molecular geometry and force constants to compute the values of the fundamental frequencies. In practice the force constants are rarely known and the more usual form of the problem is the calculation of these from measured vibrational frequencies. However, the number of independent force constants required is almost always greater than the number of vibration frequencies, even when the equivalence of many force constants due to symmetry is taken into account. It is therefore necessary to use approximations to the complete force field involving fewer independent terms. An obvious simplification is to consider only those forces which resist the extension, compression, bending or torsion of valence bonds, neglecting interactions between non-bonded atoms. This gives only diagonal terms in the F matrix when the internal coordinates are the bond lengths, bond angles etc. Whilst this method may not be particularly accurate for calculating unknown frequencies, it is very useful in assigning observed frequencies to vibrational modes (3). If additional frequency data are available then the simplified force field can be refined by the addition of selected interaction constants.

Once a satisfactory force field has been obtained, it may be used to estimate the frequencies of the non-infrared active modes of the molecule, and these data can then be used to calculate thermodynamic quantities.

The calculation of the thermodynamic properties of simple gases from a knowledge of their structure and vibration frequencies is a well-established and important method of obtaining such data (7). The derivation of the method is described in detail elsewhere (8); a brief summary together with the formulae used are given in the next sections.

6. CALCULATION OF THERMODYNAMIC QUANTITIES

The central quantity linking spectroscopic measurements with thermodynamic quantities is the partition function, Q, which expresses the way in which the total energy of a system is distributed over its various energy states. The partition function is defined as:

$$Q = \sum_n g_n e^{-E_n/kT} \qquad [18]$$

where E_n is the total energy of a molecule in state n, g_n is the statistical weight (or degeneracy) of n, and k is the Boltzmann constant. The summation is over all states n of the molecule.

The total energy E_n of a perfect gas molecule arises from translational, rotational, vibrational and electronic contributions. These terms are very nearly additive and so can be treated separately. The partition function can therefore be expressed as the product of the corresponding terms Q_{tr}, Q_r, Q_v, and Q_e, and these are considered below.

(a) Translational contribution

The translational partition function is given by

$$Q = V\left(\frac{2\pi mkT}{h^2}\right)^{3/2} \qquad [19]$$

where V is the volume of gas, m is the molecular mass and h is Planck's constant. Calculation of the translational contribution to the partition function therefore requires only a knowledge of the molecular mass.

(b) Rotational Contribution

The derivation of the rotational partition function is different for linear and non-linear molecules, and is formed by summation over all rotational levels. Assuming that the temperature is high enough for a significant number of rotational levels to be populated, then

$$Q_r = \frac{kT}{\sigma hcB} \text{ (linear molecule)}$$

and [20]

$$Q = \frac{1}{\sigma}\sqrt{\frac{\pi}{ABC}\left(\frac{kT}{hc}\right)^3} \text{ (non-linear molecule)}$$

where the symmetry number, σ, is the number of indistinguishable positions into which the molecule can be turned by simple rigid rotations. The rotational constants A, B and C are obtained from the principal moments of inertia of the molecule using the equation

$$A,B,C, = \frac{h}{8\pi^2 cI_{A,B,C}}$$

Calculation of the rotational contribution to the partition function therefore requires structural information: molecular shape, bond lengths and bond angles.

(c) Vibrational Contribution

The vibrational partition function is

$$Q_v = \sum_v g_v e^{-E_v/kT} \quad , \qquad [21]$$

and the vibrational energy levels, in the harmonic oscillator approximation, are given by

$$E_v = hc \sum_i \omega_i v_i$$

where ω_i are the fundamental vibration frequencies of the molecule and v_i the vibrational quantum numbers. Since E_v is the sum of independent contributions, Q_v becomes a product of terms, each of which is due to one vibration frequency. The final result is therefore

$$Q_v = \left(1-e^{-\omega_1 hc/kT}\right)^{-d_1}\left(1-e^{-\omega_2 hc/kT}\right)^{-d_2} \ldots \qquad [22]$$

where d_1, d_2, d_3 ... are the degeneracies of the vibrations of frequencies ω_1, ω_2, ω_3, ... The vibrational contribution to the partition function can thus be calculated from a knowledge of the frequencies and degeneracies of the fundamental vibrations.

(d) Electronic Contribution

The electronic contribution to the partition function has the same form as the vibrational contribution given in equation [21] above. However, the electronic energy levels of most species are sufficiently energetic not to exert a great influence on the thermodynamic properties of the molecule except at very high temperaures. In a very few cases, for example NO, low-lying electronic states do exist and make a significant contribution to the thermodynamic properties. Usually, however, the statistical weight of the ground state is the only quantity which needs to be known, and this is unity for most polyatomic molecules (7,9). The formulae given below assume that only the electronic ground state is of any importance.

The enthalpy, heat capacity, entropy and free energy of a gas at a given temperature can all be expressed in terms of the partition function Q.

The total internal energy E^o of one mole of a perfect gas is given by

$$E^o = E_o^o + \sum_n N_n E_n$$

where E_o^o is the zero-point energy and N_n the number of molecules having energies E_n above the lowest energy. According to the Maxwell-Boltzmann distribution law,

$$N_n = N_A \frac{g_n e^{-E_n/kT}}{Q}$$

where N_A is Avogadro's number. This gives

$$E^o = E_o^o + RT^2 \frac{d(\ln Q)}{dT}$$

The molar heat content or enthalpy, H^o, is the sum of the total internal energy E^o and the external energy pV (=RT). The quantity usually tabulated is $(H^o - E_o^o)$, which is given by

$$(H^o - E_o^o) = RT + RT^2 \frac{d(\ln Q)}{dT} \qquad [23]$$

The molar heat capacity at constant pressure is therefore

$$C_p^o = \frac{dH^o}{dT} = R + R \frac{d}{dT}\left(T^2 \frac{d(\ln Q)}{dT}\right) \qquad [24]$$

The molar entropy is given by

$$S^o = R(1-\ln N_A) + RT \frac{d(\ln Q)}{dT} + R \ln Q \qquad [25]$$

The molar free energy, G^o, is obtained by substituting equations [23] and [25] into

$$G^o = H^o - TS^o$$

giving

$$G^o = E_o^o + RT \ln N_A - RT \ln Q$$

The quantity usually tabulated is

$$-\frac{G^o - E_o^o}{T} = R \ln Q - R \ln N_A \qquad [26]$$

Since Q is the product of Q_{tr}, Q_r, Q_v and Q_e, the above functions of ln Q can be expressed as the sum of the four corresponding contributions. The contributions to each of the thermodynamic quantities are listed below; in each case the constant term, which does not involve Q, is included in the expression for the translational contribution.

(a) Enthalpy

$$H_{tr}^o = E_o^o + \frac{5}{2} RT$$

$$H_r^o = RT \text{ (linear molecule)}$$

$$= \frac{3}{2} RT \text{ (non-linear molecule)}$$

$$H_v^o = R \frac{hc}{k} \sum_i \frac{d_i \omega_i e^{-\omega_i hc/kT}}{1-e^{-\omega_i hc/kT}}$$

$$H_e^o = 0$$

(b) Heat Capacity

$$C_{p,tr}^o = \frac{5}{2} R$$

$$C_{p,r}^o = R \text{ (linear molecule)}$$

$$= \frac{3}{2} R \text{ (non-linear molecule)}$$

$$C_{p,v}^o = R \left(\frac{hc}{kT}\right)^2 \sum \frac{d_i \omega_i^2 e^{-\omega_i hc/kT}}{(1-e^{-\omega_i hc/kT})^2}$$

$$C_{p,e}^o = 0$$

(c) Entropy

$$S_{tr} = \left[R \left(\frac{5}{2} \ln T + \frac{3}{2} \ln M + \ln \left\{ \left(\frac{2\pi}{N_A}\right)^{3/2} \left(\frac{k^{5/2}}{h^3}\right) \right\} + \frac{5}{2} - \ln p \right) \right]$$

$$S_r = R\left(\ln T + \ln\frac{k}{hc} - \ln B - \ln\sigma + 1\right) \text{(linear molecule)}$$

$$= \frac{1}{2}R\left\{3\ln T - \ln ABC - 2\ln\sigma + \ln\left[\pi\left(\frac{k}{hc}\right)^3\right] + 3\right\}$$

(non-linear molecule)

$$S_v^o = -R\sum_i d_i \ln(1-e^{-\omega_i hc/kT}) + R\frac{hc}{kT}\sum_i \frac{d_i\omega_i e^{-\omega_i hc/kT}}{1-e^{-\omega_i hc/kT}}$$

$$S_e^o = R\ln g_e$$

(d) Free Energy

$$\frac{-(G^o-E_o^o)_{tr}}{T} = S_{tr}^o - \frac{5}{2}R$$

$$\frac{-(G^o-E_o^o)_r}{T} = S_r^o - R \text{ (linear molecule)}$$

$$= S_r^o - \frac{3}{2}R \text{ (non-linear molecule)}$$

$$\frac{-(G^o-E_o^o)_v}{T} = -R\sum_i d_i \ln(1-e^{-\omega_i hc/kT})$$

$$\frac{-(G^o-E_o^o)_e}{T} = R\ln g_e$$

It can be seen from the formulae given above that all the thermodynamic quantities of a molecule can be calculated

provided that its molecular mass, moments of inertia, symmetry number, fundamental vibration frequencies and electronic ground state degeneracy are known. A BASIC computer program "TDFUN2" was used for the calculations in this thesis; the program is listed in Appendix 1. The product of the principal moments of inertia was calculated from:

$$I_A I_B I_C = \begin{vmatrix} I_{xx} & -I_{xy} & -I_{xz} \\ -I_{xy} & I_{yy} & -I_{yz} \\ -I_{xz} & -I_{yz} & I_{zz} \end{vmatrix}$$

(10), where I_{xx}, I_{xy}, etc are the moments and products of inertia with respect to any coordinate system, and are given by

$$I_{xx} = \sum m_i (y_i^2 + z_i^2) - M^{-1} (\sum m_i y_i)^2 - (\sum m_i z_i)^2 \quad , \text{ etc}$$

and

$$I_{xy} = \sum m_i x_i y_i - M^{-1} (\sum m_i x_i)(\sum m_i y_i), \text{ etc}$$

where $M = \sum m_i$. A BASIC computer program "INERTS" was used in these calculations, and this is listed in Appendix 1.

There are a number of approximations implicit in the above treatment arising from the neglect of various contributions such as nuclear spin, centrifugal distortion of the molecule, change of moment of inertia with vibrational state, vibrational anharmonicity and non-ideality of the gas. The neglect of the nuclear spin contribution means that the calculated entropy is less than the absolute entropy by R ln g_s, where g_s is the nuclear spin weight $(2I_1 + 1)(2I_2 + 1)\ldots$. However, this difference only

becomes significant at very low temperatures, and the calculated or virtual entropy is used in practice.

Corrections for vibrational anharmonicity and centrifugal distortion are seldom possible for polyatomic molecules, although calculational methods for some types of molecule have been developed (11). For diatomic molecules, however, the required data usually exist allowing the appropriate corrections to be made (12).

REFERENCES

1. Nakamoto, K, "Infrared and Raman Spectra of Inorganic and Coordination Compounds", 3rd edition, John Wiley and Sons, New York, 1978.

2. Wilson, E B, Decius, J C and Cross, P C, "Molecular Vibrations", Dover Publications Inc., New York, 1980.

3. Banwell, C N "Fundamentals of Molecular Spectroscopy", 2nd Edition, McGraw-Hill, London, 1972.

4. Decius, J C, J Chem Phys, 16, 1025, 1948.

5. Beattie, I R, Cheetham, N, Gardner, M and Rogers, D E, J Chem Soc (A), 1971, 2240.

6. Cotton, F A, "Chemical Applications of Group Theory", 2nd Edition, John Wiley and Sons, New York, 1971.

7. Wilson, E B, Chem Rev, 27, 17, 1940.

8. Herzberg, G H, "Molecular Spectra and Molecular Structure, II, Infrared and Raman Spectra of Polyatomic Molecules", Van Nostrand, New Jersey, 1966.

9. Snelson, A, Int Rev Sci, Phys Chem Ser 2, 10, 81, 1975.

10. Hirschfelder, J O, J Chem Phys, 8, 431, 1940.

11. See for example:

Gordon, A R, J Chem Phys, 2, 1934;
Gordon, A R, J Chem Phys, 3, 1935;
Kassel, L S, Chem Rev, 18, 277, 1936.

12. Stull, D R and Prophet, H, in "The Characterisation of High-Temperature Vapors", ed J L Margrave, John Wiley and Sons, New York, 1967.

CHAPTER FIVE

STANNNOUS TELLURIDE, LEAD SELENIDE AND LEAD TELLURIDE

1. INTRODUCTION

The vaporisation behaviour of stannous telluride (SnTe) is of considerable interest in severe reactor accident analyses because of its influence on the timing and chemical form of the release of fission product tellurium from the damaged fuel. A number of experimental studies (1) have shown that significant quantities of tellurium begin to be released from the fuel when the temperature exceeds 1200°C. The released tellurium reacts readily with the Zircaloy fuel cladding to form zirconium telluride, and this results in a substantial decrease in the tellurium volatility (2). Indeed, the low release of tellurium from the reactor core observed after the accident at Three Mile Island has been attributed to the extensive reaction of tellurium with Zircaloy and other structural materials (3). In the steam-containing atmospheres expected in most severe accident scenarios, the Zircaloy cladding would become increasingly oxidised as the fuel temperature increased. If an area of the cladding became completely oxidised then the zirconium telluriude in this region would be broken down in favour of continued zirconium oxide formation, resulting in the re-release of tellurium. It has been shown experimentally that the release of tellurium from overheated fuel is strongly dependent on the extent of cladding oxidation (2,4,5,6). Furthermore, the volatility and chemical reactivity of the re-released tellurium have been found to be lower than expected for elemental tellurium vapour (7,8). It was also observed that some of the released tellurium was deposited in association with tin (9), and it was therefore postulated that tellurium was released from the cladding and transported as tin telluride, formed by the reaction of tellurium with the trace tin component of the Zircaloy fuel cladding.

This chapter describes mass spectrometric and matrix isolation-infrared spectroscopic studies of the

vaporisation behaviour of stannous telluride to identify directly the chemical form(s) in which tellurium vaporises after reaction with Zircaloy. Similar studies were also made of the analogous compounds PbSe and PbTe, for which published infrared data (10) were incomplete.

2. EXPERIMENTAL DETAILS

To investigate the chemical form in which tellurium was released after reaction with Zircaloy, a coupon of Zircaloy was laid on top of an alumina crucible containing a small quantity (~ 10 mg) of tellurium. The coupon and crucible were then heated in an argon flow to 550 or 950°C to vaporise the tellurium and allow it to react with the Zircaloy. After cooling, the coupon was transferred to a silica holder for mass spectrometric analysis.

Commercially-prepared stannous telluride was obtained from Cerac Ltd. Lead telluride and selenide were prepared by heating equimolar quantities of the elements to 450°C in alumina boats under a flowing atmosphere of 4% hydrogen in argon. The identities of the products were confirmed by x-ray diffraction analysis.

For mass spectrometric analysis, the samples were contained in silica-tube holders and heated gradually until molecular ions were observed in the mass spectra. The vaporisation temperatures varied between about 500°C for the prepared compounds to about 800°C for the tellurium-Zircaloy samples. Infrared spectra were obtained by heating the samples in the range 750 to 800°C and co-condensing the vapour species with argon onto a silicon window. The spectra were monitored over the range 400 to 80 cm^{-1}.

3. MASS SPECTROMETRY

The general pattern of vaporisation behaviour was very similar for the three compounds studied. In the early stages of heating, only X^+ and X_2^+ ions were observed in the mass spectrum. However, as the sample temperature was increased, MX^+ ions were detected and the X_2^+ ion intensities decreased, and above 500°C the mass spectra were dominated by the MX^+ ions. The observed MX^+ spectra are shown in Figures 1 and 2, together with calculated intensities for the different isotope combinations.

Additional higher-mass ions were observed in the mass spectrum of stannous telluride, and comparison with calculated spectra showed these to be $SnTe_2^+$ and $Sn_2Te_2^+$ (Figure 1). No such higher-mass ions were observed in the spectrum of lead telluride or lead selenide.

Fairly strong peaks due to M^+ and X^+ ions were also observed in all the mass spectra. The appearance potentials of these ions were measured to determine whether they were parent species or fragments of MX. Samples of elemental tellurium and selenium were also vaporised, and the appearance potentials of the X^+ and X_2^+ ions measured for comparison. The results of these measurements are shown in Table 1.

The appearance potentials of the M^+ and X^+ ions were significantly higher than their first ionisation potentials (11), showing that these ions arose principally from fragmentation. Comparison of the appearance potentials of the X^+ ions with those measured when the elements were vaporised showed that the parent species were not the X_2 molecules, and that these ions therefore arose from fragmentation of MX molecules in all cases. The appearance potential of the $SnTe_2^+$ ion was consistent with it being a fragment of Sn_2Te_2.

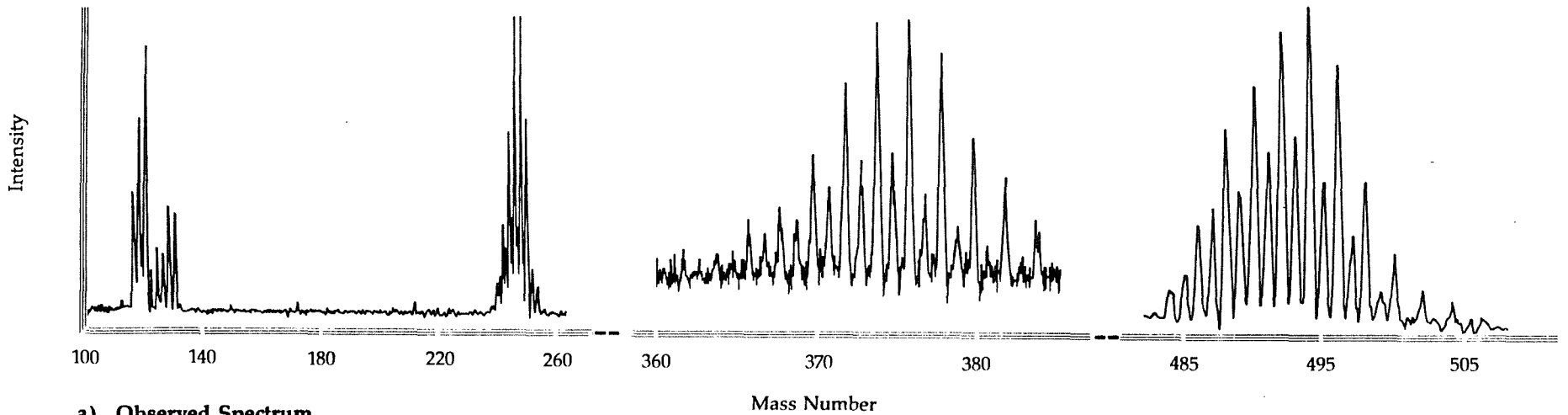

a) **Observed Spectrum**

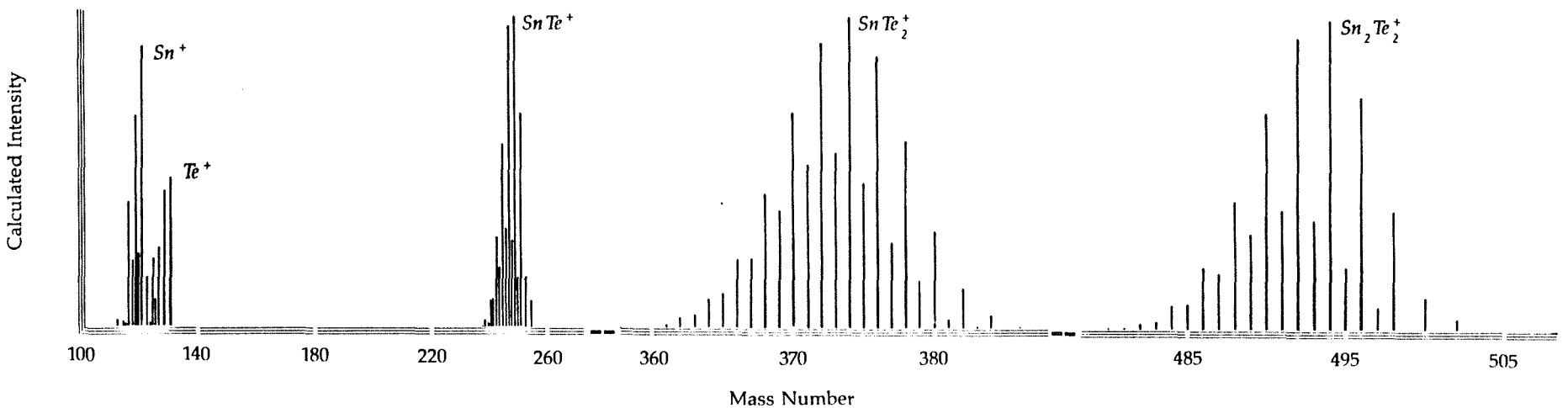

b) **Calculated Spectrum**

Figure 1 Mass Spectrum from Tin Telluride Vaporisation

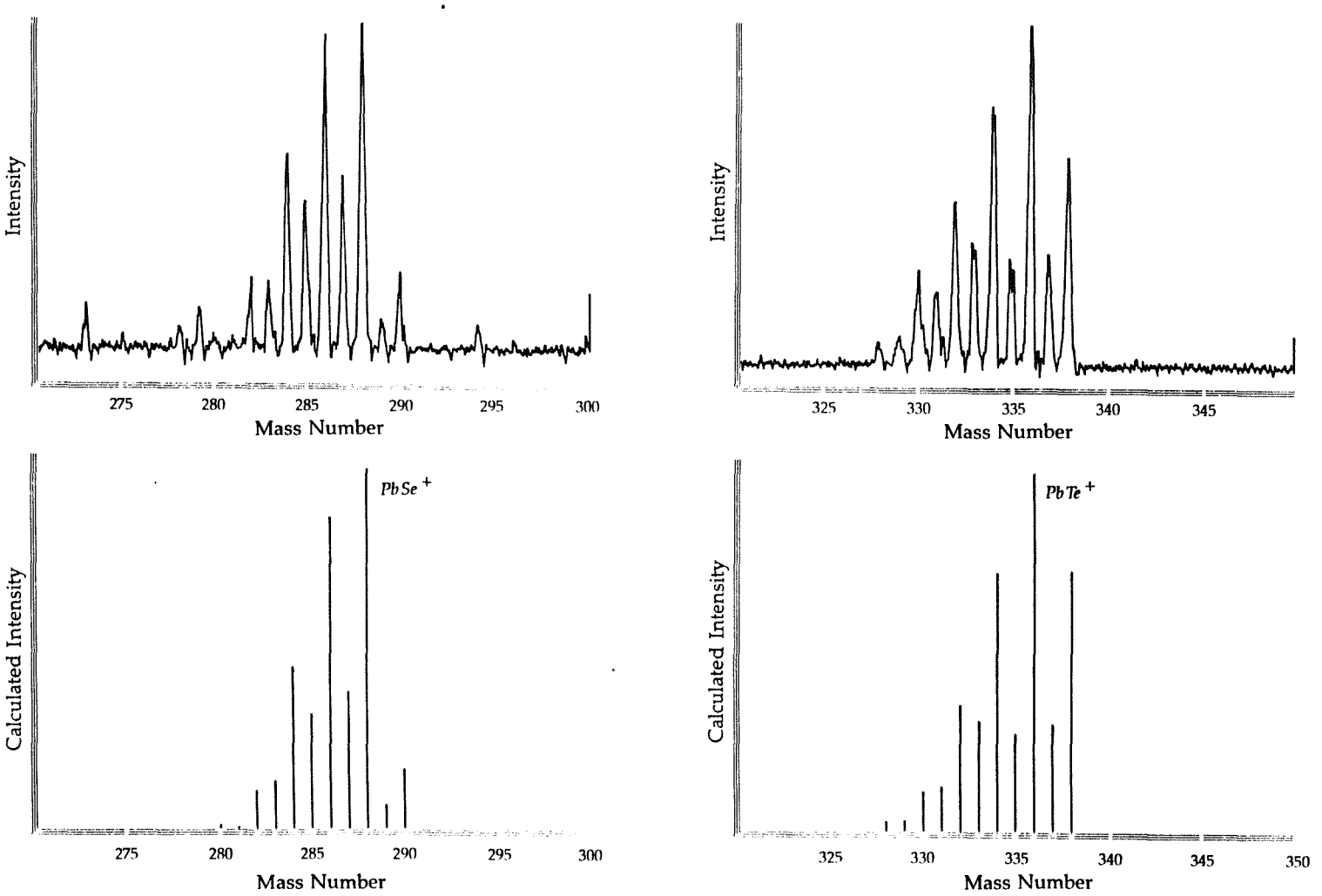

Figure 2 Observed and Calculated Mass Spectra of Parent Ions from Lead Selenide and Lead Telluride Vaporisation

TABLE 1

APPEARANCE POTENTIALS (eV) OF IONS OBSERVED IN MASS SPECTRA OF SnTe, PbSe AND PbTe VAPOUR SPECIES

Ion	SnTe	PbSe	PbTe	Se	Te
M^+	10.8	9.8	10.5	-	-
X^+	13.2	12.4	11.3	13.4	13.2
X_2^+	-	-	-	9.7	8.1
MX^+	8.5	8.9	8.3	-	-
MX_2^+	8.2	-	-	-	-
$M_2X_2^+$	7.6	-	-	-	-

First ionisation potentials (from Reference 11)

Se = 9.75 eV

Sn = 7.34 eV

Te = 9.01 eV

Pb = 7.42 eV

The mass spectra observed from Zircaloy coupons which had been exposed to tellurium vapour at 550 and 950°C are shown in Figure 3. The spectrum from the sample prepared at 550°C was dominated by Te_2^+, but the peaks at 244, 246, 248 and 250 mass numbers were somewhat more intense than expected, indicating the presence of a small amount of $SnTe^+$. The vaporisation of stannous telluride was more clearly apparent in the case of the Zircaloy coupon which had been exposed to tellurium vapour at 950°C; the mass spectrum showed that SnTe was the dominant vapour species produced when this sample was heated. It should be noted that the absolute intensities of the SnTe peaks were very similar for both the Zircaloy samples, and that the main difference between the two mass spectra shown in Figure 3 lies in the much greater quantity of Te_2^+ detected from the sample prepared at the lower temperature.

The observed Te_2 may have arisen from elemental tellurium adsorbed onto the Zircaloy surface, or from the breakdown of a Zr-Te compound; substantial Te_2 evolution has been observed from $ZrTe_2$ under vacuum at 700°C (12). Earlier experiments have shown (13) that tellurium vapour reacts readily with zirconium metal, and the small quantities of alloying elements contained in Zircaloy do not significantly influence the reaction rate. It is therefore reasonable to assume that the initial product of the reaction is a zirconium-tellurium compound. The phase diagram for the Zr-Te system shows a number of such compounds, ranging in composition from $ZrTe_5$ to Zr_5Te_4 (14). Given the large excess of zirconium, a mixture of Zr and Zr_5Te_4 would be expected if the system was at equilibrium. In these experiments, however, the elemental composition of the sample would have been very non-uniform, with a relatively high tellurium concentration at the surface, decreasing with penetration into the coupon. The concentration of tellurium in the bulk of the coupon would depend on the rate of diffusion of tellurium into the

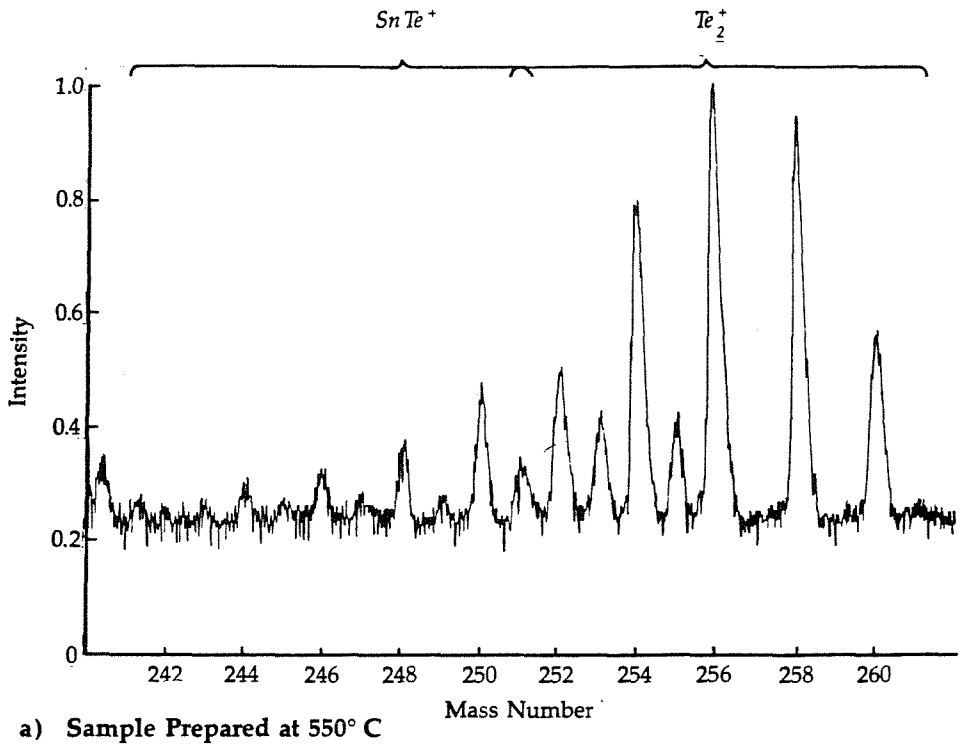

a) **Sample Prepared at 550° C**

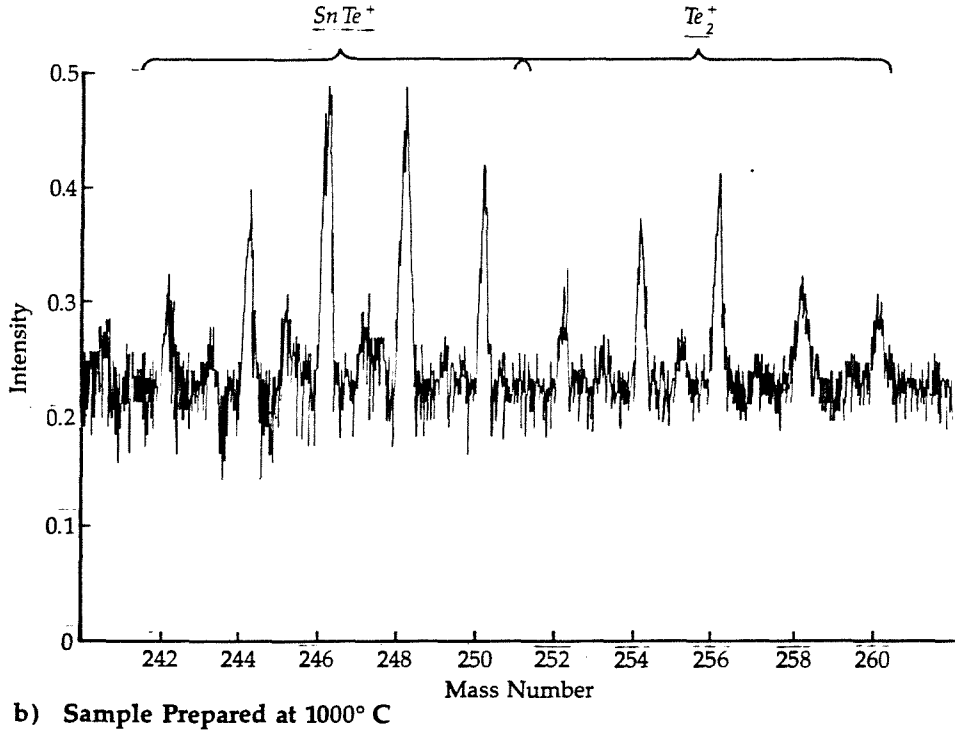

b) **Sample Prepared at 1000° C**

Figure 3 Mass Spectra of Vapour Released from Zircaloy Coupons After Exposure to Tellurium Vapour

alloy, and this would be expected to be less in the sample prepared at lower temperature. This is consistent with the experimental observation that less Te_2 was released from the sample prepared at 950°C, suggesting the formation of a more stable Zr-Te compound at the higher temperature. However, steam oxidation of the Zircaloy would result in the breakdown of this compound and, given that the quantity of tin contained in the Zircaloy cladding of a PWR is an order of magnitude greater than the tellurium inventory (15), the tellurium thus released could react with the tin component to be released as SnTe.

These studies have clearly demonstrated the potential importance of SnTe in the revaporisation and transport of tellurium after reaction with Zircaloy.

4. MATRIX ISOLATION-INFRARED SPECTROSCOPY

Infrared spectra of the matrix-isolated vapour species produced from tin telluride, lead selenide and lead telluride are shown in Figures 4, 5 and 6. The spectra are characterised by a single band, or closely-spaced multiplet, above 200 cm^{-1} together with a pair of bands at lower frequency. The frequencies of the observed bands are summarised in Table 2 together with reported frequencies for the gas-phase diatomic molecules.

The spectra of tin telluride shown in Figure 4 were obtained using different vaporisation temperatures and matrix gas flows to study the effect of varying the matrix-to-solute ratio. The higher-frequency band was assigned to monomeric SnTe, since the observed frequency is in good agreement with the reported gas-phase value (16, 17). The intensity of the lower-frequency doublet was found to increase relative to the monomer band when a lower matrix-to-solute ratio was used, although the intensity ratio of the two bands was not significantly affected

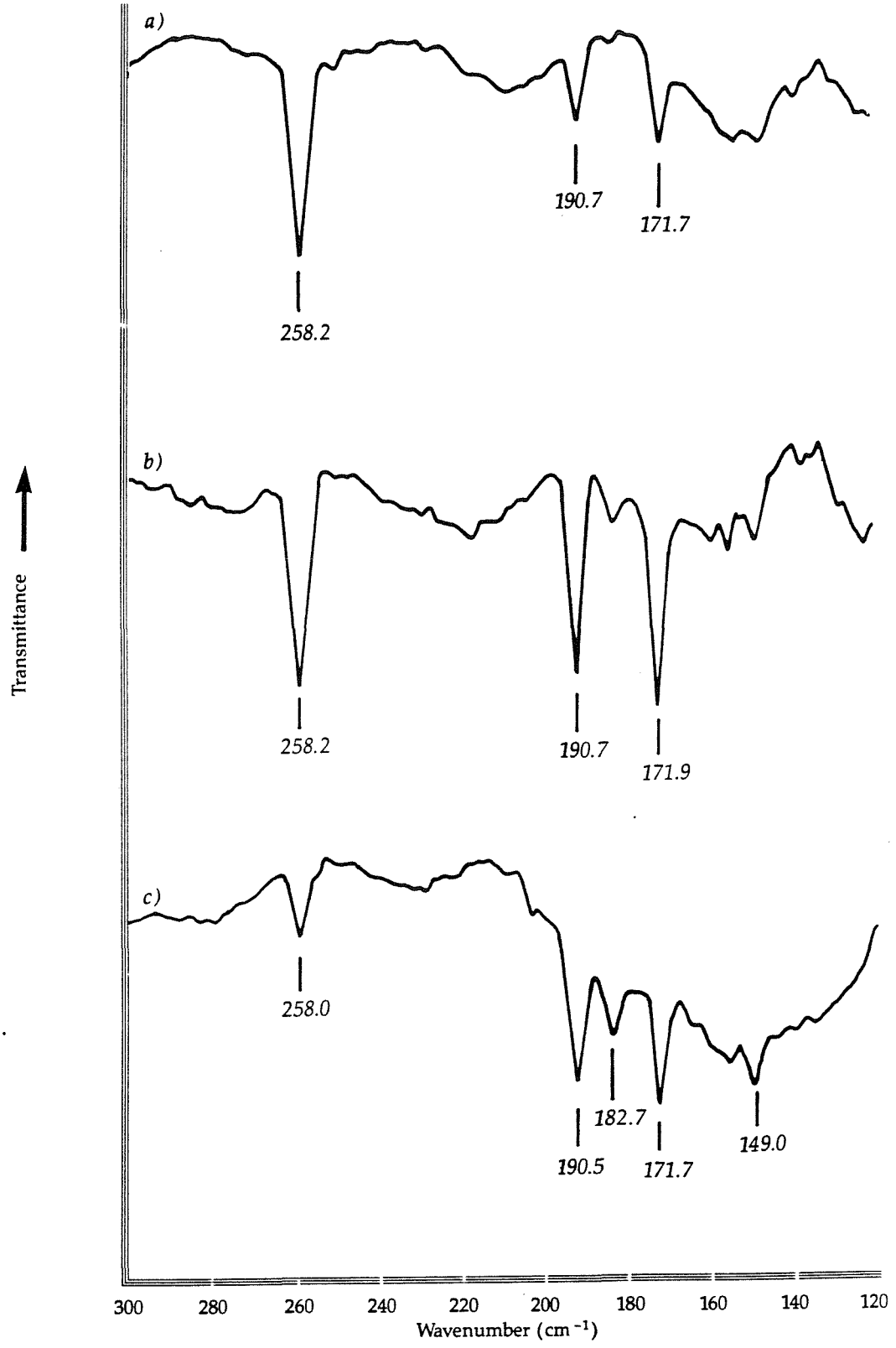

a—Vaporisation Temperature = 750° C, High Ar Flow

b—Vaporisation Temperature = 790° C, High Ar Flow

c—Vaporisation Temperature = 770° C, Low Ar Flow

Figure 4 Argon Matrix Infrared Spectra of Tin Telluride

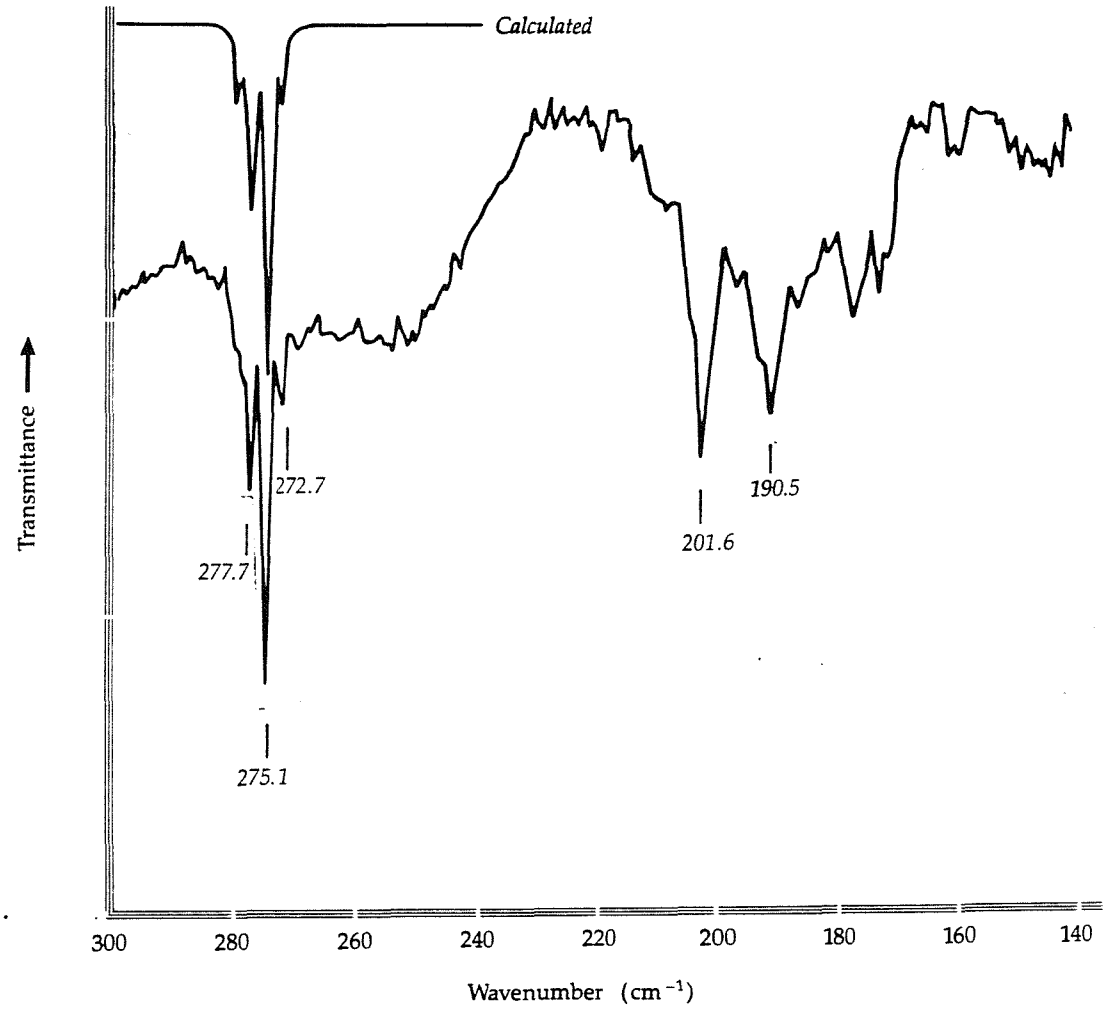

Figure 5 Argon Matrix Infrared Spectrum of Lead Selenide, with Calculated Spectrum for PbSe

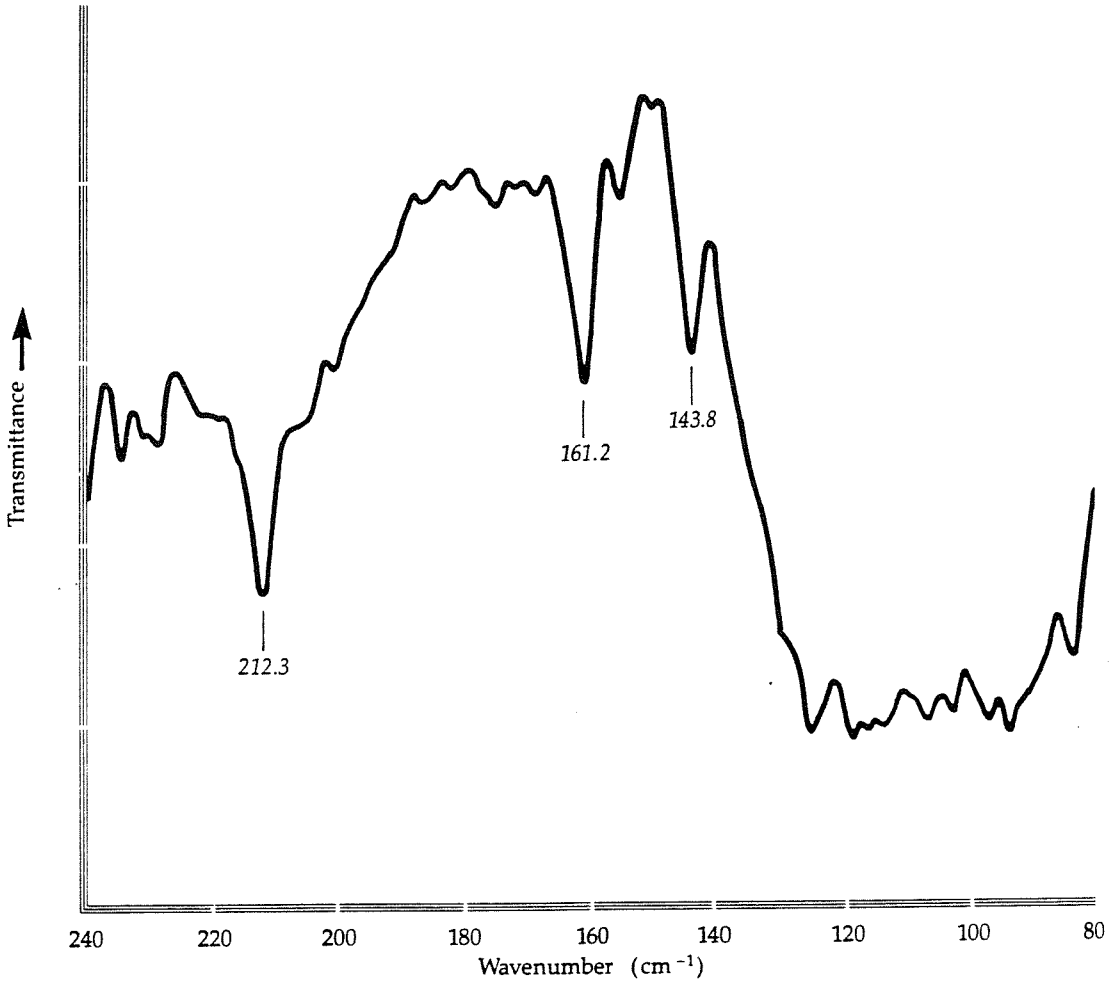

Figure 6 Argon Matrix Infrared Spectrum of Lead Telluride

TABLE 2

BANDS OBSERVED IN ARGON MATRIX INFRARED SPECTRA

Sample	Observed Frequencies (cm^{-1})		MX gas phase frequency (cm^{-1})*
SnTe	258.2 (m)	190.7 (d) 182.7 (p) 171.7 (d) 149.0 (p)	259.5
PbSe	277.1 275.1 (m) 272.7	201.6 (d) 190.5 (d)	277.6
PbTe	212.3 (m)	161.2 (d) 143.1 (d)	211.8

(m) = monomer
(d) = dimer
(p) = higher polymer

*from Reference 16

by the spray-on conditions (Figure 4b). These observations indicate that the lower-frequency bands arose from a single polymeric species whose concentration in the matrix was increased under conditions of increased sample-to-matrix gas ratio. Additional low-frequency bands were observed at very low matrix to solute ratio (Figure 4c), indicating the formation of other polymeric species in the matrix under these conditions.

The assignment of the high-frequency band to the MX monomer is supported by the high-resolution spectrum of lead selenide vapour, shown in Figure 5. This spectrum clearly shows fine structure due to the different selenium isotopes. The calculated spectrum for PbSe, assuming a linewidth of 1 cm^{-1}, is also shown and is in good agreement with the shape of the observed high-frequency band. The less well-defined isotopic structure on the lower-frequency bands indicates that more than one selenium atom is involved in the vibrations giving rise to these absorptions. No fine structure could be resolved in the stannous telluride spectra, and this is expected since the many Te and Sn isotopes would give rise to a large number of very closely-spaced components. In the case of lead telluride (Figure 6), the tellurium isotope bands are also too close together to be resolved.

Matrix isolation studies of many analogous Group IV-Group VI compounds have been reported, including the monoxides of silicon, germanium, tin and lead (18-22). Marino et al (10) reported spectra for germanium sulphide, selenide and telluride, tin sulphide and selenide, and lead sulphide and selenide, although the lower-frequency bands of lead selenide were beyond the wavelength range of that study. In all of these studies, the spectra showed the same features (monomeric MX and two dominant polymer bands). The polymer bands were assigned in all cases to dimers with

planar ring structures (D_{2h} symmetry). Such a structure is consistent with the observation of two infrared active bands, and has been supported by Raman studies in the case of Pb_2O_2 (22).

The normal coordinate analysis for a M_2X_2 molecule with D_{2h} symmetry (see Appendix 2) gives the following expressions for the five in-plane vibrations:

$$\lambda_1 + \lambda_2 = 2(F_r)(\mu_m\cos^2\theta + \mu_x\sin^2\theta) + 4(\mu_m\sin^2\theta + \mu_x\cos^2\theta)\ (F_\alpha + F_\beta)$$

$$\lambda_1\lambda_2 = 8(F_r)\ \mu_m\mu_x\ (F_\alpha + F_\beta) \qquad \text{both symmetry } A_g$$

$$\lambda_3 = 2(F_r)(\mu_m\sin^2\theta + \mu_x\cos^2\theta) \qquad B_{2g}$$

$$\lambda_4 = 2(\mu_m + \mu_x)\ (F_r\cos^2\theta + 2\sin^2\theta\ F_{\gamma_1}) \qquad B_{2u}$$

$$\lambda_5 = 2(\mu_m + \mu_x)\ (F_r\sin^2\theta + 2\cos^2\theta\ F_{\gamma_2}) \qquad B_{3u}$$

where μ_m and μ_x are the reciprocals of the masses of the two elements, and the potential constants are defined by

$$2V = F_r \sum_i \Delta r_i^2 + F_\alpha \sum_i (r_o\Delta\alpha_i)^2 + F_\beta \sum_i (r_o\Delta\beta_i)^2$$

in which the r_is represent the MX bond lengths, the α_is the two XMX angles and the β_is the two MXM angles, and $\theta = \alpha/2$.

An expression for the out-of-plane B_{1u} mode of the D_{2h} ring has been derived by Berkowitz (23) following the original treatment by Bell (24). Using the notation defined above, this takes the form:

$$\bar{\nu}_6 = 0.149c(hF_\gamma/r^2)^{1/3}\ (\tan^2\theta + \cot^2\theta)^{1/3}(\mu_m/2 + \mu_x/2)^{2/3},$$

where h is Planck's constant, c is the velocity of light and $F_\alpha = F_\beta = F_\gamma$. However, this expression only holds if there is free rotation about the M-X bonds, and if there is no strain in the ring (25). Ring strain or restricted rotation introduces additional quadratic terms into the potential function, and so the above expression gives the lower limit for $\bar{\nu}_6$ (18).

The B_{2u} and B_{3u} modes are the only in-plane vibrations which are active in the infrared, corresponding to the two dimer bands observed in all cases (the B_{1u} mode is also infrared active, but is expected to occur at a very low frequency beyond the range of these investigations). If it is again assumed that $F_\alpha = F_\beta = F_\gamma$, then

$$F_r + 2F_\gamma = \frac{\lambda_4 + \lambda_5}{2(\mu_m + \mu_x)} = \frac{2\pi^2c^2\ (\bar{\nu}^2_{B_{2u}} + \bar{\nu}^2_{B_{3u}})}{(\mu_m + \mu_x)}$$

An approximate value for the bond angle can also be obtained, since

$$\frac{\lambda_5}{\lambda_4} = \tan^2\theta\ \left(1 + \frac{F_\gamma}{F_r}\mathrm{ctn}^2\theta - \frac{F_\gamma}{F_r}\tan^2\theta + \ldots\right)$$

If F_r is much larger than F_γ, this simplifies to

$$\frac{\lambda_5}{\lambda_4} = \tan^2\theta \quad \text{and therefore} \quad \frac{\bar{\nu}_{B_{3u}}}{\bar{\nu}_{B_{2u}}} = \tan\theta$$

The value of θ thus obtained depends on how the observed frequencies are assigned. For consistency with previous work on related systems (10), the higher frequencies were assigned to the B_{2u} modes, giving 2θ values of less than 90°. Since the covalent radii for Sn (0.14 nm) and Pb (0.144 nm) are larger than those of Se (0.177 nm) and Te (0.137 nm) (26), packing considerations suggest that the M-M distance should be greater than X-X, and this is consistent with the chosen assignment. The force constants and bond angles calculated from the above equations are given in Table 3.

In order to evaluate the frequencies of the remaining four bands, it is necessary to estimate separate values of F_r and F_γ. Whilst it may appear possible to substitute the calculated values of θ into the expressions for λ_4 and λ_5, and hence obtain F_r and F_γ, in practice this is unsatisfactory since the values so obtained are very sensitive to variations in the estimated bond angle. In the case of Sn_2Te_2, for example, varying θ between 82 and 86° produces values of F_γ of -15 to 8 N m^{-1}. F_γ was therefore arbitrarily set at approximately 0.025 F_r and the frequencies thus calculated are given in Table 3.

The sensitivity of these calculated frequencies to variations in the estimated force constant was assessed by repeating the calculations using different values of F_r and F_γ. An uncertainty of ± 5 cm^{-1} on the measured $\bar{\nu}_4$ and $\bar{\nu}_5$ frequencies would result in an error of approximately ± 5% in the $(F_r + 2F_\gamma)$ term, and this would produce corresponding uncertainties of approximately ± 5 cm^{-1} in the calculated $\bar{\nu}_1$ and $\bar{\nu}_3$ frequencies. The $\bar{\nu}_2$ frequency, which can be identified with the A_g bending mode, is particularly sensitive to the selected value of F_γ; varying the value of this constant between $0.01F_r$ and $0.05F_r$ results in changes of ± 20 cm^{-1} in this frequency.

TABLE 3

FORCE CONSTANTS, BOND ANGLES AND CALCULATED VIBRATION FREQUENCIES OF M_2X_2 MOLECULES

Molecule	(F_r+2F_γ) (N m^{-1})	θ	ν_1 (cm^{-1})	ν_2 (cm^{-1})	ν_3 (cm^{-1})	ν_4 (cm^{-1})	ν_5 (cm^{-1})	ν_6 (cm^{-1})
Sn_2Te_2	121.6	42.0	177.5	57.3	176.8	190.1	173.0	5.4
Pb_2Se_2	131.7	43.4	191.4	55.7	194.0	201.5	191.6	6.0
Pb_2Te_2	110.1	41.8	147.4	47.5	150.8	160.2	144.9	4.3

The planar ring structure postulated for the M_2X_2 molecules is in contrast with that of the isoelectronic M_4 molecules (M = P, As), which are tetrahedral (27). However, this apparent anomaly can be explained by consideration of the nature of the bonding of the M_2X_2 molecule, using Sn_2Te_2 as an example. If it is assumed that the s electrons in divalent Sn and Te are inert, then a molecular orbital description can be constructed for planar Sn_2Te_2 by considering the symmetry properties of the p orbitals (Figure 7). For a D_{2h} structure, with the Sn and Te atoms on the x and y axes respectively, the p_x and p_y orbitals of both Sn and Te transform as $A_g + B_{1g} + B_{2u} + B_{3u}$, whereas the p_z orbitals of Sn and Te transform as $B_{2g} + B_{1u}$ and $B_{3g} + B_{1u}$ respectively. These atomic orbitals combine to give five bonding (a_g, b_{1g}, b_{1u}, b_{2u} and b_{3u}), two non-bonding (b_{2g} and b_{3g}) and five antibonding (a_g^*, b_{1g}^*, b_{1u}^*, b_{2u}^* and b_{3u}^*) molecular orbitals. The b_{1u}, b_{1u}^*, b_{2g} and b_{3g} can be identified as pi orbitals, since they arise from combination of the out-of-plane p_z orbitals. As Sn_2Te_2 has a total of 12 p electrons, all of the bonding and one of the non-bonding orbitals will be fully occupied, and there will therefore be an element of pi-bonding in the ring. If the molecule had a non-planar shape, then this pi-bonding would be lost, and such a structure would therefore be less stable.

5. CALCULATION OF THERMODYNAMIC FUNCTIONS

In order to calculate the thermodynamic functions of MX and M_2X_2, the moments of inertia of the molecules must be evaluated. This requires estimates of the bond lengths and, in the case of the dimers, the bond angles.

An empirical relationship between the bond length and stretching force constant of a diatomic molecule has been derived by Badger (28,29):

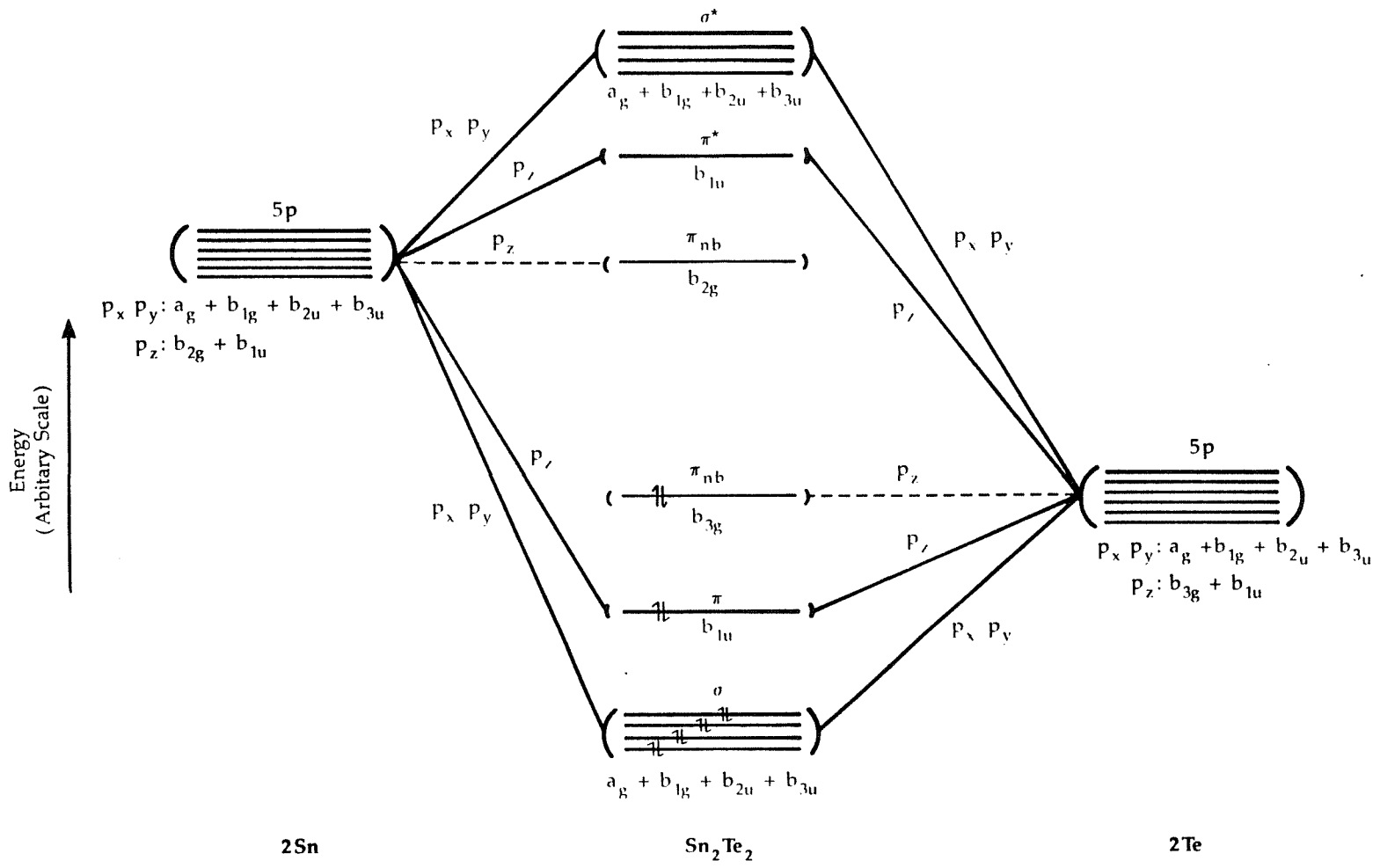

Figure 7 Molecular Orbital Diagram for Planar Sn_2Te_2

$$r = (C_{ij}/F_r)^{1/3} + d_{ij}$$

where C_{ij} and d_{ij} are constants characteristic of all diatomic molecules made up of one element in the ith row and one in the jth row of the periodic table. Values of C_{ij} and d_{ij} for molecules in which both atoms are in the 4th row of the periodic table (eg, SnTe) are given as 0.240 and 0.176, for r in nm and F_r in N m^{-1}. This gives a Sn-Te bond length of 0.276 nm. However, the constants are based on a single molecule of this type, I_2, and no constants are available for PbSe- and PbTe-type molecules. For consistency, therefore, all the bond lengths of the MX molecules were calculated using another empirical relationship derived by Gordy (30), in the form:

$$\frac{1}{r^2} = \left(\frac{F_r - a}{bN} \right)^{4/3} \cdot \frac{1}{x_A x_B}$$

where N is the bond order and x_A and x_B are the electronegativities of the bonded atoms. If F_r is in N m^{-1} and r is in nm, the constants a and b take the values 30 and 5.28 respectively (although different values of these constants are required if both atoms have only one valence electron). For these calculations, the bond orders were taken to be 2, and the electronegativities were those used by Gordy in verifying the above relationship. The data used, together with the calculated bond lengths, are shown in Table 4. The calculated r values were found to be quite sensitive to variation of the electronegativities used; for lead in particular, considerable variation was found in the tabulated Pauling electronegativity (27,31,32), in the most extreme case giving bond lengths for PbX of 0.05 nm greater than given in Table 4

TABLE 4

MOMENTS OF INERTIA OF MX AND M_2X_2 MOLECULES

Monomer	x_m	x_x	F_r (N m^{-1})	r (nm)	I_B (amu nm^2)	Dimer	r* (nm)	<XMX	$I_A I_B I_C$ (amu^3 nm^6)
SnTe	1.8	2.1	245	0.253	3.94	Sn_2Te_2	0.277	84.0	1655
PbSe	1.5	2.4	260	0.243	3.38	Pb_2Se_2	0.261	86.8	1537
PbTe	1.5	2.1	214	0.264	5.50	Pb_2Te_2	0.281	83.6	4365

*Calculated from the sum of the covalent radii given in Reference 27

The Gordy equation was also used to calculate the bond lengths of the M_2X_2 molecules, assuming a bond order of 1.25 (due to the contribution of π-bonding, see Section 4 above). The resulting bond lengths were about 0.1 nm larger than those obtained from summation of the single bond covalent radii of the atoms. This was thought to be unrealistic, and may indicate that these molecules lie beyond the range of applicability of the Gordy equation. Moments of inertia for the dimer molecules were therefore calculated assuming the bond lengths to be the sum of the covalent radii, and the bond angles to be those derived from the vibrational data (see Section 4 above).

The other data required for the thermodynamic calculations were the vibration frequencies, symmetry numbers and electronic ground state degeneracies of the molecules. For the monomers, the single observed frequencies were used. In the dimer calculations, the observed B_{2u} and B_{3u} frequencies were used together with the calculated frequencies for the other in-plane modes shown in Table 3. The frequency of the out-of-plane mode was arbitrarily set at 20 cm^{-1} for all the molecules; the calculated $\bar{\nu}_6$ values were not used since these represent the lower limits rather than the true frequencies. The symmetry numbers of the monomer and dimer molecules are 1 and 4 respectively, and the degeneracy of the electronic ground state was taken to be unity in all cases.

The thermodynamic functions of all the molecules, over the temperature range 100 to 2500°C, are tabulated in Appendix 3.

5.1 Vaporisation Thermodynamics

Several studies have been made of the vaporisation thermodynamics of SnTe. Vapour pressure vs. temperature

relationships have been determined by several groups of workers (33-40), and with the exception of that of Lyubimov (33), there is reasonable agreement between them. Good agreement was also obtained between the third law enthalpies at 298 K, which ranged from 217.8 to 222.0 kJ mol^{-1} (34-38) with a mean value of 220.06 kJ mol^{-1}. An 'average' expression for the vapour pressure:

$$\ln p\ (atm) = 16.39 - 24640/T(K)$$

was obtained by calculating the vapour pressure at 50 K intervals using each reported equation (34-40) within its range of applicability, and carrying out a least-squares fit.

The enthalpy of formation of SnTe(s) at 298 K has been calculated as -59.83 kJ mol^{-1}, based on a number of reported determinations at different temperatures (41). This is in reasonable agreement with the value of 61.9 kJ mol^{-1} selected by Mills (42).

Similar studies have been made of the vaporisation behaviour of PbTe (35,38,43-47). The mean third law enthalpy of sublimation at 298 K (35,38,47) was 225.19 kJ mol^{-1}, and the average expression for the vapour pressure, calculated as described above, was

$$\ln p\ (atm) = 19.30 - 27860/T(K)$$

Shamsuddin (48) has tabulated the results of nine separate determinations of the enthalpy of formation of PbTe(s) at 298 K; the mean value of six of these was -68.94 kJ mol^{-1}, with a relative standard deviation of less than 1%. There was poor agreement between the remaining three determinations, which differed from this mean value by at least 10 kJ mol^{-1}, and have therefore been disregarded. A more recent determination (49) gave a value of -68.52 kJ

mol^{-1}, in good agreement with the earlier work. Taking this into account gives a mean value of -68.88 kJ mol^{-1}. This is close to the value of -68.6 kJ mol^{-1} selected by Mills (42).

The mean value of the enthalpy of sublimation of PbSe at 298 K, based on four determinations, is 227.8 kJ mol^{-1} (42). Combining the corresponding vapour pressure-temperature relationships as above gives

$$\ln p\ (atm) = 14.76 - 23980/T(K)$$

The enthalpy of formation of PbSe(s) at 298 K was selected (42) as -99.9 kJ mol^{-1}. An additional value of -99.5 kJ mol^{-1} was reported by Shamsuddin (50), in good agreement with this average value.

The data discussed above can be combined to obtain the enthalpies of formation of the gaseous molecules at 298 K, which can then be used in conjunction with the data in Appendix 3 to evaluate the enthalpies and free energies of SnTe(g), PbTe(g) and PbSe(g) as functions of temperature. These results are summarised in Table 5.

The enthalpy of the dimerisation reaction

$$2\ SnTe(g) \rightarrow Sn_2Te_2(g)$$

has been calculated by Colin and Drowart (37) as -196.04 kJ mol^{-1}. This calculation was based on mass spectrometric measurements of the vapour pressures of SnTe and Sn_2Te_2, together with estimated free energy functions (Ø), since

$$T\Delta(\text{Ø}) = -(G_T - H_{298})_d + 2(G_T - H_{298})_m$$

$$= (H_d - 2H_m)_{298} - (G_d - 2G_m)_T$$

TABLE 5

THERMODYNAMIC QUANTITIES AT 298 K

System	$\Delta H^{\circ}_{f,298}[MX_{(s)}]$ kJ mol^{-1}	$\Delta H^{\circ}_{subl,298}$ kJ mol^{-1}	$\Delta H^{\circ}_{f,298}[MX_{(g)}]$ kJ mol^{-1}	$\Delta H^{\circ}_{dim,298}$ kJ mol^{-1}*	$\Delta H^{\circ}_{f,298}[M_2X_{2(g)}]$ kJ mol^{-1}
SnTe	-59.8	220.1	160.3	-148.3	172.3
PbSe	-100.0	227.8	127.8	-151.1**	104.5**
PbTe	-68.9	225.2	156.3	-151.3**	161.3**

*Enthalpy change for the reaction:

$$2MX_{(g)} \rightarrow M_2X_{2(g)}$$

**estimated

$$= \Delta H_{298} - \Delta G_T$$

$$= \Delta H_{298} + RT \ln K_p$$

where the subscripts m and d refer to monomer and dimer respectively.

The free energy functions which were used for SnTe were very close to those obtained in this work. However, those for Sn_2Te_2, which were estimated by interpolation from As_4 and Sb_4, differed substantially from the values determined here.

Although measured vapour pressures of SnTe and Sn_2Te_2 were not reported, the equilibrium constant could be obtained from the given free energy functions and calculated dimerisation enthalpy. This gives a K_p value of 21.5 atm^{-1} at 1000 K. The vapour pressure of SnTe at this temperature was calculated using the relationships discussed above, and the average value obtained was 2.68×10^{-4} atm. Since $p(Sn_2Te_2) = K_p p(SnTe)^2$, the Sn_2Te_2 pressure at 1000 K would be 1.5×10^{-6} atm, less than 1% of the monomer pressure.

Combining the free energy functions listed in Appendix 3 with the equilibrium constant calculated from the data in Reference 37 gives a dimerisation enthalpy of -150.7 kJ mol^{-1}. Combining this with the enthalpy of formation of SnTe(g) discussed above gives the enthalpy of formation of Sn_2Te_2(g) at 298 K as 169.9 kJ mol^{-1}.

There are no available data on the equilibrium constants for the dimerisation of PbSe and PbTe, although Pb_2Se_2 molecules have been reported in previous mass spectrometric studies (42). A reasonable estimate for K_p at 1000 K is 20 atm^{-1}, based on the value for SnTe. Using the data in Appendix 3, the enthalpies of dimerisation for PbSe and

PbTe are calculated as -151.1 and -151.3 kJ mol^{-1} respectively; the corresponding enthalpies of formation of Pb_2Se_2(g) and Pb_2Te_2 (g) at 298 K are 104.5 and 161.3 kJ mol^{-1}.

6. CONCLUSIONS

Mass spectrometric studies of the vaporisation of tin telluride, lead selenide and lead telluride have shown that the predominant vapour-phase species in each case was the MX molecule, with smaller quantities of X_2 and M_2X_2. The presence of MX_2 as a neutral vapour species was not confirmed.

The vaporisation of molecular tin telluride from a Zircaloy surface after exposure to tellurium vapour has been demonstrated. This observation confirms previous conclusions concerning the transport of fission product tellurium in severe reactor accidents.

The infrared vibration frequencies of the MX and M_2X_2 molecules have been determined by matrix isolation-infrared spectroscopy. These have been used to calculate the thermodynamic functions for these molecules for use in severe reactor accident modelling codes. Previously-reported data have been used to calculate the standard enthalpies of formulation of the molecules.

REFERENCES

1. Lorenz, R A, Beahm, E C and Wichner, R P, Proc Int Mtg LWR Severe Accident Evaluation, Cambridge, Mass., 28 August-1 September 1983.

2. Osborne, M F, Collins, J L and Lorenz, R A, Nucl Technol, 78, 157, 1987.

3. Vinjamuri, K, Sallach, R A, Osetek, D J, Hobbins, R R and Akers, D W, 13th Water Reactor Safety Research Information Mtg, Gaithersburg, 22-25 October 1985.

4. Osetek, D J, Cronenburg, A W, Hagram, D L, Broughton, J M and Rest, J, Int Mtg on Thermal Nuclear Reactor Safety, Karlsruhe, 10-14 September 1984.

5. Osborne, M F, Collins, J L, Lorenz, R A and Strain, R V, IAEA Symposium on Source Term Evaluation for Accident Conditions, Columbus, Ohio, 28 October-1 November 1985, 89, IAEA, Vienna, 1986.

6. Schlenger, B J, Dunn, P F, Herceg, J E, Simms, R, Horton, E L, Baker, I and Ritzman, R L, Proc ACS Symposium on Chemical Phenomena Associated with Radioactivity Releases During Severe Nuclear Plant Accidents, Anaheim, USA, 9-12 September 1986, NUREG/CP-0078, 2-65, 1987.

7. Vinjamuri, K, Osetek, D J, Meikrantz, D H and Baker, J D, Proc ACS Symposium on Chemical Phenomena Associated with Radioactivity Releases During Severe Nuclear Plant Accidents, Anaheim, USA, 9-12 September 1986, NUREG/CP-0078, 4-99, 1987.

8. Baker, J D, Meikrantz, D H and Simpson, O D, Proc ACS Symposium on Chemical Phenomena Associated with Radioactivity Releases During Severe Nuclear Plant Accidents, Anaheim, USA, 9-12 September 1986, NUREG/CP-0078, 4-113, 1987.

9. Collins, J L, Osborne, M F and Lorenz, R A, Nucl Tech, 77, 18, 1987.

10. Marino, C P, Guerin, J D and Nixon, E R, J Mol Spec, 51, 160, 1974.

11. CRC Handbook of Chemistry and Physics, 64th Edition, CRC Press, Boca Raton, 1984.

12. Beard, A M, Bowsher, B R, Dickinson, S and Nichols, A L, 2nd ACS Symposium on Nuclear Reactor Severe Accident Chemistry, Toronto, 7-10 June 1988.

13. Bowsher, B R, Dickinson, S, Gomme, R A, Jenkins, R A, Nichols, A L and Ogden, J S, Proc Workshop on Chemical Reactivity of Oxide Fuel and Fission Product Release, CEGB Berkeley Nuclear Laboratories, April 1987, Vol 2, 55, 1988.

14. Sodeck, H, Mikler, H and Komarek, K L, Monatsh fur Chem, 110, 1, 1979.

15. Bowsher, B R, Prog Nucl Energy, 20, 199, 1987.

16. Nakamoto, K, "Infrared and Raman Spectra of Inorganic and Coordination Compounds, John Wiley and Sons, New York, 1978.

17. Barrow, R F and Vago, E E, Proc Phys Soc, 56, 78, 1944.

18. Anderson, J S and Ogden, J S, J Chem Phys, 51, 4189, 1969.

19. Ogden, J S and Ricks, M J, J Chem Phys, 52, 352, 1970.

20. Ogden, J S and Ricks, M J, J Chem Phys, 53, 896, 1970.

21. Ogden, J S and Ricks, M J, J Chem Phys, 56, 1658, 1972.

22. Khanna, R J and Park, Y J, Spectrochim Acta, 42A, 603, 1986.

23. Berkowitz, J, J Chem Phys, 29, 1386, 1958.

24. Bell, R P, Proc Roy Soc (London), 183, 328, 1944-45.

25. Webb, A N, Neu, J T and Pitzer, K S, J Chem Phys, 17, 1007, 1949.

26. Cotton, F A and Wilkinson, G, "Advanced Inorganic Chemistry", 4th Edition, John Wiley and Sons, New York, 1980.

27. Cartmell, E and Fowles, G W A, "Valency and Molecular Structure", 4th Edition, Butterworths, London, 1977.

28. Badger, R M, J Chem Phys, 2, 128, 1934.

29 Badger, R M, J Chem Phys, 3, 710, 1935.

30. Gordy, W, J Chem Phys, 14, 305, 1946.

31. Heslop, R B and Jones, K, "Inorganic Chemistry", Elsevier, Amsterdam, 1976.

32. Greenwood, N N and Earnshaw, A, "Chemistry of the Elements", Pergamon Press, Oxford, 1984.

33. Lyubimov, A P and Bespal'tseva, I I, Izv Akad Nauk SSSR, Neorg Mater, 5, 1289, 1969.

34. Hirayama, C, Ichikawa, Y and DeRoo, A M, J Phys Chem 67, 1039, 1963.

35. Northrop, D A, J Phys Chem 75, 118, 1971.

36 Hansen, E E and Munir, Z A, J Electrochem Soc: Solid State Sci, 118, 983, 1971.

37. Colin, R and Drowart, J, Trans Faraday Soc, 60, 673, 1964.

38. Sokolov, V V, Pashchinkin, A S, Novoselova, A V, Ryazantsev, A A, Dolgikh, V A and Klinchikova, S A, Izv Akad Nauk SSSR, Neorg Mater, 5, 15, 1969.

39. Brebrick, R F and Strauss, A J, J Chem Phys, 41, 197, 1964.

40. Nesterova, Y M, Pashinkin, A S and Novoselova, A V, Russ J Inorg Chem, 6, 1031, 1961.

41. Kattner, U, Lukas, H L and Petzow, G, J Less Common Metals, 114, 129, 1985.

42. Mills, K C, "Thermodynamic Data for Inorganic Sulphides, Selenides and Tellurides", Butterworths, London, 1974.

43. Brebrick, R F and Strauss, A J, J Chem Phys, 40, 3230, 1964.

44. Lyubimov, A P and Bespal'tseva, I I, Russ J Phys Chem, 41, 798, 1967.

45. Pashinkin, A S and Novoselova, A V, Russ J Inorg Chem, 4, 1229, 1959.

45. Bates, H E and Weinstein, M, Advan Energy Convers, 6, 177, 1966.

47. Hansen, E E and Munir, Z A, J Electrochem Soc: Solid State Sci, 117, 121, 1970.

48. Shamsuddin, Mat Res Bull 12, 7, 1977.

49. Yu, H and Brebrick, R F, J Electrochem Soc: Solid State Sci, 135, 468, 1988.

50. Shamsuddin and Misra, S, Curr Sci, 42, 119, 1973.

CHAPTER SIX

GALLIUM SELENIDE, GALLIUM TELLURIDE, INDIUM SELENIDE AND INDIUM TELLURIDE

1. INTRODUCTION

The tellurides of indium, silver and cadmium are potentially important in determining the transport of tellurium in severe reactor accidents, owing to the large quantities of these three elements in the reactor control rods in some designs of PWR. Tellurium vapour found reacts readily with cadmium aerosol at 1000°C, forming cadmium telluride on the surface of the aerosol particles (1), and similar reactions might be expected to occur between tellurium vapour and the indium- and silver-rich aerosols formed at higher temperatures (2). Such reactions may play an important role in determining the behaviour of tellurium during a severe reactor accident, since the transport of tellurium associated with aerosol particles will be very different from that of the vapour. Furthermore, if the tellurium-containing aerosols are subsequently exposed to higher temperatures, then the fission product tellurium could be revaporised, possibly in a different chemical form. It is this aspect which is considered in this chapter.

The vaporisation behaviour of cadmium telluride and silver telluride has been investigated previously by mass spectrometry, and both compounds were found to decompose to the elements at fairly low temperatures (3). Other workers (4,5) have reported very small quantities of CdTe molecules in the vapour phase above cadmium telluride, but this species accounted for only a very small fraction (<0.1%) of the vapour, which consisted predominantly of Cd and Te. However, a number of studies of the vaporisation behaviour of indium telluride (6-12) have demonstrated the existence of stable In-Te species in the vapour phase. Similar studies of analogous compounds - gallium selenide (7,13,14), gallium telluride (7,13,15,16) and indium selenide (7,8,12,17-19) - have provided supporting evidence for the existence and stability of such vapour species.

However, there are some inconsistencies between these different studies, particularly with regard to the interpretation of mass spectrometric data and the identification of parent species. Furthermore, whilst thermodynamic functions have been calculated for the vapour species, these have relied almost completely on estimated vibration frequencies since very few spectroscopic data have been reported (19,20).

This chapter describes mass spectrometric and matrix isolation studies of the vaporisation of gallium selenide, gallium telluride, indium selenide and indium telluride.

2. EXPERIMENTAL DETAILS

Commercially-prepared samples of gallium selenide ($GaSe_3$), gallium telluride (GaTe), indium selenide (In_2Se_3) and indium telluride (In_2Te_3) were obtained from Cerac Ltd.

For mass spectrometric analysis, the compounds were contained in zirconia holders and heated inductively to about 900°C.

Infrared spectra were obtained by heating the samples, contained in silica boats, to about 1000°C and co-condensing the vapour species with argon onto a silicon window. The spectra were monitored over the range 400 to 80 cm^{-1}.

3. MASS SPECTROMETRY

The observed vaporisation behaviour was very similar for all the compounds studied. In the early stages of heating, X^+ and X_2^+ ions were observed in the mass spectrum. The appearance of these signals was accompanied by the formation of a red (in the case of selenides) or silver-grey (in the case of tellurides) deposit on the

water-cooled vacuum jacket, indicating the sublimation of elemental selenium or tellurium. With further heating, these ions decreased in intensity and a number of new peaks were observed in the mass spectra. These were assigned to M^+, M_2^+, MX^+, M_2X^+, MX_2^+ and $M_2X_2^+$, as shown in Figures 1-4. The appearance potentials of some of these ions are listed in Table 1; the $M_2X_2^+$ and MX_2^+ peaks were not sufficiently intense for reliable appearance potential measurements to be made.

The appearance potential measurements indicate that the X_2^+ species were parents, and the X^+ ions can therefore be assigned at least partially as fragments of molecular X_2. The M^+ ions were also fragments, as shown by comparison of the appearance potentials with the first ionisation potentials of gallium and indium.

Whilst the appearance potentials of the MX^+ ions were somewhat higher than those of the corresponding M_2X^+ ions, consistent with the former being fragments, such an assignment cannot be made with certainty on the basis of these results alone. The $M_2X_2^+$ ions were almost certainly parent species, since no ions of higher mass were detected. Some fragmentation of M_2X_2 to MX_2^+ ions would be expected and, given the very low intensities of the MX_2^+ peaks, it is likely that these ions arose entirely from fragmentation.

These observations are in broad agreement with previous studies of the vaporisation behaviour of these compounds, although there is some disagreement in the literature as to which M-X ions were observed, and their sources. In most cases (8,11,13,15), M_2X^+, $M_2X_2^+$, MX^+ and MX_2^+ ions were all observed, the first two of these being assigned as parent species and the others as a mixture of parent and fragment. However, Srinivasa and co-workers (6,9,12) assigned In_2X^+ and $In_2X_2^+$ as the only significant parent ions, with InX^+

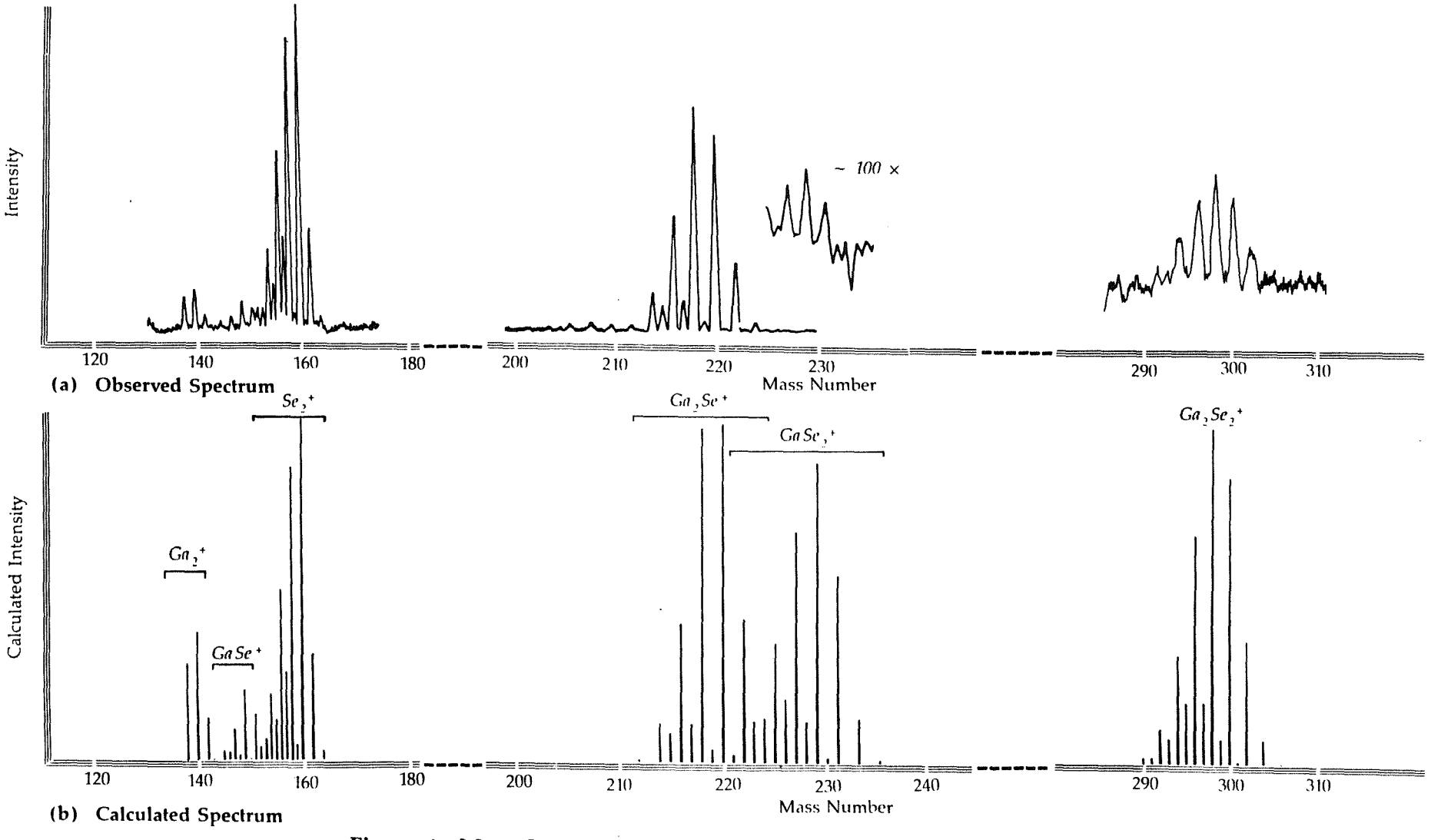

Figure 1 Mass Spectrum from Gallium Selenide Vaporisation

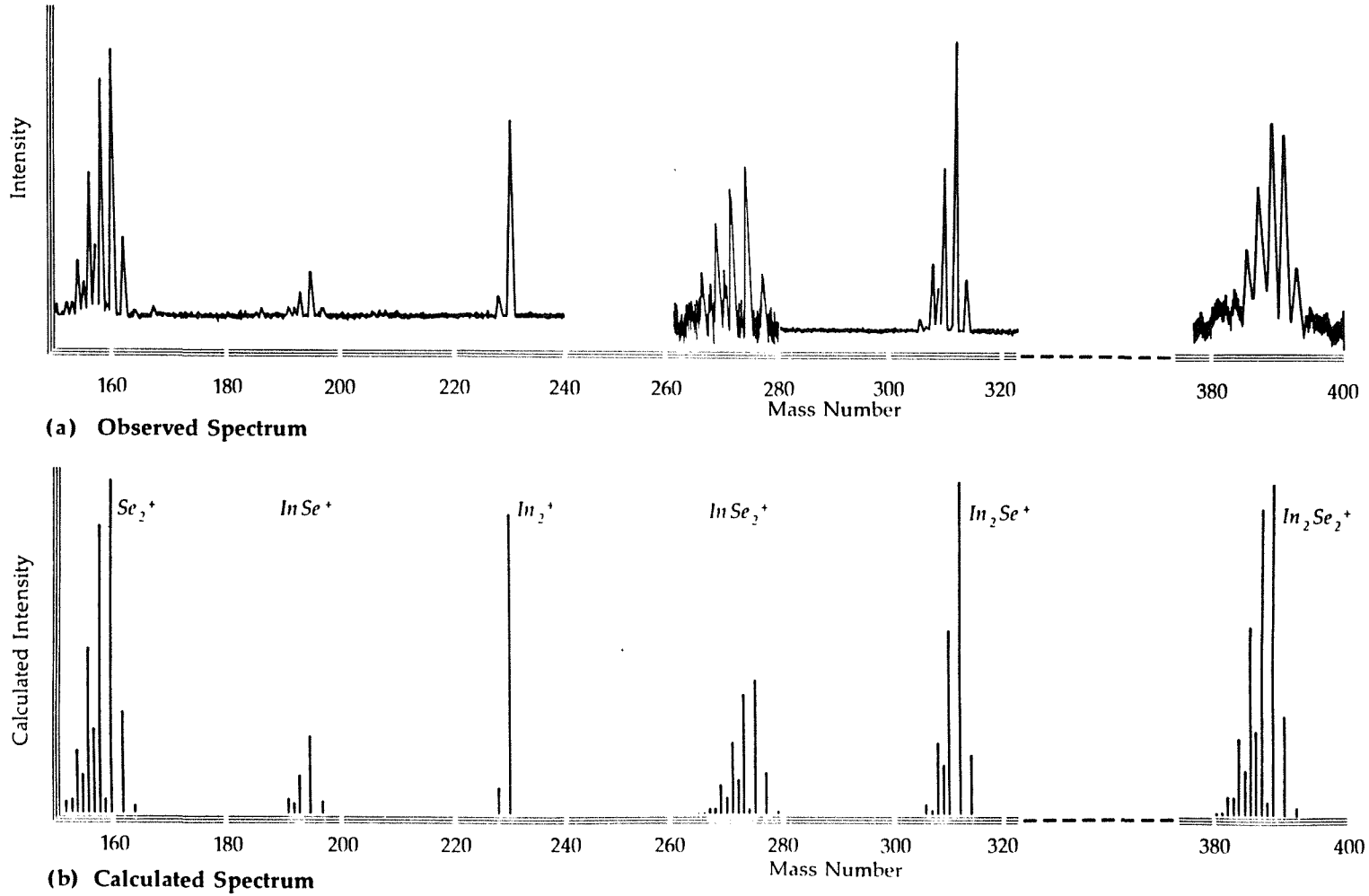

Figure 2 Mass Spectrum from Indium Selenide Vaporisation

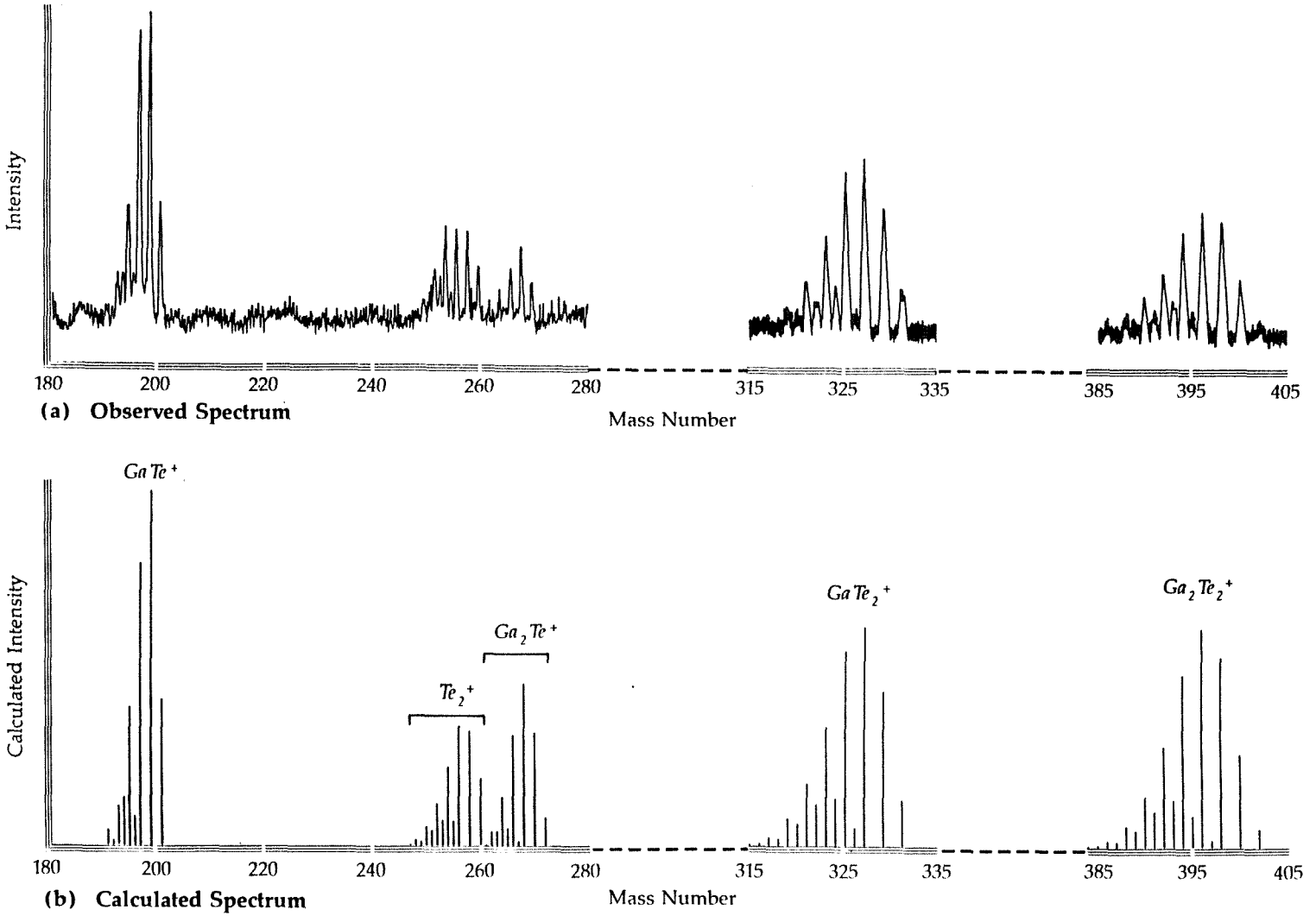

Figure 3 Mass Spectrum from Gallium Telluride Vaporisation

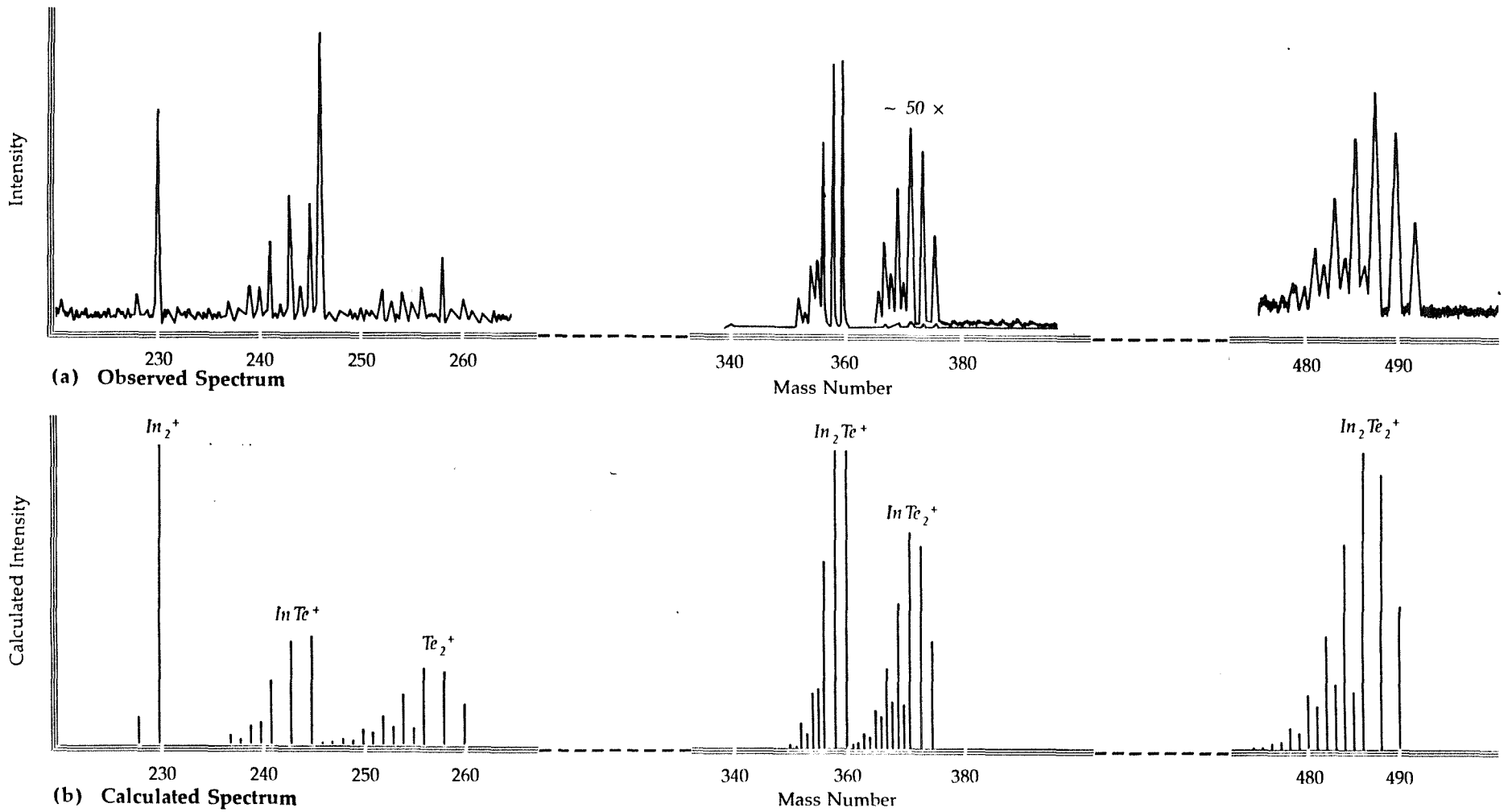

Figure 4 Mass Spectrum from Indium Telluride Vaporisation

TABLE 1

APPEARANCE POTENTIALS (eV) OF IONS OBSERVED IN MASS SPECTRA FROM $GaSe_3$, In_2Se_3, GaTe AND In_2Te_3 VAPORISATION

Ion	$GaSe_3$	In_2Se_3	GaTe	In_2Te_3
M^+	8.7	9.9	8.5	9.4
X^+	13.3	13.2	11.0	11.2
M_2^+	11.0	11.5	10.0	0.9
X_2^+	9.6	9.5	8.2	8.1
MX^+	11.7	12.2	9.8	10.2
MX_2^+	-	-	-	-
M_2X^+	8.3	7.8	7.8	7.4
$M_2X_2^+$	-	-	-	-

First ionisation potentials (from Reference 21):

Ga = 6.00 eV
In = 5.79 eV
Se = 9.75 eV
Te = 9.01 eV

arising almost entirely from fragmentation. Colin and Drowart (8) reported $InTe^+$, $InTe_2^+$, In_2Te^+ and $In_2Te_2^+$ as the vapour species above In_2Te_3, and assigned all of these as parent ions. Only $InSe^+$, In_2Se^+ and $In_2Se_2^+$ were reported from InSe vaporisation, and these were again all assigned as parents, although some of the $InSe^+$ was also assumed to arise from fragmentation. Berger et al (7) reported only MX^+ and M_2X^+ ions, of which only the latter were assigned as parents, except in the case of Ga_2Te_3 vaporisation where no Ga_2Te^+ was observed. $GaTe^+$ was therefore assigned entirely as a parent ion. Anomalous behaviour of gallium telluride was also reported by Uy et al (13); although these workers observed Ga_2Te^+ as the predominant ion, significant amounts of parent $GaTe^+$ and $GaTe_2^+$ were also found, together with trace Ga_2Te_2. These observations contrasted with those of the same workers on Ga_2Se_3 vaporisation, where only parent Ga_2Se^+ and fragment $GaSe^+$ were observed.

In summary, the present and previously-reported work has shown that the dominant vapour species produced on heating these Group III - Group VI compounds have the general formula M_2X. Much smaller quantities of M_2X_2 are also produced, but the existence of molecular MX is not proven.

4. MATRIX ISOLATION-INFRARED SPECTROSCOPY

Infrared spectra of the matrix-isolated vapour species are shown in Figures 5-8, and the frequencies of the observed bands are listed in Table 2.

The calculated spectra shown in Figures 5-7 were generated using the spectrum reconstruction routine in the Bruker software. The band frequencies and intensities for the different isotopic compositions of the M_2X molecules were calculated using SOTONVIB, assuming the molecular structures discussed in Section 4.1.

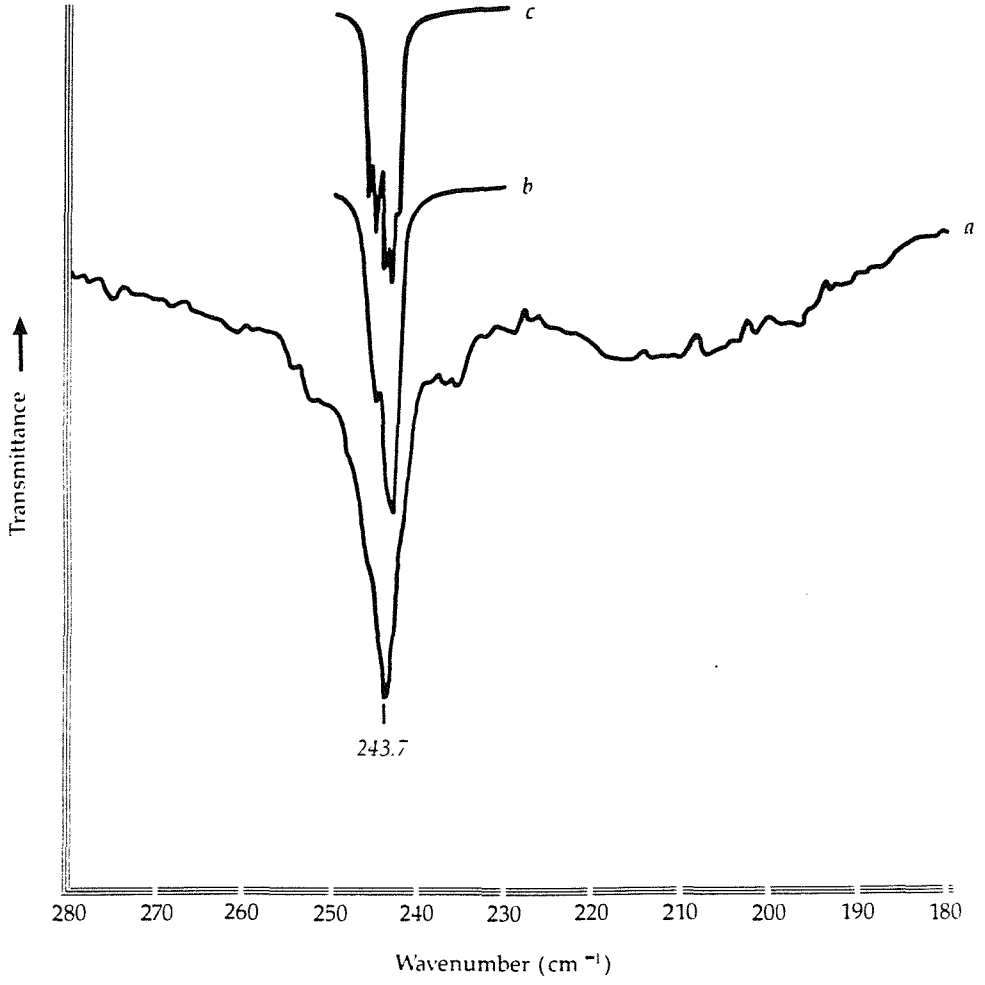

(a) Observed Spectrum
(b) Calculated Spectrum, 1 cm^{-1} linewidth
(c) Calculated Spectrum, 0.5 cm^{-1} linewidth

Figure 5 Argon Matrix IR Spectrum of Gallium Selenide

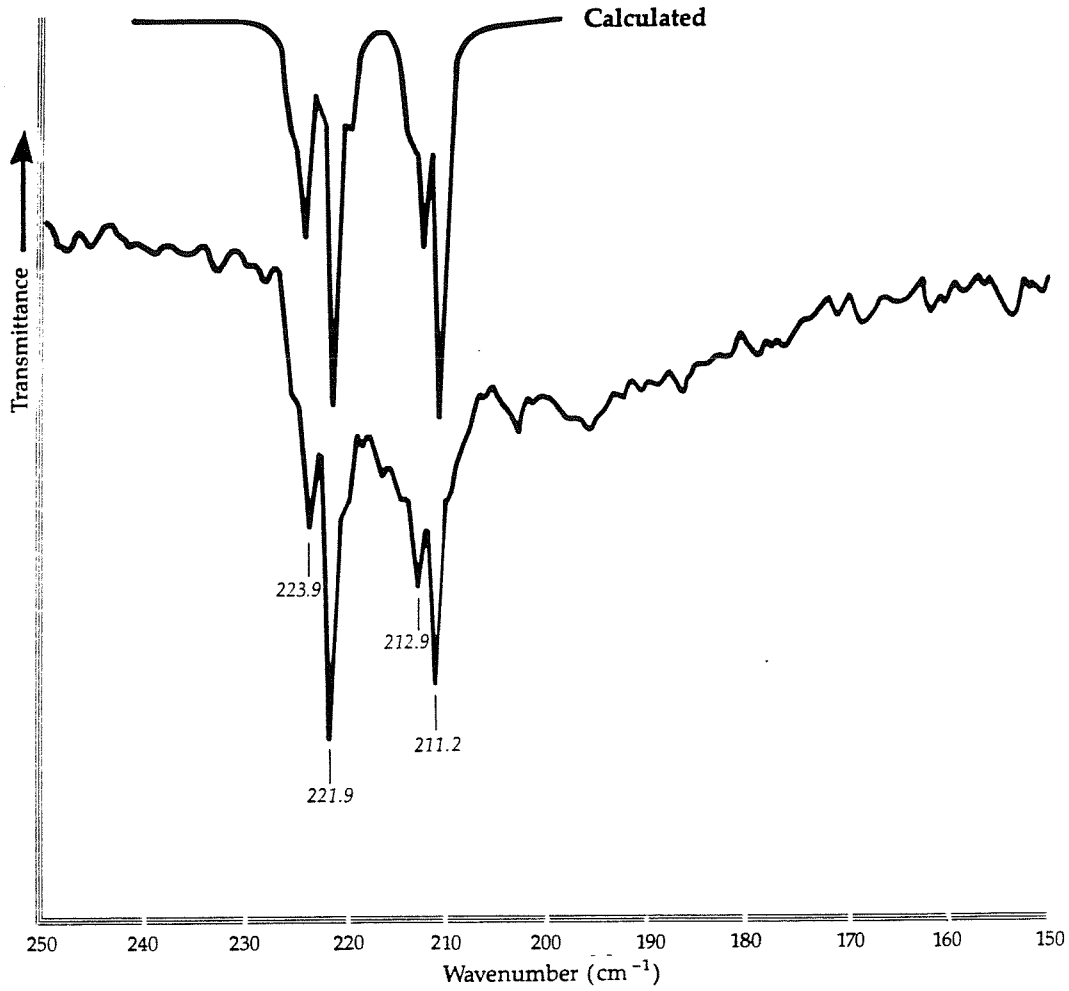

Figure 6 Argon Matrix IR Spectrum of Indium Selenide, Showing Calculated Isotope Splitting for In_2Se

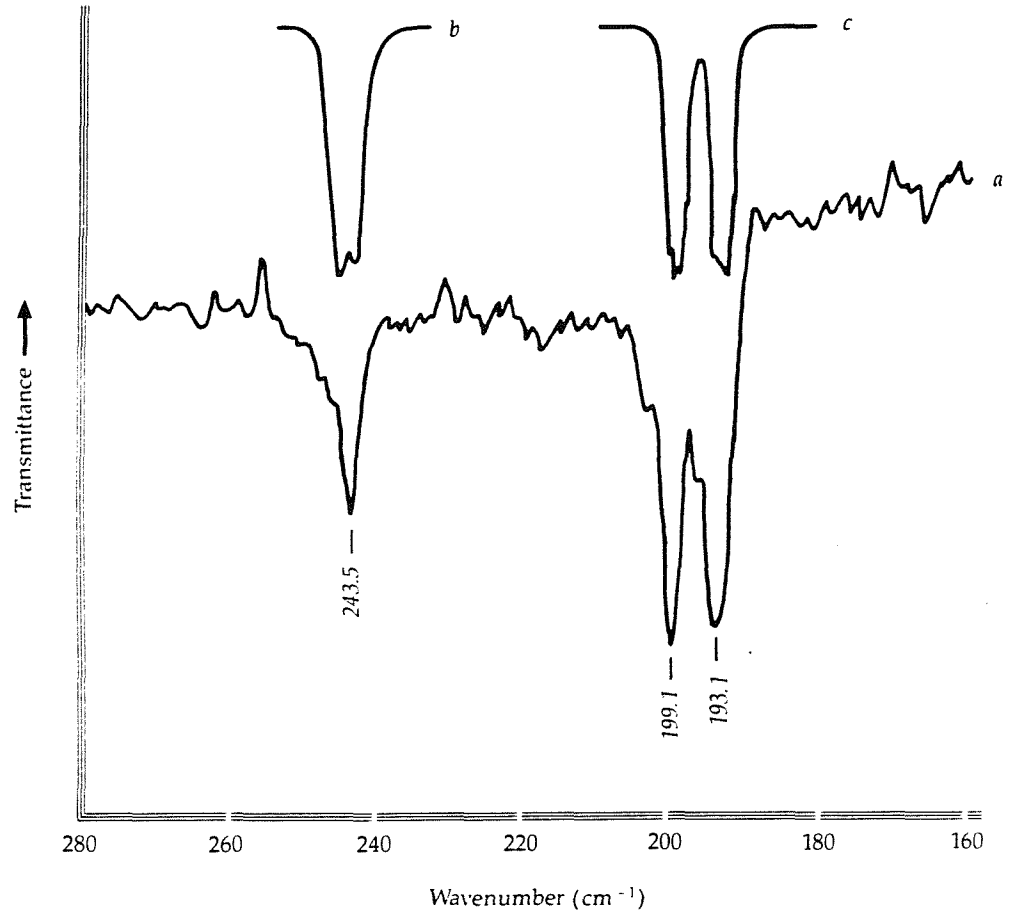

(a) Observed Spectrum
(b) Calculated Spectrum for GaTe
(c) Calculated Spectrum for Ga_2Te

Figure 7 Argon Matrix IR Spectrum of Gallium Telluride

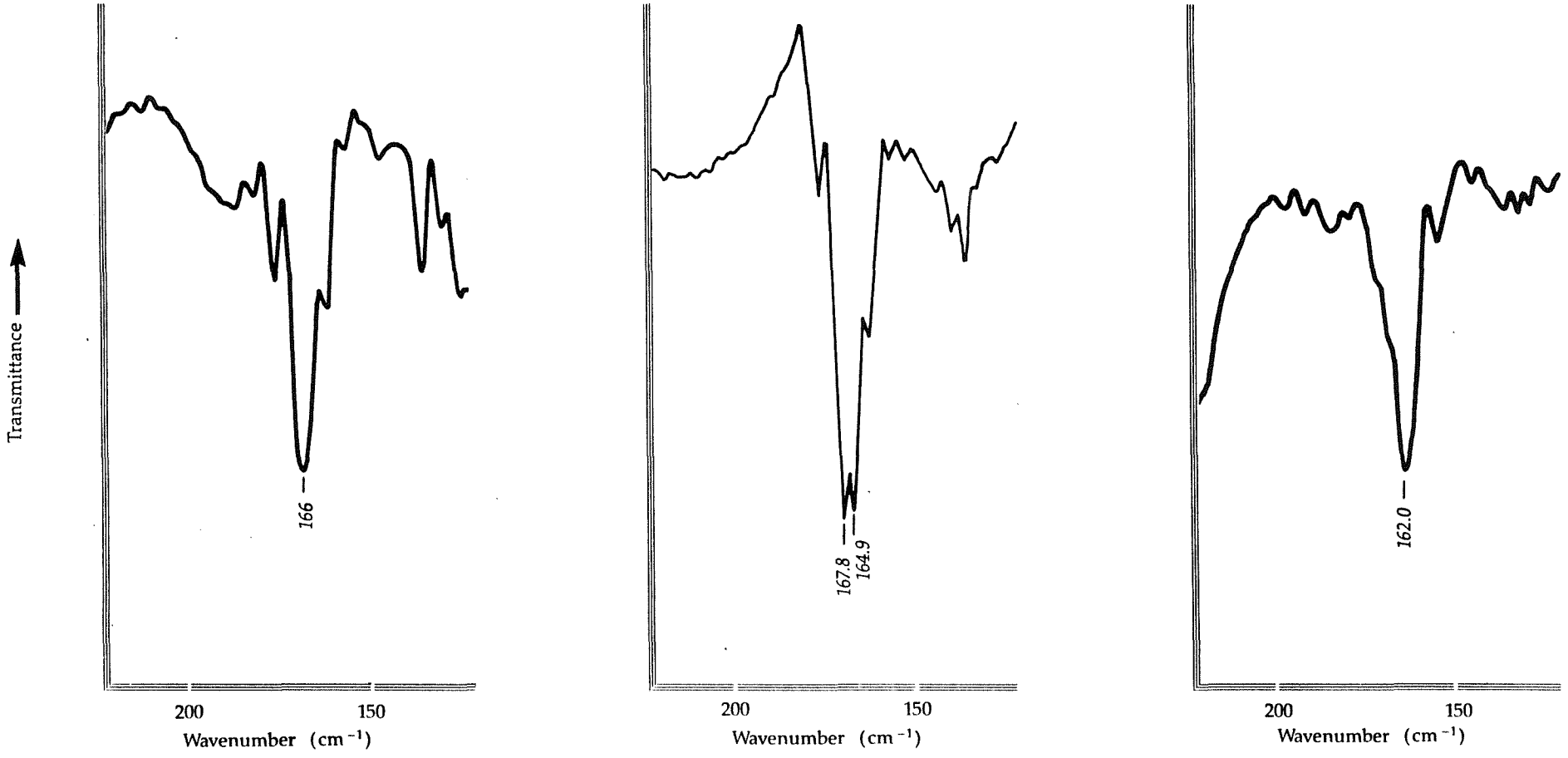

a) Ar Matrix, 4 cm^{-1} Resolution

b) Ar Matrix, 2 cm^{-1} Resolution

c) N_2 Matrix, 2 cm^{-1} Resolution

Figure 8 Infrared Spectra of Matrix-Isolated Indium Telluride

TABLE 2

BANDS OBSERVED IN ARGON MATRIX INFRARED SPECTRA

Vapour Species	Observed Frequencies (cm^{-1}) $\bar{\nu}_1$	$\bar{\nu}_3$	Other	Reported Frequencies
Ga_2Se	-	243.7	-	
In_2Se	212.9 (a) 211.2 (b)	223.9 (a) 221.9 (b)	196 (d)	208 (f) 235 (g)
Ga_2Te	193.1	199.1	243.5 (e)	
In_2Te	-	166 (c) 167.8 164.9	134 (d)	155 (f)

(a) Se-78
(b) Se-80
(c) N_2 matrix
(d) Polymeric species
(e) Ga_2Se impurity
(f) Xe matrix, reference 20
(g) Gas phase, references 18, 19.

The argon matrix spectrum obtained from the vaporisation of gallium selenide showed a single strong absorbance band, indicating that only one M-X species was present in significant quantities in the vapour phase. This was assumed to be Ga_2Se, on the basis of the mass spectrometric results; there was no evidence for the presence of GaSe in the matrix. The calculated spectra in Figure 5 show that there was good agreement with the experimental spectrum when a linewidth of 1 cm^{-1} was used to model the spectrum (Figure 5b). The contribution of the various isotopic species can be seen in the spectrum calculated with a linewidth of 0.5 cm^{-1}, (Figure 5c) but this fine structure was not resolvable in the experimental spectrum.

The spectrum obtained when indium selenide was vaporised showed two distinct doublets of approximately equal intensity (Figure 6). The intensity ratios of these bands were not affected by variations in the spray-on conditions and were therefore both assigned to a single species, molecular In_2Se. The calculated spectrum in Figure 6 shows the contributions of the different selenium isotopes and is in good agreement with the experimental spectrum. An additional band was observed at lower frequency in experiments where a low matrix gas flow was used, and this was attributed to the formation of polymeric species within the matrix.

The infrared spectrum of the vapour species released when gallium telluride was heated was similar to that described for indium selenide in that it showed two fairly closely-spaced bands of similar intensity (Figure 7), together with a lower-frequency band whose intensity varied according to the spray-on conditions. However, a further sharp band was also observed at higher frequency whose intensity relative to the two 'main' peaks did not vary appreciably with changes in the sample vaporisation temperature or the matrix gas flow rate.

The fact that this additional band occurred at a higher frequency than the Ga_2Te bands, and that its intensity was not substantially altered by changes in the matrix gas flow rate, indicate that it was not due to polymeric species. The previously-reported mass spectrometric work described above (7,13,16) suggest that the extra band could be due to GaTe. However, the observed band shape does not agree with that calculated for this molecule, which would show substantial broadening and fine structure due to the different contributions of the two gallium isotopes (Figure 7). It therefore appears likely that the additional band arises from an impurity in the gallium telluride sample. This is borne out by the close correspondence of the frequency of this band with that observed for gallium selenide.

The spectrum of indium telluride, recorded at 4 cm^{-1} resolution in an argon matrix, showed a single band at 166 cm^{-1} together with a lower-frequency polymer band of variable intensity (Figure 8a). The width of the principal band was about 10 cm^{-1}, which was about twice that observed for the other compounds studied in this section. When the spectrum was recorded at 2 cm^{-1} resolution, the band was resolved into two components of approximately equal intensity, with a frequency separation of about 3 cm^{-1} (Figure 8b). However, when nitrogen was used as the matrix gas, no such splitting was observed (Figure 8c).

The frequencies observed in this work are in moderate agreement with the few previously reported data (Table 2). Perov et al (20) reported frequencies for In_2Se and In_2Te in xenon matrices of 208 and 155 cm^{-1} respectively. Grinberg et al (18,19) reported a single strong band at 235 cm^{-1}, together with a higher-frequency combination band, in the gas phase IR spectrum of In_2Se. However, the width of the main band was not reported, and it is likely that the two bands observed in the present work, which were

separated by about 10 cm^{-1}, would not have been resolvable in the gas-phase spectrum.

4.1 Interpretation of the Infrared Spectra

The mass spectrometric studies discussed in Section 3 indicated that the vapour released from all of these compounds consists predominantly of M_2X molecules. In contrast with the consistency of the mass spectra, however, there are a number of dissimilarities between the infrared spectra, which are discussed below.

The M_2X molecules considered here may be either linear (D_{2h} symmetry) or bent (C_{2v} symmetry). The normal coordinate analysis for a non-linear triatomic molecule gives the following expressions for the three normal vibrations, all of which are infrared active:

$$\lambda_1+\lambda_2 = (2\mu_x \cos^2\theta + \mu_m)(F_r+F_{rr}) + 2(\mu_m + 2 \sin^2\theta\mu_x)F_\alpha$$

$$\lambda_1\lambda_2 = 2(\mu_m^2 + 2\mu_m\mu_x)(F_r+F_{rr})F\alpha \quad \text{(both } A_1 \text{ symmetry)}$$

$$\lambda_3 = (2\mu_x \sin^2\theta + \mu_m)(F_r-F_{rr}) \quad (B_1 \text{ symmetry})$$

where the potential constants are defined by

$$2V = F_r \sum_i \Delta r_i^2 + F_{rr} \sum_{i,j} \Delta r_i \Delta r_j + F_\alpha \sum_i (r_o \Delta\alpha_i)^2$$

in which μ_m and μ_x are the reciprocal atomic masses, the r_i's represent the M-X bond length, α is the M-X-M angle and $\theta = \alpha/2$. The symmetry species are assigned on the basis that the molecule lies in the xz plane.

Neglecting any interaction with the bending mode, the relative intensities of the A_1 and B_1 stretching modes in a C_{2v} molecule can be shown to satisfy the relationship:

$$\frac{I_{A_1}}{I_{B_1}} = \tan^2\theta \; \frac{(2\,\mu_x \sin^2\theta + \mu_m)}{(2\,\mu_x \cos^2\theta + \mu_m)}$$

This implies that the intensities of the two stretching modes are equal when the interbond angle is 90°, and the relative intensity of the A_1 mode approaches zero as the bond angle increases towards 180°. In the following discussion, all of the molecules are assumed to have C_{2v} symmetry, although in some cases no A_1 band was observed.

4.1.1 Gallium Selenide

The observation of a single strong band in the gallium selenide spectrum indicates that the M_2X molecule is practically linear in this case. If a limit of detection for the A_1 band of 5% of the B_1 band intensity is assumed, then the bond angle is at least 145°. Substituting an angle of 150° into the expression for the B_1 vibration gives an $(F_r - F_{rr})$ value of 92.5 N m^{-1}.

4.1.2 Gallium Telluride

The two most intense bands in this spectrum were assigned to the A_1 and B_1 stretching vibrations of molecular Ga_2Te. The approximately equal intensity of these two bands indicates that, in contrast to gallium selenide, this molecule has a significantly bent structure. The intensity ratio of the bands is approximately 1.1, and assigning the most intense band as the B_1 vibration gives an interbond angle of 93°. Substituting this angle into the expression for the B_1 vibration gives the $(F_r - F_{rr})$ value as 96.7 N m^{-1}.

4.1.3 Indium Selenide

The appearance of selenium isotope structure on the two principal bands of this spectrum confirms that they both arise from a species containing one selenium atom. Like gallium telluride, this molecule is substantially bent, the intensity ratio of approximately 1.4 indicating an interbond angle of 96°.

The value of the bond angle can also be calculated from the isotopic splitting of the bands, since for the B_1 mode:

$$\frac{\lambda'}{\lambda} = \frac{\bar{\nu}'^2}{\bar{\nu}^2} = \frac{2\mu_x' \sin^2\theta + \mu_m}{2\mu_x \sin^2\theta + \mu_m}$$

where $\bar{\nu}'$ is the observed frequency corresponding to the isotope of reduced mass μ_x'. This can be rearranged to:

$$\sin^2\theta = \frac{\mu_m (\bar{\nu}^2 - \bar{\nu}'^2)}{2(\mu_x \bar{\nu}'^2 - \mu_x' \bar{\nu}^2)}$$

Applying this formula to the Se-80 and Se-78 components of the B_1 doublet gives a bond angle of 130°. However, this result is very sensitive to small errors in the frequency measurements, since frequency ratios of 1.0075 and 1.0095 correspond to interbond angles of 90° and 180° respectively. The bond angle of 96°, obtained from the intensity ratios of the A_1 and B_1 bands, is therefore a more reliable value.

The isotopic splitting of the A_1 band can be used similarly to obtain separate values for the force constants F_r and F_{rr}, and these were calculated as 126 and 10 N m^{-1}

respectively. However, these results are again very sensitive to small errors in the frequency measurements; for example, varying the frequencies by ± 0.1 cm^{-1} results in a $\pm 100\%$ change in the calculated value of F_{rr}. The value of $(F_r - F_{rr})$, calculated from the B_1 frequency expression, was 129.0 N m^{-1}.

4.1.4 Indium Telluride

The spectrum of indium telluride vapour was anomalous in that, although two bands were observed, they were much more closely spaced than in the In_2Se and Ga_2Te spectra, and could not be resolved in a nitrogen matrix. There are three possible explanations for these observations:

(i) In_2Te has a large bond angle (analogous to Ga_2Se), and the band splitting observed in the argon matrix spectra arises from matrix shifts due to two different trapping sites;

(ii) In_2Te has a small bond angle (analogous to In_2Se and Ga_2Te), but the closely-spaced B_1 and A_1 modes are not resolved in the nitrogen matrix,

(iii) In_2Te has a large bond angle when isolated in a nitrogen matrix, but a fairly small angle when isolated in argon.

The third of these possibilities is extremely unlikely since the perturbation of the bond angle by the matrix would have to be very large to give the observed spectra. The first possibility is supported by the presence of other, weaker bands to either side of the main peak which could also indicate multiple trapping sites in the argon matrix. Furthermore, the separation of the two bands in the argon matrix is considerably less than would be expected from the studies of the In_2Se and Ga_2Te analogues (3 cm^{-1} compared to 10 cm^{-1}). The fact that the band width

in the nitrogen matrix is not substantially narrower than in argon may however indicate the presence of two unresolved components, supporting (ii).

In the absence of any decisive factors, it was decided to treat In_2Te as having a large bond angle analogous to Ga_2Se, and to attribute the observed band splitting to a matrix site effect. The value of $(F_r - F_{rr})$, calculated from the B_1 frequency assuming a bond angle of 150°, was 69.8 N m^{-1}.

4.2 Estimation of IR-Inactive Frequencies

In order to calculate the frequencies of the non-active modes, the three force constants F_r, F_{rr} and F_α must be separately estimated. In the cases where the A_1 frequency can be measured, F_r and F_{rr} are not independent, so that fixing the value of one of these constants constrains the value of the other. For all of the molecules, the bending force constant F_α was arbitrarily set at $0.1F_r$, and hence the F_{rr} values for Ga_2Se and In_2Se were fixed at 3.4 and -4.5 N m^{-1} respectively. In the cases of Ga_2Se and In_2Te, where only one measured frequency was available, the interaction constants F_{rr} were set to zero as this was approximately midway between the values obtained for In_2Se and Ga_2Te. The selected values of all the force constants, together with the frequencies thus calculated, are given in Table 3.

5. VAPORISATION BEHAVIOUR AND THERMODYNAMICS

The overall reaction for the vaporisation of the M_2X_3 compounds, neglecting the contribution of minor species such as MX or M_2X_2, is generally expressed as:

$$M_2X_3(s) \rightleftharpoons M_2X(g) + X_2(g) \qquad [1]$$

TABLE 3

ESTIMATED FORCE CONSTANTS, FREQUENCIES AND MOMENTS OF INERTIA OF M_2X MOLECULES

Molecule	Force Constants (N m^{-1})			Calculated Frequencies			X-M-X angle	I_A I_B I_C (amu^3nm^6)
	F_r	F_{rr}	F_α	$\bar{\nu}_1$	$\bar{\nu}_2$	$\bar{\nu}_3$		
Ga_2Se	92.5	0	10	164	107	244	150	11.0
In_2Se	124.5	-4.5	13	211	77	222	96	159.6
Ga_2Te	100.1	3.4	10	199	81	193	93	74.0
In_2Te	69.8	0	7	110	70	166	150	122.9

Similar equations can be written for different solid phase compounds, involving more or less evolution of $X_2(g)$. The above equilibrium has been assumed in calculating the enthalpies of formation of $Ga_2Se(g)$ and $Ga_2Te(g)$ (7, 13).

However, more detailed studies of the vaporisation of indium telluride (6,10) indicate that the vaporisation is not congruent, as implied above. Initially, only $Te_2(g)$ is evolved, resulting in an increasingly indium-rich condensed phase. In the intermediate stage of the vaporisation, both $In_2Te(g)$ and $Te_2(g)$ are produced, until the composition of the condensed phase reaches InTe(s), which vaporises congruently by the reaction

$$2\ InTe(s) \rightarrow In_2Te(g) + \tfrac{1}{2}\ Te_2(g)$$

The observation of substantial Se_2 and Te_2 vaporisation in the early stages of the mass spectrometic experiments indicates that all the compounds studied have similar non-congruent vaporisation schemes.

Previous calculations of the thermodynamic functions of the M_2X molecules (8,13,15,18,19) have been based almost entirely on estimated vibration frequencies and molecular shapes. The frequencies estimated by different workers vary considerably, and are generally in poor agreement with the experimental values determined here (Table 4). Thermodynamic functions based on the present experimental values are tabulated in Appendix 3, and the input data for these calculations are summarised in Table 3. The estimation of the bond angles and non-observed frequencies is described above, and the bond lengths were estimated by summation of the covalent radii (22, 23). The degeneracies of the electronic ground states were assumed to be unity in all cases.

Enthalpies of formation of these M_2X molecules have been calculated by Mills (24) on the basis of mass spectrometric

TABLE 4

DATA USED IN CALCULATIONS OF M_2X THERMODYNAMIC FUNCTIONS

Molecule	$\bar{\nu}_1$ (cm^{-1})	$\bar{\nu}_2$ (cm^{-1})	$\bar{\nu}_3$ (cm^{-1})	r_{m-x} (nm)	θ	Ref
Ga_2Se	302	132	345	0.26	110	13
	164	107	244	0.24	150	*
	303	109	321	0.27	100	8
In_2Se	160	75	235	0.25	140	18, 19
	211	77	222	0.27	96	*
	240	107	267	0.29	110	13
Ga_2Te	252	90	264	0.27	99	15
	199	81	193	0.26	93	*
In_2Te	215	88	240	0.29	100	8
	110	70	166	0.29	150	*

* Present work

studies of the vaporisation reaction [1] at temperatures of 1000 to 1800K (7,8,13). The high temperature reaction enthalpies were corrected to 298 K using estimated enthalpy and free energy functions, and the M_2X formation enthalpies thus obtained from the known heats of formation of $M_2X_3(s)$ and $X_2(g)$. The estimated M_2X functions were in good agreement with those in Appendix 3 for the gallium compounds, such that the $\Delta H°_{f,298}$ values for $Ga_2Se(g)$ and $Ga_2Te(g)$ calculated from these new data differ by less than 1 kJ mol^{-1} from those given by Mills. The agreement is not so good in the case of the indium compounds; the enthalpies of formation of $In_2Se(g)$ and $In_2Te(g)$ based on the new data differ by +9 and -7 kJ mol^{-1} respectively from the values given by Mills.

6. CONCLUSIONS

The vaporisation behaviour of gallium selenide, gallium telluride, indium selenide and indium telluride has been studied using mass spectrometry and matrix isolation-infrared spectroscopy.

The predominant vapour species was found to be M_2X in all cases, although small quantities of M_2X_2 were detected by mass spectrometry. The existence of MX and MX_2 in significant quantities was not confirmed by matrix isolation-infrared studies.

Considerable differences in the infrared spectra of the molecules were observed, consistent with Ga_2Se and In_2Te being almost linear and Ga_2Te and In_2Se having bond angles approaching 90°.

The observed infrared frequencies differed substantially from previously estimated values. The thermodynamic functions of the M_2X molecules have been calculated over the temperature range 100 to 2500 K.

REFERENCES

1. Beard, A M, Benson, C G and Bowsher, B R, UKAEA Report AEEW-R 2470, 1988.

2. Bowsher, B R, Prog Nucl Energy, 20, 199, 1987.

3. Dickinson, S, UKAEA Report AEEW-R 2227, 1987.

4. Grade, M and Hirschwald, W, Z Anorg Allg Chem, 460, 206, 1980.

5. Grade, M and Hirschwald, W, Ber Bunsenges Phys Chem, 86, 899, 1982.

6. Srinivasa, R S and Edwards, J G, Monatch für Chem, 117, 695, 1986.

7. Berger, L I, Strel'chenko, S S, Bondar, S A, Molodyk, A D, Balanevskaya, A E and Lebedev, V V, Izv Akad Nauk SSSR, Neorg Mater, 5, 872, 1969.

8. Colin, R and Drowart, J, Trans Farad Soc, 64, 2611, 1968.

9. Srinivasa, R S and Edwards, J G, J Electrochem Soc, 131, 2954, 1984.

10. Fiorani, P, Ferro, D and Piacente, V, J Mater Sci Lett, 6, 57, 1987.

11. Belousov, V I, Vendrikh, N F, Novozhilov, A F and Pashinkin, A S, Izv Akad Nauk SSSR, Neorg Mater, 17, 1190, 1981.

12. Srinvasa, R S, Diss Abstr Internat, 47, 648-B, 1986.

13. Uy, O M, Muenow, D W, Ficalora, P J and Margrave, J L, Trans Faraday Soc, 64, 2998, 1968.

14. Grimes, L E, Diss Abstr Internat, 46, 1935-B, 1985.

15. Belousov, V I, Vendrikh, N F, Gorbov, S I, Novozhilov, A F and Pashinkin, A S, Izv Akad Nauk SSSR, Neorg Mater, 20, 1319, 1984.

16. Nappi, B M, Ferro, D, Pelino, M and Piacente, V, Mater Chem, 2, 133, 1977.

17. Grinberg, Y K, Boryakova, V A and Shevel'kov, V F, Izv Akad Nauk SSSR, Neorg Mater, 7, 769, 1971.

18. Grinberg, Y K, Boryakova, V A and Shevel'kov, V F, Izv Akad Nauk SSSR, Neorg Mater, 8, 1206, 1972.

19. Greenberg, J H, Borjakova, V A and Shevelkov, V F, J Chem Thermodynamics, 5, 233, 1973.

20. Perov, P A, Shevel'kov, V F and Mal'tsev, A A, Vestn Mosk Univ Khim, 16, 109, 1975.

21. CRC Handbook of Chemistry and Physics, 64th Edition, CRC Press, Boca Raton, 1984.

22. Cotton, F A and Wilkinson, G, "Advanced Inorganic Chemistry", 4th Edition, John Wiley and Sons, New York, 1980.

23. Stark, J G, and Wallace, H G, "Chemistry Data Book", 2nd ed, John Murray, London, 1984.

24. Mills, K C, "Thermodynamic Data for Inorganic Sulphides, Selenides and Tellurides", Butterworths, London, 1974.

CHAPTER SEVEN

CAESIUM MOLYBDATE

1. INTRODUCTION

Caesium molybdate, Cs_2MoO_4, is of particular interest in severe accident studies since it contains two important fission product elements, caesium and molybdenum. This compound is less volatile than either caesium hydroxide or caesium iodide, which are predicted to be the dominant caesium vapour species in the primary circuit of a PWR during a severe accident (1). Evidence for the existence of a relatively involatile caesium species has been obtained in fission product release experiments (2, 3, 4), and observations of co-deposition of caesium and molybdenum suggest that this may be caesium molybdate.

The formation of caesium molybdate, Cs_2MoO_4, and possibly the bimolybdate, $Cs_2Mo_2O_7$, within the fuel matrix has been postulated, and the available thermodynamic data for these compounds have been reviewed (5). Caesium molybdate is considerably more volatile than elemental molybdenum, which is predicted to be the main form of molybdenum within the fuel (6,7). The formation of this compound may therefore provide a route whereby molybdenum, which is usually assumed to be non-volatile, could be transported out of the fuel at relatively low temperatures. However, whilst it is recognised that Cs_2MoO_4 is a stable vapour molecule, the gas-phase thermodynamic functions of this compound have not previously been calculated.

Molecules of the type M_2XO_4 (M = Na, K, Rb, Cs, X = Cr, Mo, W) have been studied quite extensively by matrix isolation and infrared spectroscopy (8 - 16). These studies have been mainly restricted to the X-O stretching frequency region of the spectrum, with very few reported studies of the O-X-O bending modes or the M-O stretching frequencies. This chapter describes mass spectrometric and matrix isolation-infrared studies of the vaporisation of caesium

molybdate with particular emphasis being placed on the determination of the Cs-O infrared stretching frequencies.

2. EXPERIMENTAL PROCEDURE

Commercially-prepared caesium molybdate, obtained from Koch-light Ltd, was used in all experiments.

A vaporisation temperature of about 1100°C was required to produce a sufficient vapour pressure above the sample; this necessitated the use of induction heating for mass spectrometric analysis, and a platinum-wound resistance furnace for the matrix isolation studies.

Two sets of matrix isolation experiments were performed to examine the Mo-O stretching region (900 to 800 cm^{-1}) and the O-Mo-O bending and Cs-O stretching regions (400 to 100 cm^{-1}). In the mid-infrared experiments, the sample was deposited onto a caesium iodide window. Nitrogen was used as the matrix gas since this was found to give better isolation. However, the use of a nitrogen matrix gave a broad absorption band at around 200 cm^{-1}, so argon was used as the matrix gas in the far infrared studies. A silicon deposition window was used for the low-frequency work.

3. MASS SPECTROMETRY

The mass spectrum of the vapour above liquid caesium molybdate at 1100°C was dominated by a strong Cs^+ ion peak, together with a much weaker group of peaks which were assigned to the $Cs_2MoO_4^+$ ion (Figure 1). No higher-mass ions were observed and it was therefore assumed that $Cs_2MoO_4^+$ was a parent species. The appearance potential of the Cs^+ ion, determined by extrapolation of the ionisation efficiency curve to zero ion current, was 5.1 eV. However,

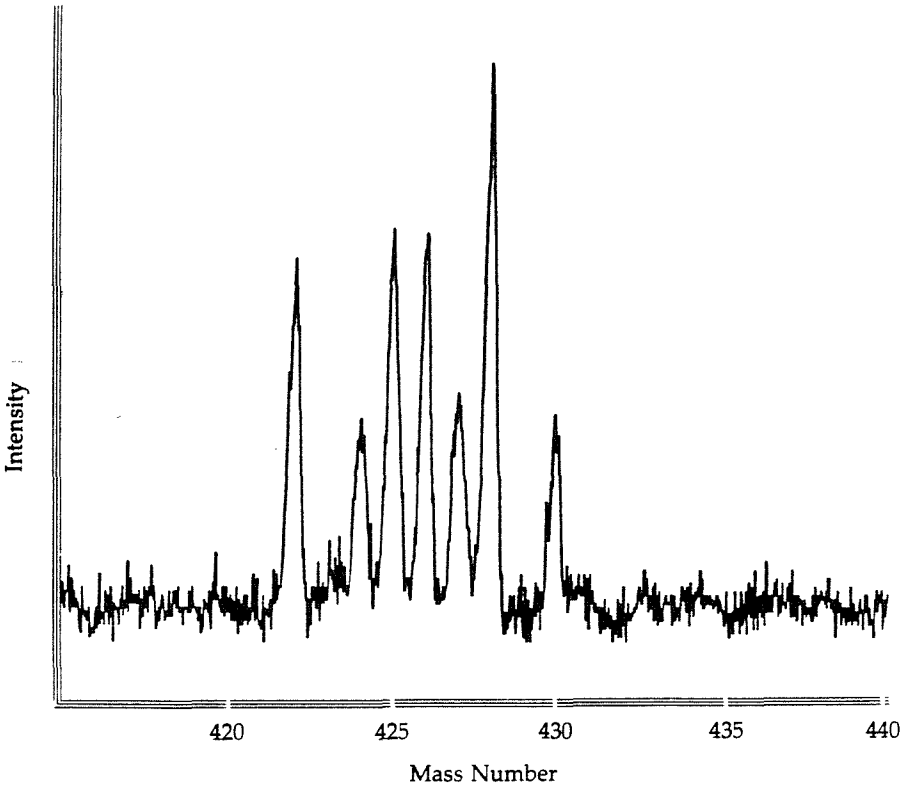

a) **Observed Spectrum**

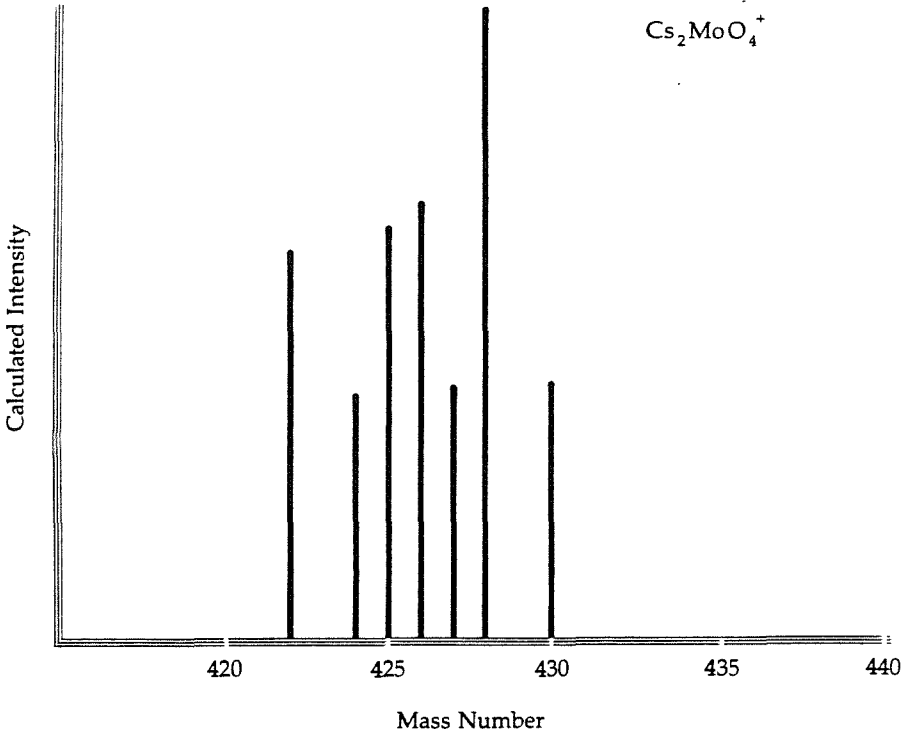

b) **Calculated Spectrum**

Figure 1 Mass Spectrum of Caesium Molybdate Parent Ion

the ion current did not fall rapidly to zero below 5 eV but remained at the same, albeit very low, value between about 5 and 4 eV before falling to zero just below 4 eV. This observation indicates that the caesium ions arose largely via a single mechanism, with a very small contribution from a second route with a lower appearance potential. The first ionisation potential of atomic caesium is 3.89 eV (17), and the observed ionisation behaviour is therefore consistent with the presence of a small amount of elemental caesium in the vapour. It can therefore be inferred that the main source of caesium ions was the fragmentation of Cs_2MoO_4 molecules.

These results are in good agreement with previously-reported mass spectrometric results of alkali metal molybdates (18, 19). Johnson (18) calculated that the appearance potential of Cs^+ produced by fragmentation of Cs_2MoO_4 would be 5.6 eV, in good agreement with the value observed in the present studies. The small quantities of elemental caesium vapour which were also observed by Johnson (18) were attributed to the dimersation reaction:

$$2Cs_2MoO_4(c) \rightarrow Cs_2Mo_2O_7(c) + 2Cs(g) + \tfrac{1}{2}O_2(g),$$

but no evidence was found for the presence of dimer molecules in the vapour.

4. MATRIX ISOLATION-INFRARED SPECTROSCOPY

The mid-infrared spectrum of matrix-isolated Cs_2MoO_4 showed a strong doublet at 827 and 837 cm^{-1}, in agreement with previous studies (8, 10, 11, 13-15). When the spectrum was recorded at 0.5 cm^{-1} resolution (Figure 2), fine structure was apparent on both bands due to molybdenum isotope effects. In the case of the higher-frequency band, seven component peaks were clearly resolved corresponding to the naturally-occuring isotopes of molybdenum: Mo-92, -94, -95,

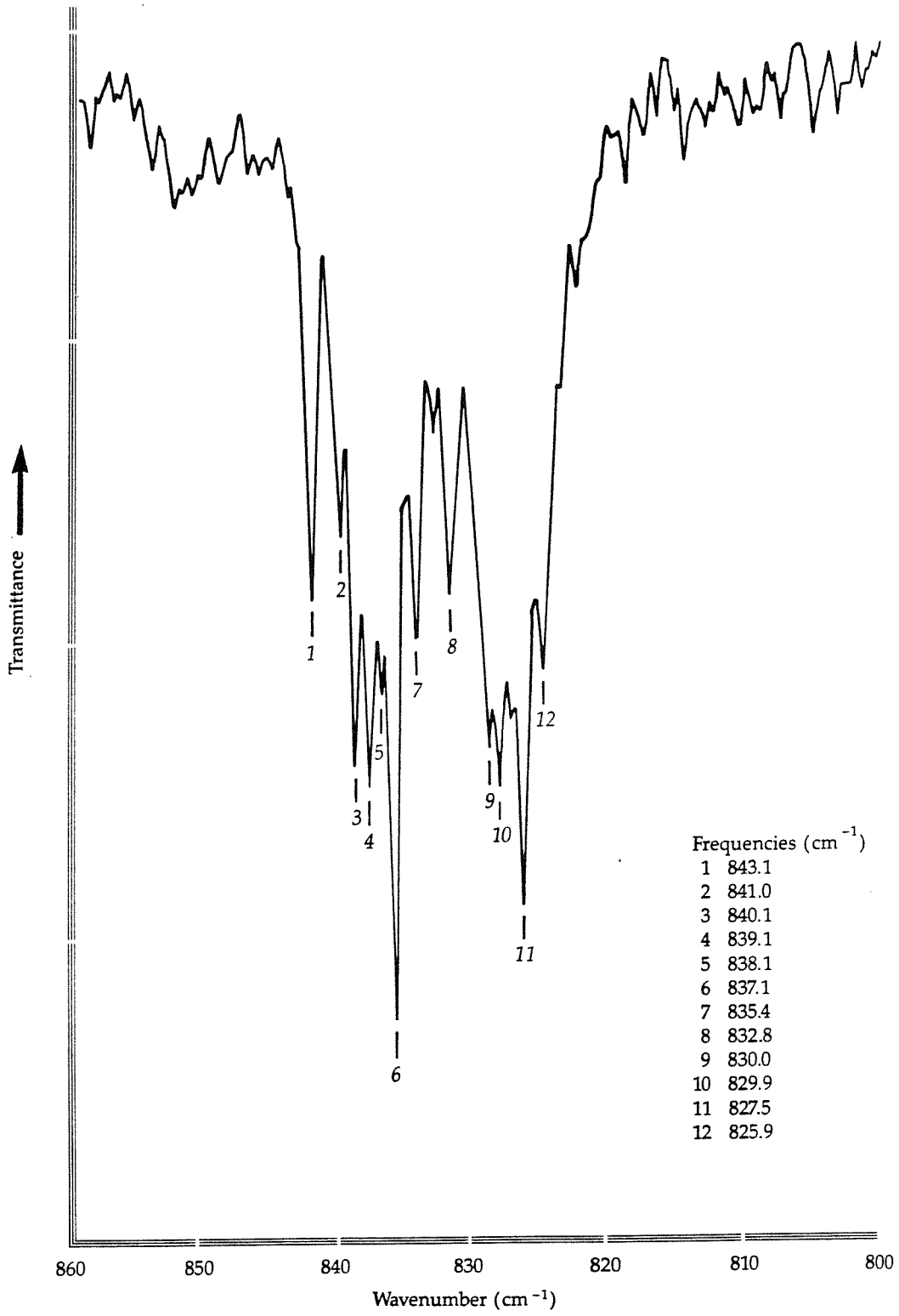

Figure 2 Nitrogen Matrix IR Spectrum of Caesium Molybdate (Mo-O Stretching Region)

-96, -97, -98 and -100. A similar pattern was discernible on the lower-frequency band, but the contributions of the different isotopes were less well resolved in this case.

A typical argon matrix spectrum of caesium molybdate, recorded over the frequency range 400 to 120 cm^{-1}, is shown in Figure 3. Spectral differences in this region from one experiment to another indicated that the bands at 369, 315, 164 and 143 cm^{-1} arose from the same species, which was assumed to be caesium molybdate. The bands at 356 and 155 cm^{-1} showed varying intensities, and in some experiments, additional bands were observed between 315 and 360 cm^{-1}.

Electron diffraction analysis of molecular caesium molybdate (20,21) has shown that its structure consists of a distorted tetrahedral MoO_4^{2-} unit with bidentate coordination to the two caesium ions (D_{2d} symmetry):

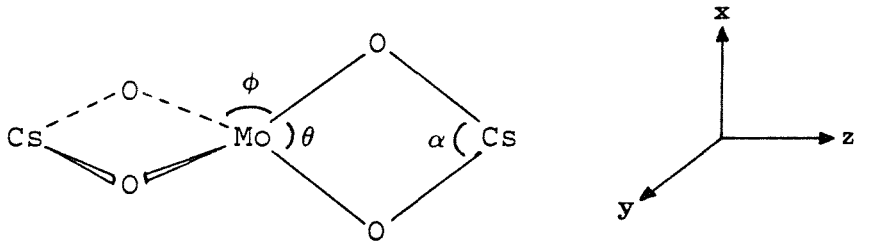

The interpretation of the caesium molybdate spectrum will be discussed in terms of this structure in three frequency ranges: 850-830 cm^{-1}, 400-300 cm^{-1} and 200-120 cm^{-1}. These regions can be identified with the Mo-O stretching, O-Mo-O bending and Cs-O stretching modes respectively.

4.1 The Mo-O Stretching Vibrations

The F-G analysis of the Mo-O stretching coordinates in terms of the D_{2d} structure shown above gives the following expressions (13,15):

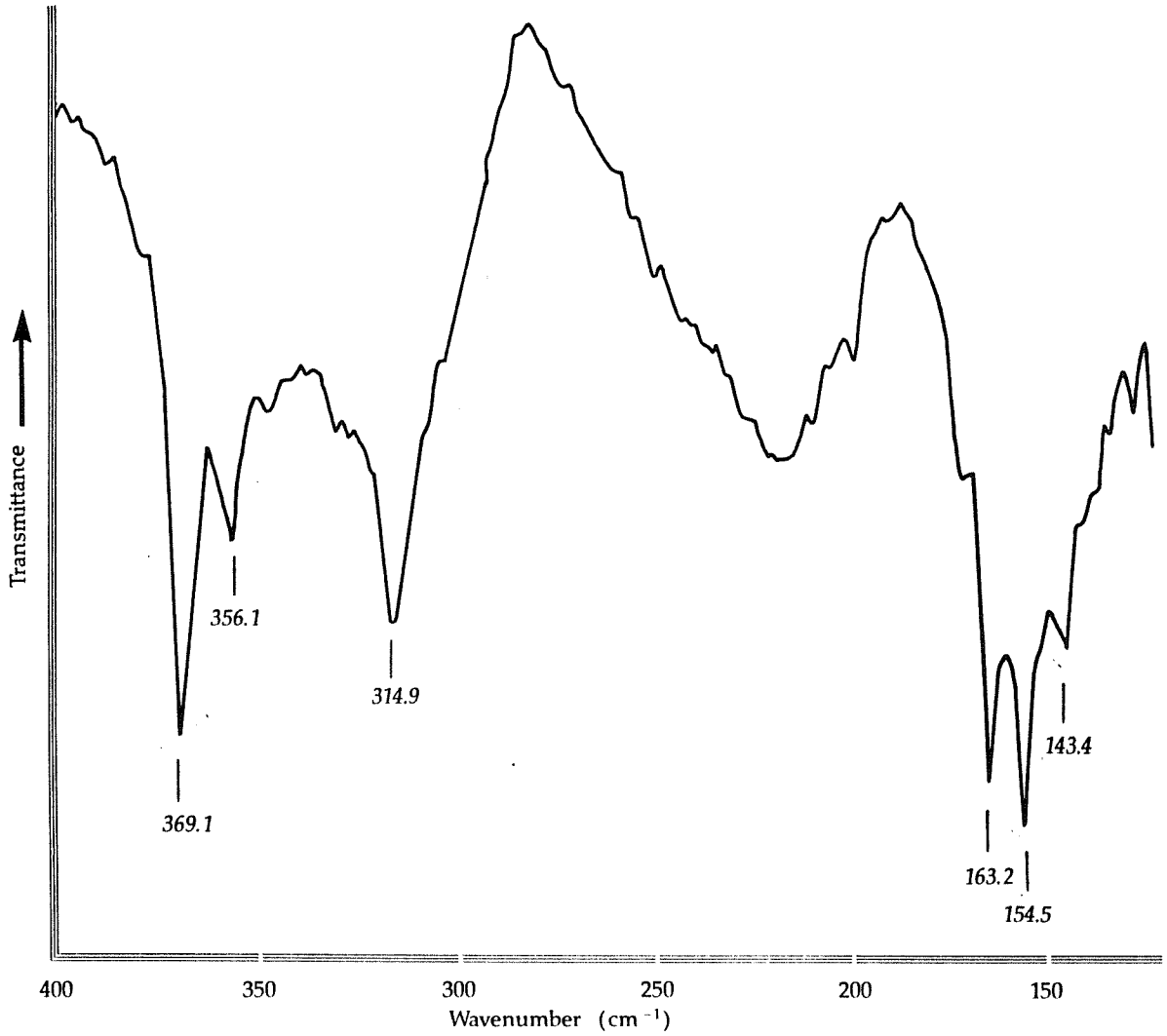

Figure 3 Argon Matrix IR Spectrum of Caesium Molybdate

$$\lambda_1 = \mu_O\ (F_r + F_{rr} + 2F'_{rr}) \qquad (A_1 \text{ symmetry})$$

$$\lambda_2 = (\mu_O + 4\ \cos^2\Theta\ \mu_{Mo})(F_r + F_{rr} - 2F'_{rr}) \qquad (B_2 \text{ symmetry})$$

$$\lambda_3 = (\mu_O + 2\ \sin^2\Theta\ \mu_{Mo})(F_r - F_{rr}) \qquad (E \text{ symmetry})$$

where the potential constants are defined by

$$2V = F_r \sum_i (\Delta r_i)^2 + F_{rr} \sum_{i,j} (\Delta r_i \Delta r_j) + F'_{rr} \sum_{i,k} (\Delta r_i \Delta r_k)$$

and Θ is half the O-Mo-O angle in which both O atoms are coordinated to the same Cs, and μ_O and μ_{Mo} are the reciprocal masses of the O and Mo atoms.

The two bands observed in this region of the spectrum can be assigned to the infrared active B_2 and E modes. The A_1 vibration is Raman active only, and its frequency has been determined for caesium molybdate in a neon matrix as 891 cm^{-1} (15).

The bond angle 2Θ can be determined from the well-resolved molybdenum isotope fine structure, using the above expression for the B_2 vibration. Two such equations can be written for the observed B_2 frequencies $\bar{\nu}$ and $\bar{\nu}'$ which arise from the molybdenum isotopes Mo and Mo' It then follows that

$$\frac{\lambda}{\lambda'} = \frac{\bar{\nu}^2}{\bar{\nu}'^2} = \frac{\mu_O + 4\ \cos^2\Theta\ \mu_{Mo}}{\mu_O + 4\ \cos^2\Theta\ \mu_{Mo'}}$$

which can be rearranged to give

$$\cos^2\Theta = \frac{(\bar{\nu}^2 - \bar{\nu}'^2)\ \mu_O}{4(\bar{\nu}'^2\ \mu_{Mo} - \bar{\nu}^2\mu'_{Mo})}$$

The higher frequency multiplet, which shows the molybdenum isotope structure most clearly, is assigned as the B_2 mode. Solving the above equation for the (Mo-92, Mo-100) and (Mo-92, Mo-98) frequency pairs gives Θ values of 49.5 and 48.8° respectively, and averaging these two results gives a bond angle of 98.3°. This is in excellent agreement with the angles obtained in previous studies of potassium molybdate (13) and caesium molybdate (16). However, in another study of caesium molybdate (15) a bond angle of 104.4° was obtained due to the somewhat larger frequency differences between the different isotopomers than were observed in the present work (see Table 1). The reason for these differences is not clear, since all of these data were obtained from nitrogen matrices at very similar temperatures.

The rather poorer resolution of the isotopic fine structure on the lower-frequency band can be attributed to the partial lifting of the degeneracy of the E mode due to low matrix site symmetry (13). This is also indicated by the low intensity of this band relative to the B_2 band. If the MoO_4 unit was truly tetrahedral, then the E mode would be twice as intense as the B_2. For the distorted tetrahedral shape, the intensity ratio can be calculated as a function of the bond angle from (11, 13):

$$\frac{I_E}{I_{B_2}} = \tan^2\Theta\ \frac{(m_{Mo} + 2\ m_O\sin^2\Theta)}{(m_{Mo} + 4\ m_O\cos^2\Theta)}$$

Substituting Θ = 49° into this relationship gives a ratio of 1.23. The observed intensity ratio is actually about

TABLE 1

MOLYBDENUM ISOTOPE STRUCTURE ON THE B_2 MODE IN NITROGEN MATRIX-ISOLATED CAESIUM MOLYBDATE

Molybdenum Isotope	B_2 Mo-O frequency (cm^{-1})		
	(a)	(b)	(c)
92	843.1	842.1	842.6
94	841.0	840.2	840.5
95	840.1	839.4	839.6
96	839.1	838.6	838.6
97	838.1	--	837.7
98	837.1	836.9	836.7
100	835.4	835.2	834.9

(a) This work
(b) Reference 15
(c) Reference 16

0.9, indicating that the two components of the degenerate mode are not exactly superimposed.

The force constants F_r, F_{rr} and F'_{rr} can be calculated if all three Mo-O frequencies are known. Using

A_1 = 891 cm^{-1} (from reference 15)
B_2 = 837.1 cm^{-1}
E = 827.5 cm^{-1}

gives

F_r = 589.0 N m^{-1}

F_{rr} = 43.9 N m^{-1}

F'_{rr} = 58.3 N m^{-1}

4.2 The O-Mo-O Bending Vibrations

The vibrational analysis of the O-Mo-O coordinates gives the following expressions:

$$\lambda_1 = 2\ F_\Theta + \frac{2\cos^2\Theta}{(1+\cos^2\Theta)} F_\phi\ \mu_O \qquad (A_1 \text{ symmetry})$$

$$\lambda_2 = 2\ F_\Theta\ (\mu_O + 4\sin^2\Theta\ \mu_{Mo}) \qquad (B_2 \text{ symmetry})$$

$$\lambda_3 = \frac{4}{(1+\cos^2\Theta)} F_\phi \mu_O \qquad (B_1 \text{ symmetry})$$

$$\lambda_4 = 2\ F_\phi\ [\mu_O + 2(1+\cos^2\Theta)\ \mu_{Mo}] \qquad (E \text{ symmetry})$$

where the force constants are defined by

$$2V = F_\Theta \sum_i (r_o \Delta\Theta_i)^2 + F_\phi \sum_i (r_o \Delta\phi_i)^2$$

and the angles Θ and ϕ are defined on the diagram on page 159.

The B_2 and the E modes are infrared active, and these can be identified with the observed bands at 369.1 and 314.9 cm^{-1} respectively. The order of these assignments is arbitrary, but is supported by the greater width of the lower frequency band which is consistent with some loss of degeneracy from the E mode. Substituting these frequencies into the appropriate expressions, together with $\Theta = 49°$, gives $F_\Theta = 47$ N m^{-1} and $F_\phi = 32$ N m^{-1}. The frequencies of the non-infrared active modes can thence be calculated as 375 (A_1) and 218 (B_1) cm^{-1} respectively.

4.3 The Cs-O Stretching Vibrations

The expressions for the Cs-O stretching modes are identical to those given for the Mo-O stretches (Section 4.1). However, the force constant F'_{RR}, which is associated with the interaction between two bonds without a common caesium atom, is likely to be very small. If this force constant is neglected, then the expressions reduce to:

$$\lambda_1 = (\mu_O + 2\cos^2\alpha\,\mu_{Cs})\,(F_R + F_{RR}) \qquad (A_1 \text{ symmetry})$$

$$\lambda_2 = (\mu_O + 2\cos^2\alpha\,\mu_{Cs})\,(F_R + F_{RR}) \qquad (B_2 \text{ symmetry})$$

$$\lambda_3 = (\mu_O + 2\sin^2\alpha\,\mu_{Cs})\,(F_R - F_{RR}) \qquad (E \text{ symmetry})$$

where the force constants are defined by

$$2V = F_R \sum_i (\Delta r_i)^2 + F_{RR} \sum_{i,j} (\Delta r_i \Delta r_j)$$

and α is half the O-Cs-O angle.

The B_2 and E modes are predicted to be infrared active and these can be identified with the bands at 163 and 143 cm^{-1} respectively. There is moderate agreement between these observed frequencies and those reported for the analogous modes of caesium sulphate in an argon matrix (196 and 170/148 cm^{-1}) (22, 23). However, the lower frequency bands were very weak in the case of the sulphate, in contrast with the molybdate spectrum (Figure 3) which shows the 163 and 143 cm^{-1} bands to have an intensity ratio of about 4.

The intensity ratio of the E and B_2 bands is given by:

$$\frac{I_E}{I_{B_2}} = \tan^2\alpha \quad \frac{(\mu_O + 2 \sin^2\alpha \, \mu_{Cs})}{(\mu_O + 2 \cos^2\alpha \, \mu_{Cs})}$$

The structural data for Cs_2SO_4 (15, 21, 24) can be used to calculate an O-Cs-O angle of 52° (α = 26°), and on the basis of this the E/B_2 intensity ratio is calculated as 0.2. The greater intensity of the lower frequency band in Cs_2MoO_4 indicates a somewhat larger bond angle.

Electron diffraction data for molecular caesium molybdate (20,21) give an O-Cs-O half-bond angle of 30°, corresponding to an E/B_2 ratio of 0.3, which is in good agreement with the observed ratio of about 0.25.

Substituting the bond angle of 30°, together with the observed frequencies, into the expression for the B_2 and E modes give values of F_R and F_{RR} of 19.8 and 1.5 N m^{-1} respectively.

4.4 SOTONVIB Calculations

In the above discussion, it was assumed that there was no interaction between vibrations involving internal coordinates of different types. However, several of the vibrational modes thus obtained belong to the same symmetry species and would therefore give off-diagonal terms in the G matrix for the full set of internal coordinates. The six observed frequencies, together with the set of seven force constants obtained above, were therefore used as input to the SOTONVIB program. The calculated frequencies and force constants, obtained by the simple model and after perturbation by SOTONVIB, are shown in Tables 2 and 3.

In the initial SOTONVIB calculations, the force field was restricted to the seven force constants defined in Sections 4.1 to 4.3. However, it was not possible to obtain a set of values of these constants which exactly fitted the observed frequency set. The differences between the calculated and observed frequencies were particularly large for the Cs-O stretching modes. When the calculated L_R vectors (which show the extent to which each internal coordinate is involved in all the normal coordinates) were examined, it was evident that these low-frequency modes involved significant contributions from all the internal coordinates. A number of interaction force constants were therefore gradually introduced into sequential calculations until good agreement between the observed and calculated frequencies was obtained.

5. THERMODYNAMIC CALCULATIONS

The above discussion has identified thirteen of the vibrational modes of the caesium molybdate molecule. However, the full representation of the vibration modes of this molecule, after the removal of the rotational and translational motions, is $3A_1 + B_1 + 3B_2 + 4E$. This means that there is another E mode which has not been observed in

TABLE 2

OBSERVED AND CALCULATED VIBRATION FREQUENCIES FOR CAESIUM MOLYBDATE

	Observed Frequency (cm^{-1})	Calculated Frequency (cm^{-1})	
		a	b
A_1 (Mo-O)	891*		891.0
A_1 (O-Mo-O)	-	375	369.0
A_1 (Cs-O)	-	163	124.4
B_1 (O-Mo-O)	-	218	278.2
B_2 (Mo-O)	837.1		837.1
B_2 (O-Mo-O)	369.1		369.0
B_2 (Cs-O)	163.2		163.0
E (Mo-O)	827.5		827.5
E (O-Mo-O)	314.9		315.0
E (Cs-O)	143.4		143.0

* = from Reference 15

a = factored force field

b = SOTONVIB

TABLE 3

CALCULATED FORCE CONSTANTS FOR CAESIUM MOLYBDATE

	Force Constant (N m^{-1})	
	a	b
F_r	589	577
F_{rr}	44	38
F'_{rr}	58	61
F_R	20	110
F_{RR}	1.5	-9.0
F_Θ	47	26
F_ϕ	32	11
F_Θ	-	1.4
$F_{R\phi}$	-	14
$F_{R\Theta}$	-	-7.2
$F_{\phi\phi}$ *	-	-8.3
$F_{\phi\Theta}$		

*applies to angles with a common bond

a = factored force field

b = SOTONVIB

the spectrum or considered in the above analysis. This mode can be visualised as the out-of-plane motion of the caesium ions with respect to the MoO_2Cs rings, and would be expected to have a very low frequency. The frequency of the analogous vibration in caesium sulphate has been calculated (21) as 30 cm^{-1}, and this value will be assumed for the molybdate.

The structural data used to calculate the product of the moments of inertia are as follows:

Mo-O bond length = 0.18 nm (20,21)

Cs-O bond length = 0.28 nm (20,21)

O-Mo-O angle = 98°

O-Cs-O angle = 58°

The symmetry number of the D_{2d} molecule is 4, and the degeneracy of the electronic ground state is assumed to be unity. The thermodynamic functions for the caesium molybdate molecule calculated from these data are given in Appendix 3.

These calculations were based on the observed frequencies together with those calculated from SOTONVIB (column (b) in Table 2). However, the frequencies calculated using the factored force field model (column (a) in Table 2) gave results which differed by less than 1% from those given in Appendix 3.

The vapour pressure of caesium molybdate has been determined by Johnson (18) over the temperature range 1070 to 1170 K, as:

$$\ln p(atm) = 15.14 - 32200/T(K)$$

This gives the enthalpy of sublimation at 1120 K as 267.7 kJ mol^{-1}. Using the free energy functions tabulated by Cordfunke et al (5) for the condensed phase, together with the gas-phase data tabulated in Appendix 3, allows an enthalpy of sublimation of 301 kJ mol^{-1} at 298 K to be calculated. Combining this value with the enthalpy of formation of solid Cs_2MoO_4 at 298 K, - 1514.6 kJ mol^{-1} (5), gives the enthalpy of formation of $Cs_2MoO_4(g)$ as -1214 kJ mol^{-1}.

6. CONCLUSIONS

The vaporisation of caesium molybdate has been studied by mass spectrometry and matrix isolation-infrared spectroscopy. The existence of molecular Cs_2MoO_4 in the vapour phase has been confirmed.

The infrared spectrum of molecular caesium molybdate has been interpreted in terms of a D_{2d} structure. The experimentally-observed frequencies have been used to construct a seven-term force field from which the frequencies of three of the non-infrared active modes have been calculated. The positions of the remaining modes have been obtained from previously-reported Raman studies and calculations, and the thermodynamic functions of the molecule have been calculated.

REFERENCES

1. Garisto, F, "Thermodynamics of Iodine, Caesium and Tellurium in the Primary Heat-Transport System under Accident Conditions", AECL-7782, 1982.

2. Lorenz, R A, Collins, J L and Malinauskas, A P, Nucl Technol, 46, 404, 1979.

3. Osetek, D J, Cronenberg, A W, Hobbins, R R, and Vinjamuri, K, Proc ANS Meeting on Fission Product Behaviour and Source Term Research, 15-19 July 1984, Snowbird, USA, NP-4113-SR,22-1, 1985.

4. Fink, J K, Roche, M F, Seils, C A, Steidl, D V, Johnson, C E and Ritzman, R L, Proc Symposium on Chemical Phenomena Associated with Radioactivity Release during Severe Nuclear Plant Accidents, Anaheim, 9-12 September 1986, NUREG/CP-0078, 2-79, 1987.

5. Cordfunke, E H P, Konings, R J M, Prins, G, Potter, P E and Rand, M H, "Thermochemical Data for Reactor Materials and Fission Products", Eur. Contract ETSN-005-NL, 1988.

6. Kleykamp, H, J Nucl Mater, 131, 221, 1985.

7. Bowsher, B R, Prog. Nucl. Energy, 20, 199, 1987.

8. Spoliti, M, Bencivenni, L, Maltese, M and Nunziante Cesaro, S, J Mol Structure, 60, 259, 1980.

9. Atkins, R M, and Gingerich, K A, High Temp Sci, 14, 103, 1981.

10. Spoliti, M, Nunziante Cesaro, S, Bencivenni, L, D'Alessio, L, Enea, L and Maltese M, High Temp Sci, 14, 11, 1981.

11. Spoliti, M, Bencivenni, L, Nunziante Cesaro, S, Teghil, R and Maltese, M, J Mol Structure, 74, 297, 1981.

12. Bencivenni, L, and Gingerich, K A, J Chem Phys, 76, 53, 1982.

13. Beattie, I R, Ogden, J S, and Price, D D, J Chem Soc, Dalton Trans, 505, 1982.

14. Spoliti, M, Bencivenni, L, Nunziante Cesaro, S, and D'Alessio, L, J Mol Structure, 80, 141, 1982.

15. Nagarantha, H M, Bencivenni, L and Gingerich, K A, J Chem Phys, 81, 591, 1984.

16. Ogden, J S and Gomme, R A, University of Southampton, Unpublished data, 1989.

17. CRC Handbook of Chemistry and Physics, 64th Edition, CRC Press, Boca Raton, 1984.

18. Johnson, I, J Phys Chem, 79, 722, 1975.

19. Yamdagni, R, Pupp, C and Porter, R F, J Inorg Nucl Chem, 32, 3509, 1970.

20. Ugarov, V V, Ezhov, Y S and Rambidi, N G, Zh Strukt Khim, 14, 359, 1973.

21. Ugarov, V V, Ezhov, Y S and Rambidi, N G, J Mol Structure, 25, 357, 1975.

22. Belyaeva, A A, Dvorkin, M I and Shcherba, L D, Opt Spectrosc (USSR), 38, 291, 1975.

23. Belyaeva, A A, Dvorkin, M I and Shcherba, L D, Opt Spectrosc (USSR), 43, 114, 1977.

24. Belyaeva, A A, Dvorkin, M I and Shcherba, L D, Opt Spectrosc (USSR), 38, 170, 1975.

CHAPTER EIGHT

INDIUM TRI-IODIDE

1. INTRODUCTION

The interactions between fission product vapour species and the control rod components (cadmium, indium and silver) could have an important influence on the transport of fission products (1). The control rods are predicted to fail, releasing large quantities of cadmium- and indium-based aerosols, at approximately the same time as the more volatile fission products such as iodine and tellurium are released from the degrading fuel (2). Simulant studies have demonstrated that iodine vapour will react with cadmium aerosols to form cadmium iodide, and that subsequent heating of the deposited aerosols produces cadmium iodide vapour (3). Such reactions might also be expected to occur involving iodine and indium-based aerosols, and this chapter describes studies of the vaporisation behaviour of a possible product of such a reaction, indium tri-iodide. Thermodynamic functions for the relevant vapour species are calculated, and other thermodynamic data are reviewed.

2. EXPERIMENTAL DETAILS

Indium tri-iodide, InI_3, was obtained from Johnson Matthey Chemicals Ltd with a stated purity of 99.999%. The compound was stored over phosphorous pentoxide, and samples transferred to the inlet systems of the instruments as quickly as possible (< 30 seconds) to avoid uptake of moisture.

Samples were vaporised from silica holders, and it was found that a temperature of 100°C was sufficient to give good infrared spectra. In the mass spectrometric experiments, it was necessary to heat the sample to about 150°C to produce satisfactory molecular ion signals.

In some experiments, the portion of the sample holder between the specimen and the entrance to the vacuum chamber was heated to higher temperatures, in the range 300 to 700°C. The heating element was positioned so that the temperature in the region of the sample was just high enough to slowly sublime the sample into the heated region. Using this arrangement it was possible to study changes in the vapour composition which occurred at higher temperatures.

3. MASS SPECTROMETRY

The mass spectrum obtained when indium tri-iodide was heated to 150°C is shown in Figure 1. The peaks at 242, 369 and 496 mass numbers can be assigned to InI^+, InI_2^+ and InI_3^+ respectively. In^+, I^+ and HI^+ and I_2^+ ions were also observed. The appearance potentials of the observed ions are shown in Table 1, together with results from previous studies of iodine and indium monoiodide vaporisation (4). The ionisation efficiency curves for the InI^+ ion measured with and without superheating the vapour are shown in Figure 2.

These results indicate that InI_3^+ was a parent species, whereas In^+ and I^+ were fragment ions. The appearance potentials of the I_2^+ and InI_2^+ ions were very close to the values obtained in the previous studies (4), in which both of these species were assigned as parent ions. However, the InI_2^+ ions may have been produced by fragmentation of heavier species such as In_2I_2 or In_2I_4. In the present studies, the main source of InI_2^+ ions was almost certainly fragmentation of InI_3 molecules. In experiments with no additional heating of the vapour, the InI^+ ion was evidently produced by fragmentation. The significant decrease in the appearance potential of this ion when the vapour was superheated to 700°C indicates that InI^+ was present as a parent species under these conditions. The

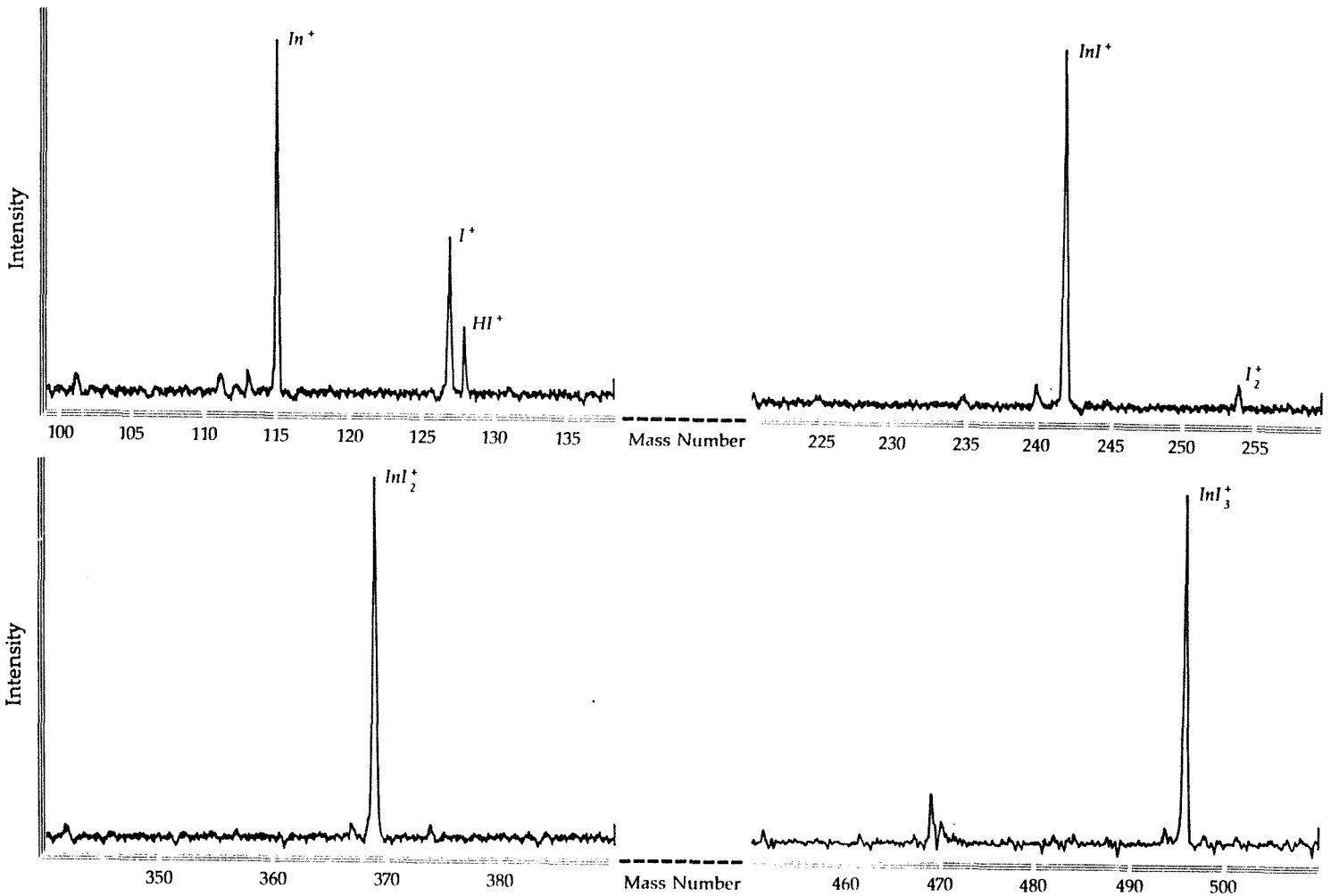

Figure 1 Mass Spectrum from Indium Tri-Iodide Vaporisation

TABLE 1

APPEARANCE POTENTIALS OF IONS OBSERVED FROM INDIUM TRI-IODIDE VAPORISATION

Ion	Appearance Potential (eV)*			
	a	b	c	d
In^+	12.0	7.3	8.4 (f)	-
I^+	14.0	12.9	13.3 (f)	13.0 (f)
I_2^+	9.7	9.5	-	9.6 (p)
InI^+	12.0	9.2	8.6 (p)	-
InI_2^+	10.0	-	9.6 (?)	-
InI_3^+	9.0	-	-	-

First ionisation potentials (from Reference 28):

$In^+ = 5.786$ eV

$I^+ = 10.451$ eV

a) InI_3 vaporisation, no superheating

b) InI_3 vaporisation, vapour superheated to 700°C

c) InI vaporisation, Reference 4

d) I_2 vaporisation, Reference 4

* = all measurements ± 0.5 eV

(p) = Ion assigned as parent species

(f) = Ion assigned as fragment

(?) = Ion assignment uncertain

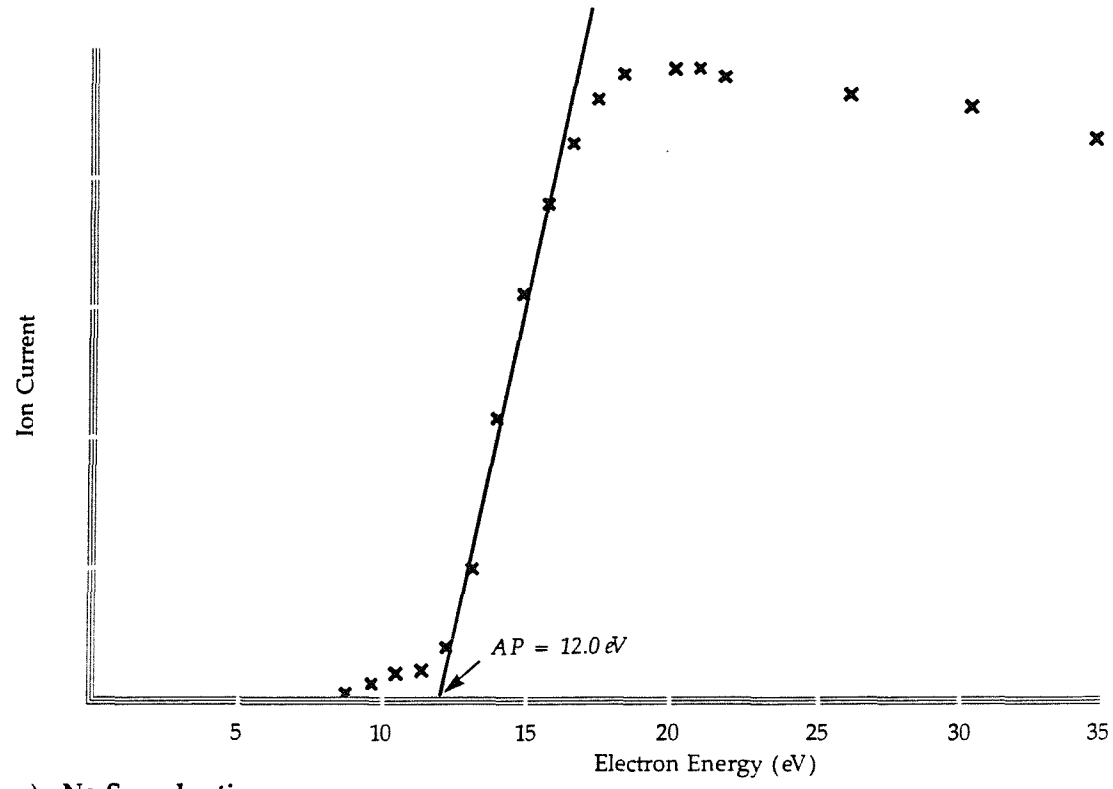

a) No Superheating

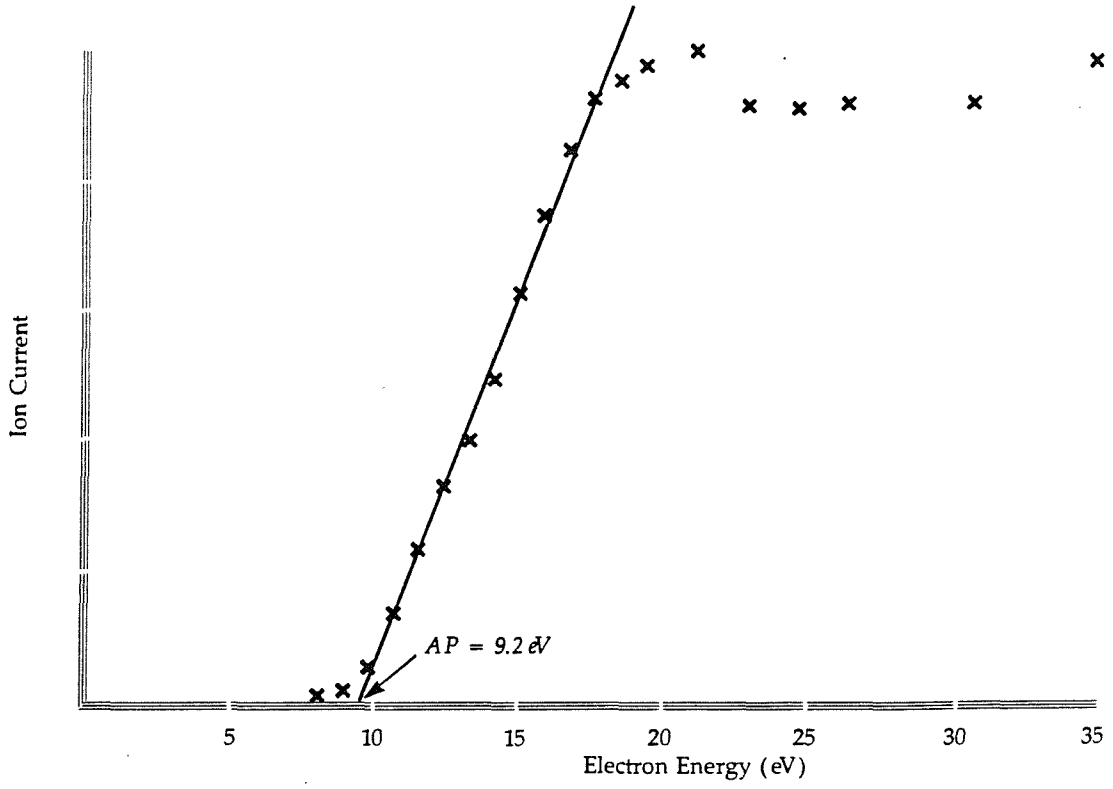

b) Vapour Superheated to 700° C

Figure 2 Ionisation Efficiency Curves for the InI^+ Ion Produced from Indium Tri-Iodide Vaporisation

slight inflexion at about 13 eV in the ionisation efficiency curve (Figure 2b) indicates that both fragment and parent InI^+ were present in the superheated vapour. The appearance potentials of the In^+ and I^+ ions were also affected by the increased temperature indicating a change in the identity of the parent molecules from InI_3 to InI and I_2.

4. MATRIX ISOLATION-INFRARED SPECTROSCOPY

The matrix isolation-infrared spectrum obtained from indium tri-iodide with no superheating of the vapour is shown in Figure 3a, whilst the spectra obtained when the vapour was passed through a hotter region before depositing on the cold window are shown in Figures 3b and 3c. All the spectra were recorded at a resolution of 1 cm^{-1} in an argon matrix. The frequencies of the observed bands are shown on the spectra, and a number of differences are apparent. In experiments with no superheating of the vapour, the spectrum was dominated by a rather broad band at 231 cm^{-1}, with a shoulder on the high frequency side. Five weaker bands were also observed in the frequency range 200 to 100 cm^{-1}. However, when the sample was vaporised at 150°C and the vapour heated to about 500°C before depositing in the matrix, the lower frequency bands were no longer apparent, and the higher-frequency peak was split into two components at 236 and 232 cm^{-1}, the former being the dominant feature. When the superheat temperature was increased to 700°C, the spectrum was dominated by a sharp band at 167.7 cm^{-1}.

4.1 Interpretation of the IR Spectrum

The changes which occurred in the infrared spectra as the spray-on conditions were varied indicate that four different vapour species were present. The bands at 231, 180, 160 and 124 cm^{-1}, which were predominant in the spectrum obtained without superheating the vapour, are very

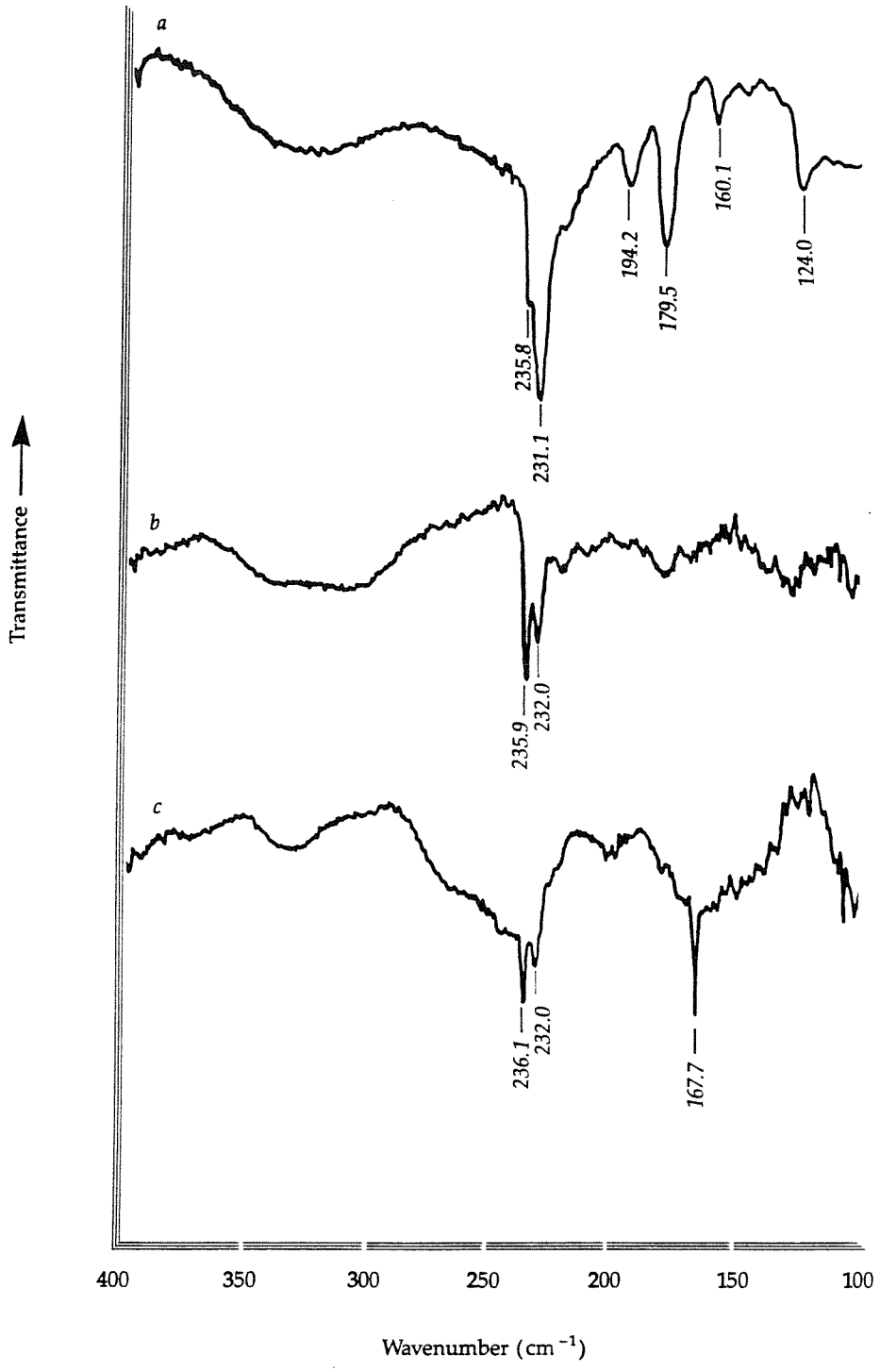

a) No Superheating
b) Vapour Superheated to 500° C
c) Vapour Superheated to 700° C

Figure 3
Argon Matrix IR Spectra from Indium Tri-Iodide Vaporisation at 120° C

TABLE 2

FREQUENCIES OBSERVED IN ARGON MATRIX INFRARED SPECTRA OF INDIUM TRI-IODIDE

Observed Frequencies (cm^{-1})	Reported Frequencies (cm^{-1})					Assignment
	a	b	c	d	e	
235.9	225			200-300		$InI_3, \bar{\nu}_3$
231.1	288	228	226			In_2I_6
194.2						In_2I_2/In_2I_4?
179.5	177	178	179			In_2I_6
167.7					177.1	InI
160.1	150	158	157			In_2I_6
124.0	122	125	125			In_2I_6

a) Xe matrix (7)
b) Solid (5)
c) Nujol Mull (6)
d) Gas-phase InI_3 (8)
e) Gas-phase InI (9)

close to the In-I stretching frequencies reported for solid indium tri-iodide in a nujol mull (5,6). There is also good agreement, with the exception of the 231 cm^{-1} band, with the frequencies reported for indium tri-iodide dimer in a krypton matrix (7) (see Table 2). The band at 194 cm^{-1} indicates that a second low-temperature species was present; possible assignments are to In_2I_2 or In_2I_4 arising from mono- or di-iodide impurities in the sample. The single band at 236 cm^{-1}, which was the dominant feature of the spectrum when the vapour was heated to 300 - 500°C, can be assigned to molecular InI_3. The observed frequency is similar to the value of 225 cm^{-1} reported for InI_3 in a krypton matrix (7) and to the gas-phase frequency of 200 - 230 cm^{-1} (8). The additional single band at 167.7 cm^{-1}, which was observed when the vapour was heated above 650°C, can be assigned to InI, and the frequency is in reasonable agreement with the value of 177 cm^{-1} reported for this molecule in the gas phase (9).

These observations are entirely consistent with other studies of indium tri-iodide and its analogues. In the solid state, indium tri-iodide is believed to consist of discrete In_2I_6 molecules (5,6,10,11) with a bridged structure:

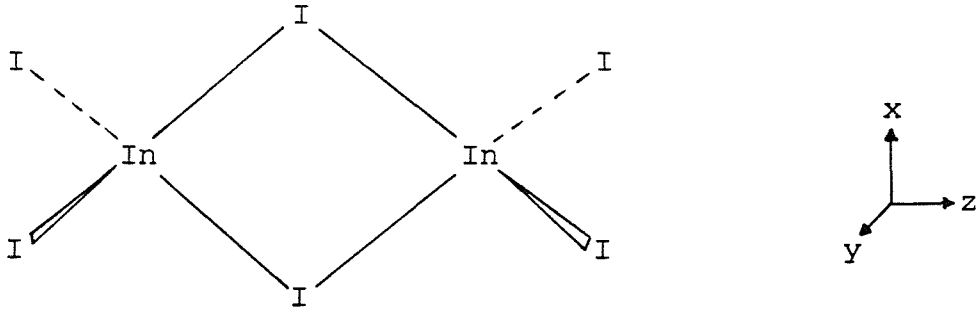

The weak lattice forces between these units result in low melting and boiling points (210 and 500°C respectively (12)), and the dimer molecules persist in the liquid phase (11). Previous studies of the vaporisation of Group III

halides (13 - 19) have indicated that dimeric molecules are also present in the vapour phase at low temperatures, with increasing dissociation to the monomer as the temperature is increased. Further decomposition to the monohalide at higher temperatures has also been reported (17), and these dissociation reactions are clearly reflected in the IR spectra shown in Figure 3.

4.2 Vibrational Analysis

4.2.1 Indium Tri-iodide Monomer

Electron diffraction studies (18) have shown that the InI_3 molecule has a planar triangular shape (D_{3h} symmetry). The normal coordinate analysis gives the following expressions for the vibration frequencies:

$$\lambda_1 = \mu_1 F_{11} \qquad A_1' \text{ symmetry}$$

$$\lambda_2 = (\mu_I + 3\mu_{In}) F_{22} \qquad A_2'' \text{ symmetry}$$

$$\lambda_3 + \lambda_4 = (1.5\mu_{In} + \mu_I)\ \{F_{33} + 3F_{44}\} + 3\sqrt{3}\ \mu_{In} F_{34}$$

$$\lambda_3\lambda_4 = 3(\mu_I^2 + 3\mu_{In}\mu_I)\ (F_{33}\ F_{44} - F_{34})$$

both E symmetry

where μ_{In} and μ_I are the reciprocal masses of the atoms, $F_{11} = (F_r + 2F_{rr})$, $F_{22} = (F_\sigma + 2F_{\sigma\sigma})$, $F_{33} = (F_r - F_{rr})$, $F_{44} = (F_\theta - F_{\theta\theta})$, $F_{34} = (F_{r\theta} - F_{r\theta'})$ and the potential constants are defined by

$$2V = F_r \sum_i (\Delta r_i)^2 + F_\theta \sum_i (r_o \Delta\theta_i)^2 + F_\sigma \sum_i (r_\sigma \Delta\sigma_i)^2$$

$$+ F_{rr} \sum_{i,j} \Delta r_i \Delta r_j + F_{\theta\theta} \sum_{i,j} r_o^2 \Delta\theta_i \Delta\theta_j$$

$$+ F_{\sigma\sigma} \sum_{i,j} r_o^2 \Delta\sigma_i \Delta\sigma_j + F_{r\theta} \sum_{i,j} r_o \Delta r_i \Delta\theta_j$$

$$+ F_{r\theta'} \sum_{i,k} r_o \Delta r_i \Delta\theta_k$$

in which the r_is represent the In-I bond lengths, the θ_i's the I-In-I angles, and σ the angle between the In-I bond and the I-In-I plane.

Both of the E modes, and the out-of-plane A_2" mode, are predicted to be active in the infrared. The observed band at 236 cm^{-1} can be assigned as $\bar{\nu}_3$, which can be largely identified with In-I bond stretching. $\bar{\nu}_2$ and $\bar{\nu}_4$ are principally bending modes, and may be expected to occur at frequencies beyond the range of these studies.

Previous studies of gas-phase InI_3 by infrared (8) and Raman (19) spectroscopies have placed the $\bar{\nu}_1$, $\bar{\nu}_2$ and $\bar{\nu}_4$ frequencies at 151, 56 and 44-48 cm respectively.

The eight force constants in the above expressions cannot be uniquely determined since there are only four known frequency values. The following set of force constants were obtained from SOTONVIB calculations based on the observed in-plane frequencies, and the out-of-plane constant was determined from the expression for λ_2 given above.

F_{11} = 170.5 N m^{-1}
F_{22} = 5.45 N m^{-1}
F_{33} = 154.2 N m^{-1}
F_{44} = 3.02 N m^{-1}
F_{34} = 0.48 N m^{-1}

From the F_{11} and F_{33} values, it is possible to obtain

$$F_r = 159.6 \text{ N m}^{-1}$$

$$F_{rr} = 5.44 \text{ N m}^{-1}$$

4.2.2 Indium Tri-iodide Dimer

The representation of all the vibrational modes of the bridged dimer molecule with the D_{2h} structure shown above reduces to:

$$\Gamma_{vib} = 4A_{1g} + B_{1g} + 2B_{2g} + 2B_{3g} + A_u + 3B_{1u} + 3B_{2u} + 2B_{3u}$$

The symmetry species are assigned on the basis that the ring lies in the xz plane as shown. Reference to character tables shows that only the B_{1u}, B_{2u} and B_{3u} species are infrared active.

The four observed frequencies of In_2I_6 can all be assigned to modes which are predominantly In-I stretching vibrations. Treating the terminal and bridging In-I bonds separately gives the following representations:

$$\Gamma_t = A_g + B_{3g} + B_{1u} + B_{2u}$$

$$\Gamma_b = A_g + B_{2g} + B_{1u} + B_{3u}$$

There are therefore predicted to be four infrared active stretching modes ($2B_{1u} + B_{2u} + B_{3u}$), in agreement with the observed spectrum. On the basis of previous condensed-phase studies, the four bands can be assigned as follows:

231 cm^{-1} : B_{2u}
180 cm^{-1} : B_{1u}
} terminal stretch

160 cm^{-1} : B_{3u}
124 cm^{-1} : B_{1u}
} bridging stretch

5. CALCULATION OF THERMODYNAMIC FUNCTIONS

The excellent agreement between the frequencies observed for the matrix-isolated In_2I_6 molecule and those reported for the solid and liquid phases indicate that the structure and force field of the free dimer molecule are not significantly perturbed in the condensed phase. This is confirmed by other reported studies of gas-phase or matrix-isolated M_2X_6 molecules (7, 13-19). It is therefore justifiable to assume previously-reported condensed-phase values for the frequencies not observed in the present work. Of the eighteen normal frequencies of the In_2I_6 molecule, fifteen have been evaluated by infrared and Raman spectroscopy. The exceptions are the B_{2u} InI_2 rocking mode, the A_u InI_2 twisting mode (which has no infrared or Raman activity), and the B_{2u} ring deformation. The first two of these have been calculated by Adams (20) on the basis of a thirteen-parameter force field; the ring deformation was not included in these calculations since no data were available to indicate the magnitude of the relevant force constant. Studies of the diborane molecule (20) indicate that the frequency of this mode is substantially lower than all the other frequencies, and a value of 15 cm^{-1} was therefore adopted in the present calculations. The moments of inertia were calculated on the basis of the established solid-phase structure (21):

In-I (terminal) = 0.264 nm

In-I (bridging) = 0.284 nm

I-In-I (terminal) = 125.1°

I-In-I (ring) = 93.7°

The symmetry number of the D_{2h} structure is 4, and the degeneracy of the electronic ground state was taken to be unity.

Experimental values are available for all the vibration frequencies of the InI_3 molecule. The moments of inertia were calculated on the basis of a D_{3h} structure (symmetry number 6) with In-I bond lengths of 0.264 nm. The electronic ground state degeneracy is unity.

The argon matrix frequency of the InI vibration is lowered by about 10 cm^{-1} compared to the gas-phase value. This fairly significant matrix shift is typical of a polar molecule (22), and can be attributed to inductive interactions between the matrix and the trapped molecules (see Chapter 3). The gas-phase value of 177 cm^{-1} (9) has therefore been used in the calculation, and the In-I distance was taken as 0.275 nm (23). The symmetry number and electronic ground state degeneracy of the molecule are both unity.

The thermodynamic functions calculated for these three molecules are tabulated in Appendix 3. The frequencies and other input data are shown at the head of each tabulation.

5.1 Vaporisation Behaviour and Thermodynamics

The vapour pressure of solid indium tri-iodide in the temperature range 100 to 130°C has been determined (24); these results fitted the expression

$$\ln p\ (atm) = 21.27 - 13900/T(K)$$

and the enthalpy of sublimation over this temperature range was thus evaluated as 115.6 kJ mol^{-1}. The heat of vaporisation of liquid InI_3 at 163°C was estimated as 88.2 kJ mol^{-1}. A more extensive study of the vaporisation of

liquid InI_3 (25) reported the heat of vaporisation over the temperature range 200 to 300°C as 95.3 kJ mol^{-1}; however, the reliability of this value is difficult to judge since it is not consistent with the data given. The reported vapour pressure data fit the equation

$$\ln p\ (atm) = 13.58 - 10310/T(K)$$

which gives the vaporisation enthalpy as 85.7 kJ mol^{-1}.

The above results apply to the reaction

$$2InI_3(c) \rightarrow In_2I_6\ (g) \qquad [1]$$

and the enthalpy of this reaction at 298 K is given by

$$\Delta H_{298} = \Delta H_T - \Delta(H_T - H_{298})$$

The enthalpy functions of solid and liquid indium tri-iodide have not been evaluated. If the corresponding functions for AlI_3 (26) are used, the sublimation and vaporisation enthalpies for InI_3 at 298K can be estimated as 118 and 98 kJ mol^{-1} respectively. The heat of fusion of InI_3 is therefore estimated to be 10 kJ mol^{-1}. This is in reasonable agreement with the value of 14 kJ mol^{-1} obtained by differential thermal analysis (27). Combining the sublimation enthalpy with the heat of formation of solid InI_3 (-238 kJ mol^{-1} (28)) gives the enthalpy of formation of $In_2I_6(g)$ as -358 kJ mol^{-1}.

Measurement of the vapour pressure of indium tri-iodide above 300°C is complicated by the increasing degree of dissociation of the dimer (17, 23). The equilibrium constant for the reaction

$$In_2I_6(g) \rightleftharpoons 2InI_3(g) \qquad [2]$$

has been found to fit the equation

$$\ln K_p \text{ (atm)} = 14.24 - 10690/T(K)$$

over the temperature range 440 to 660°C (18). The enthalpy and entropy of dissociation in this temperature range are therefore 88.7 kJ mol^{-1} and 118.3 J mol^{-1} K^{-1} respectively. The thermodynamic functions tabulated in Appendix 3 can be used to calculate the reaction enthalpy at 289 K by either the second or third law method; these two methods give values of 97.1 and 120.7 kJ mol^{-1} respectively. The discrepancy between these two results is reflected in the rather poor agreement between the entropy change calculated from the tabulated data (149 J mol^{-1} K^{-1}) and that given above. The enthalpy of reaction [2] can also be calculated from the formation enthalpies of the monomer and dimer gases, which are -116.4 (23) and -358 kJ mol^{-1} respectively. This gives a value of 125.2 kJ mol^{-1}, in reasonable agreement with the third law value obtained above.

The enthalpy and entropy changes for the dissociation reaction

$$InI_3(g) \rightleftharpoons InI(g) + I_2(g) \qquad [3]$$

have been calculated from pressure measurements in the temperature ranges 475 to 950°C (23) and 800 to 980°C (17). These two studies gave the following expressions for the equilibrium constant of [3]:

$$\ln K_p \text{ (atm)} = 12.03 - 19773/T(K) \qquad 800\text{-}980°C$$

(ΔH_T = 164.2 kJ mol^{-1}, ΔS_{1200} = 100 J mol^{-1} K^{-1}) (17)

and $\ln K_p$ (atm) = 15.77 - 21644/T(K) 475 - 950°C

(ΔH_T = 179.7 kJ mol^{-1}, ΔS_{1000} = 130.8 J mol^{-1} K^{-1}) (23)

Using the data in Appendix 3 for InI_3 and InI, together with the JANAF tabulation for I_2 (26) gives the corresponding reaction enthalpies at 298 K as 171.1 and 185.1 kJ mol^{-1} (2nd law method) and 191.0 and 171.2 kJ mol^{-1} (3rd law method), and the calculated entropy change is 116 J mol^{-1} K^{-1}. The enthalpy change for reaction [3] can also be calculated from the heats of formation of the reactants. Literature values are available for I_2(g) (62.38 kJ mol^{-1} (26)) and InI_3(g) (-116.4 kJ mol^{-1} (23)), but the reported data for InI(g) (23) are rather inconsistent. A value of 13.8 kJ mol^{-1}, based on vapour pressure data (see below) has therefore been used. The enthalpy of reaction [3] at 298 K can thus be estimated as 192.6 kJ mol^{-1}, which is again in reasonable agreement with that obtained from the third law treatment of the data of Zaidova et al (17).

A number of studies have been made on the vaporisation of indium monoiodide (29 - 32). The vapour pressure above solid (29) and liquid (30 - 32) indium monoiodide have been determined, and the enthalpies of sublimation and vaporisation obtained at a variety of temperatures. Enthalpy and heat capacity functions for solid and liquid InI have been derived (32), and these can be used to estimate the enthalpies of sublimation at 298 K. The results obtained from three of the sets of data (29, 30, 32) were in excellent agreement, giving values of 130 ± 1 kJ mol^{-1}, whilst the remaining result (31) was somewhat lower at 122 kJ mol^{-1}. The enthalpy of formation of InI(s) at 298 K has been reported as -116.2 kJ mol^{-1} (33); the heat of formation of InI(g) can thus be estimated as 13.8 kJ mol^{-1}.

The thermodynamic quantities discussed above are summarised in Table 3. These data can be used in conjunction with the tabulated functions in Appendix 3 to calculate the equilibrium contents of reactions [2] and [3] at selected temperatures (Table 4).

6. CONCLUSIONS

The vaporisation behaviour of indium tri-iodide has been studied using mass spectrometry and matrix isolation-infrared spectroscopy.

Dimeric In_2I_6 molecules predominated in the vapour at low temperatures, with increasing dissociation to InI_3 and then InI as the temperature was increased.

The infrared studies indicated that the structure and vibration frequencies of the matrix-isolated In_2I_6 molecule were practically identical to those of the solid-phase compound. This allowed the use of previously-determined Raman and low-frequency data in calculating the thermodynamic functions of the dimer molecule.

The measured infrared frequency for matrix-isolated InI_3 was used in conjunction with gas-phase Raman data to calculate the thermodynamic functions of this molecule. The vibration frequency of the InI molecule in an argon matrix was shifted by about 10 cm^{-1} with respect to the gas-phase value, and so the latter was used in calculating the thermodynamic functions.

Previous studies of the vaporisation behaviour and thermodynamics of the indium-iodine system were discussed. The equilibrium constants of the gas-phase dissociations of In_2I_6 and InI_3 were evaluated over the temperature range 500 to 2500°C.

TABLE 3

SUMMARY OF THERMODYNAMIC DATA FOR THE INDIUM-IODINE SYSTEM

$In_2I_6\ (g) = 2InI_3(g)$ $\quad \Delta H_{298} = 121\ kJ\ mol^{-1}$

$InI_3\ (g) = InI(g) + I_2(g)$ $\quad \Delta H_{298} = 191\ kJ\ mol^{-1}$

$\Delta H_{f,298}\ (In_2I_6(g)) = -358\ kJ\ mol^{-1}$

$\Delta H_{f,298}\ (InI_3(g)) = -116.4\ kJ\ mol^{-1}$ (ref 23)

$\Delta H_{f,298}\ (InI(g)) = 13.8\ kJ\ mol^{-1}$

$\Delta H_{sub,298}\ (In_2I_6) = 118\ kJ\ mol^{-1}$

$\Delta H_{sub,298}\ (InI) = 130\ kJ\ mol^{-1}$

TABLE 4

EQUILIBRIUM CONSTANTS OF INDIUM IODIDE GAS-PHASE DISSOCIATION REACTIONS AT SELECTED TEMPERATURES

1. $In_2I_6(g) = 2InI_3(g)$ $\Delta H_{298,r} = 121$ kJ mol^{-1}

Temp (K)	$\Delta\emptyset^*$ (J mol^{-1} K^{-1})	ΔG_T (kJ mol^{-1})	K_p (atm)
500	162.2	39.9	6.7×10^{-5}
1000	155.6	-34.6	6.7×10^{1}
1500	150.4	-104.6	4.4×10^{3}
2000	146.5	-172.0	3.0×10^{4}
2500	143.3	-237.4	8.9×10^{4}

2. $InI_3(g) = InI(g) + I_2(g)$ $\Delta H_{298,r} = 191$ kJ mol^{-1}

Temp (K)	$\Delta\emptyset^*$ (J mol^{-1} K^{-1})	ΔG_T (kJ mol^{-1})	K_p (atm)
500	126.2	127.9	2.3×10^{-13}
1000	123.2	68.7	2.9×10^{-4}
1500	120.8	9.8	4.6×10^{-1}
2000	119.0	-47.0	1.7×10^{1}
2500	117.6	-102.9	1.4×10^{2}

* $\emptyset = -(G_T - H_{298})/T$

REFERENCES

1. Beard, A M, Benson, C G and Bowsher, B R, UKAEA Report AEEW-R 2470, 1988.

2. Bowsher, B R, Prog Nucl Energy, 20, 199, 1987.

3. Beard, A M, Bowsher, B R, Dickinson, S, and Nichols, A L, 2nd ACS Symposium on Nuclear Reactor Severe Accident Chemistry, Toronto, 7-10 June 1988.

4. Dickinson, S, UKAEA Report AEEW-R 2227, 1987.

5. Adams, D M, and Churchill, R G, J Chem Soc (A), 2141, 1968.

6. Beattie, I R, Gilson, T and Ozin, G A, J Chem Soc (A), 813, 1968.

7. Perov, P A, Nedyak, S V and Mal'tsev, A A, Vestn Mosk Univ Khim, 15, 201, 1974.

8. Selivanov, G K and Mal'tsev, A A, Zh Strukt Khim, 14, 943, 1973.

9. Nakamoto, K, "Infrared and Raman Spectra of Inorganic and Coordination Compounds", 3rd ed, John Wiley and Sons, New York, 1978.

10. Kniep, R, Bless, P and Poll, W, Angew Chem, 94, 370, 982.

11. Bues, W., Akhras, Z and Okon, G. Z Anorg Allg Chem, 425, 193, 1976.

12. Klemm, W, Z Anorg Chem, 152, 252, 1926; and Klemm, W, Z Anorg Chem, 163, 240, 1927.

13. Radloff, P L and Papatheodorou, G N, J Chem Phys, 72, 992, 1980.

14. Rytter, E, Einarsrud, M A and Sjφgren, C E, Spectrochim Acta, 42A, 1317, 1986.

15. Tomita, T, Sjφgren, C E, Klaeboe, P, Papatheodorou, G N and Rytter, E, J. Raman Spectrosc, 14, 415, 1983.

16. Sjφgren, C E, Klaeboe, P and Rytter, E, Spectrochim Acta 40A, 457, 1984.

17. Zaidova, G A, Gadzhiev, S M and Kuliev, A A, Russ J Phys Chem, 48, 617, 1974.

18. Giricheva, N I, Petrov, V M, Girichev, G V, Titov, V A, Chusova, T P and Kokovin, G A, Izv Sib Otd Akad Nauk SSSR, Ser Khim Nauk, (3), 23, 1986.

19. Beattie, I R and Horder, J R, J Chem Soc (A), 2655, 1969.

20. Adams, D M and Churchill, R G, J Chem Soc (A), 697, 1970.

21. Cotton, F A and Wilkinson, G, "Advanced Inorganic Chemistry", 4th ed, John Wiley and Sons, New York, 1980.

22. Downs, A J and Peake, S C, Mol Spectrosc, 1, 523, 1973.

23. Grinberg, Y K, Boryakova, V A and Shevel'kov, V F, Izv Akad Nauk SSSR, Neorg Mater, 12, 402, 1976.

24. Smith, F J and Barrow, R F, Trans Faraday Soc, 54, 826, 1958.

25. Fedorov, P I, Dudareva, A G and Drobot, N F, Russ J Inorg Chem, 8, 667, 1963.

26. JANAF Thermochemical Tables, 2nd ed, NSRDS-NBS 37, 1971.

27. Newland, M S, Private Communication, Winfrith Technology Centre, 1989.

28. CRC Handbook of Chemistry and Physics, 64th ed, CRC Press, Boca Raton, 1984.

29. Barrow, R F, Pugh, A C P and Smith, F J, Trans Faraday Soc, 51, 1657, 1955.

30. Grinberg, Y K, Boryakova, V A, Shevel'kov, V F and Medvedeva, Z S, Izv Akad Nauk SSSR, Neorg Mater, 8, 67, 1972.

31. Fedorov, P I, Malova, N S and Denisov, Y N, Russ J Inorg Chem, 21, 640, 1976.

32. Chusova, T P, Stenin, G G, Titov, V A, Kokovin, G A and Karpova, T D, Izv Sib Otd Akad Nauk SSSR, Ser Khim Nauk, 6, 62, 1983.

33. Smith, F J and Barrow, R F, Trans Faraday Soc, 51, 1748, 1955.

APPENDIX 1

LISTINGS OF COMPUTER PROGRAMS 'TDFUN2' AND 'INERTS'

```
10      REM   TDFUN  by S Dickinson, February 1987
                Version 1.2, March 1989
                Mod 3, 04-09-89
                Program calculates thermodynamic functions from
                vibrational data
100     GOSUB DO_IT      (go to main body of program)
120     REM variables used...
        in subroutine INITIALISE
        fundamental constants:  R,H,KB,CC,NA     KON=H*CC/KB
        rotational constants & product:          BMIN,A,B,C,PR
        atm. pressure and pressure factor:       P,PF
        anharmonicity correction:                ANH$, XEWE
        functions:      FNVIB(X,T),FNROT1(X),FNROT2(X)TR
        in subroutine ANHARM
        VIB0, VIBE, XE, DE, GAMMA, DELTA, U, ANT1, ANT2
        in subroutine ENTHALPY
        HTR,HR,HV,
        HT1,HT2,HT3,HTA
        H0(),HREL()
        frq counter: F
        SUM,VIB,X,Y
        in subroutine HEAT_CAPACITY
        CPTR,CPR,CPV
        CPT1,CPT2,CPT3,CPT4
        CPA,CP0()
        frq counter: F
        SUM,VIB,X,Y
        in subroutine ENTROPY
        T1,T2,t3a,t3b,t3c,T3,T4
        STR,SR,SV,SE
        ST1,ST2,ST3,ST4
        STA,S0()
        frq counter: F
        SUM1,SUM2,X,Y
        in subroutine FREE_ENERGY
        FRELTR,FRELR,FRELV,FRELE
        FT1,FT2,FT3,FTA
        FREL0(),FREL()
        in subroutine SUMS
        ordering temps: X,MJ,S()
        NT,T()
        counter I,J,L,TEMP
        rot const B , ABC
        in subroutine  SYMNO
        C$,N$,N,LIN$,SIGMA
        in subroutine FILE_READ
        FILE$
        MOL$,M,P$
        R1$  [R/M]
        R2$  [S/P]
        BMIN,A,B,C,PR
        NF,FRQ()
        counter I
        EDEG [degeneracy of electronic ground state)
        TF,TL,TI,PF,TREF
        XEWE [anharmonicity correction]

200     REM   data is read in from a file which should have
```

```
            the extension .tdi
        The file should have the following format:
        Run title
        Molecule name, molecular mass, point group
          then for LINEAR molecules:
        M,I(B) or R,B
          for NON_LINEAR molecules:
        M,S,              (moments of inertia, separately)
        I(A),I(B),I(C)    or
        R,S               (rotational constants, separately)
        A,B,C             or
        M,P               (moments of inertia, product)
        I(A)*I(B)*I(C)    or
        R,P               (rotational constants, product)
        A*B*C
           then
        number of fundamentals
        frq 1
        frq 2
         .
         .
         .
        frq n
        electronic ground state degeneracy,
        start temp, end temp, interval, pressure factor, ref temp,
        anharmonicity correction

        all frqs in cm-1
        moments of inertia in amu.nm
        rotational constants in m
        temperatures in K
        molecular wt in amu

299     GO$="y"

 DO_IT:

300     GOSUB INITIALISE
305     GOSUB SET_TT14
310     GOSUB FILE_READ
315     GOSUB FORMATS
320     GOSUB SUMS
330     GOSUB SHOW
340     GOSUB RESET_TT14
399     GOTO 9999

 SET_TT14:       (set up printer)

400     OPEN "TT14:" FOR OUTPUT AS FILE£1
        PRINT£1,"<csi>2w<csi>z<csi>72t<csi>9;99s<csi>2;66r"
        CLOSE£1
        RETURN

 RESET_TT14:

410     OPEN "TT14:" FOR OUTPUT AS FILE£1
        PRINT£1,"<csi>72t<csi>2;66r"
        CLOSE£1
        RETURN
```

```
 INITIALISE:

500      REM define constants
510      R=8.3143
         H=6.6262E-34
         KB=1.38062E-23
         CC=2.99792E10
         NA=6.02217E23
520      KON=H*CC/KB
530      DIM T(40),FRQ(40)
         DIM H0(40),HREL(40)
         DIM CP0(40),S(40),S0(40)
         DIM FREL(40),FREL0(40)
535      TREF=298
         A=1
         B=1
         C=1
         PR=1
         P=1.0132E5
         PF=1
         XEWE=0
         ANH$="N"
         HTA=0
         CPTA=0
         STA=0
         FTA=0
540      FOR I=1 TO 20
         H0(I)=0
         HREL(I)=0
550      NEXT I
560      RETURN

700      DEF FNVIB(X,T)=EXP(-1*X*KON/T)
         DEF FNROT1(X)=(H*NA*1E23)/(8*PI^2*CC*X)
         DEF FNROT2(X)=((H*NA*1E23)/(8*PI^2*CC))^3/X

 ANHARM:

1000     IF ANH$="N" THEN RETURN
1010     U=KON*VIB0/T
         ANT1=8*GAMMA/U
         ANT2=EXP(U)-1
1020     RETURN

 ENTHALPY:

1120     HTR=2.5*R*T
         SUM=0
1130     IF LIN$="L" THEN HR=R*T ELSE HR=1.5*R*T
1140     FOR F=1 TO NF
         VIB=FRQ(F)
         X=(VIB*FNVIB(VIB,T))
         Y=1-(FNVIB(VIB,T))
         SUM=SUM+X/Y
         NEXT F
         HV=R*KON*SUM
1150     IF ANH$="N" THEN 1170
1160     HT1=ANT1
```

```
        HT2=U*(DELTA*EXP(U)-2*XE)/ANT2^2
        HT3=4*XE*U^2*EXP(U)/ANT2^3
        HTA=R*T*(HT1+HT2+HT3)
1170    HO(TEMP)=HTR+HR+HV+HTA
1180    HREL(TEMP)=HO(TEMP)-HO(0)
1200    RETURN

 HEAT_CAPACITY:

1405    CPTR=2.5*R
        IF LIN$="L" THEN CPR=R
        ELSE CPR=1.5*R
1410    SUM=0

1420    FOR F=1 TO NF
        VIB=FRQ(F)
        X=VIB^2*FNVIB(VIB,T)
        Y=(1-FNVIB(VIB,T))^2
        SUM=SUM+X/Y
        NEXT F
1430    CPV=R*(KON/T)^2*SUM
1440    IF ANH$="N" THEN 1460
1450    CPT1=2*ANT1
        CPT2=DELTA*U^2*EXP(U)/ANT2^2
        CPT3=U^2*EXP(U)*(2*DELTA*EXP(U)-4*XE*U-8*XE)/ANT2^3
        CPT4=12*XE*U^3*EXP(2*U)/ANT2^4
        CPA=R*(CPT1-CPT2+CPT3+CPT4)
1460    CPO(TEMP)=CPTR+CPR+CPV+CPA
1500    RETURN

 ENTROPY:

1720    T1=(2.5*R*LOG(T))
        T2=(1.5*R*LOG(M))
        T3a=(1.5*LOG(2*PI/NA))
        t3b=(2.5*LOG(KB))
        t3c=(3*LOG(H))
        t3=r*(t3a+t3b-t3c)
        T4=(2.5*R) - (R*LOG(P))
1730    STR=T1+T2+T3+T4
1735    IF LIN$="L" THEN
        SR=R*(LOG(T)-LOG(KON/100)-LOG(B)- LOG(SIGMA)+1)
        GOTO 1740
1736    T1=(3*LOG(T))
        T2=LOG(ABC)
        T3=(2*LOG(SIGMA))
        T4=LOG(PI/((KON/100)^3))
        SR=(R/2)*(T1-T2-T3+T4+3)
1740    SUM1=0
        SUM2=0
1750    FOR I=1 TO NF
        VIB=FRQ(I)
        X=VIB*FNVIB(VIB,T)
        Y=1-FNVIB(VIB,T)
        SUM1=SUM1+LOG(Y)
        SUM2=SUM2+(X/Y)
        NEXT I
1760    SV=-1*R*SUM1+R/T*KON*SUM2
1770    SE=R*LOG(EDEG)
```

```
1780    IF ANH$="N" THEN 1800
1790    ST1=2*ANT1
        ST2=DELTA/ANT2
        ST3=DELTA*U*EXP(U)/ANT2^2
        ST4=4*XE*U^2*EXP(U)/ANT2^3
        STA=R*(ST1+ST2+ST3+ST4)
1800    S0(TEMP)=STR+SR+SV+SE+STA
1810    RETURN

 FREE_ENERGY:

2000    FRELTR=STR-(HTR/T)
        FRELR=SR-(HR/T)
        FRELV=SV-(HV/T)
        FRELE=SE
2010    IF ANH$="N" THEN 2030
2020    FT1=ANT1
        FT2=DELTA/ANT2
        FT3=2*XE*U/ANT2^2
        FTA=R*(FT1+FT2+FT3)
2030    FREL0(TEMP)=FRELTR+FRELR+FRELV+FRELE+FTA
        FREL(TEMP)=FREL0(TEMP)+H0(0)/T
2040    RETURN

 SHOW:

2200    REM   print out results on VDU
2210    PRINT TITLE$
        PRINT MOL$
2220    FMA$="££££   ££££££££.£  ££££££££.£  "
        FMB$="  £££.££      £££.££      £££.££      £££.££"
        FM$=FMA$+FMB$
2230    PRINT
        PRINT"Temp      HT-H0      HT-Href  ";
        PRINT"    Cp(T)       S(T)    -(GT-H0)/T  -(GT-Href)/T"
        PRINT"  K       J/mol      J/mol    ";
        PRINT"  J/mol/k     J/mol/K    J/mol/K     J/mol/K"
        PRINT
2240    FOR T=1 TO NT
        PRINT USING FM$, T(T),H0(T),HREL(T),CP0(T),S0(T),frel0(T),frel(T)
        NEXT T
2250    INPUT "Hard copy (y/n) ";R$
2260    IF R$="N" OR R$="n" THEN 2360
2300    REM   print£1 out results on printer
2305    OPEN "TT14:" FOR OUTPUT AS FILE£1
2310    PRINT£1
        PRINT£1,TITLE$
        PRINT£1,DATE$(0),TIME$(0)
        PRINT£1
        PRINT£1,"Input data read from ";FILE$;":"
        PRINT£1
        PRINT£1, MOL$
        PRINT£1,"molecular weight :";M;" kg.mol^-1"
        PRINT£1,"point group      : ";P$
2315    IF LIN$="L" THEN PRINT£1 USING MINF$,BMIN
        ELSE IF R2$="P" THEN PRINT£1 USING MINF$,PR
        ELSE IF R2$="S" THEN PRINT£1 USING MINF$,A,B,C
2316    PRINT£1
        PRINT£1,"vibration frequencies (cm-1)"
```

```
        FOR I=1 TO NF
        PRINT£1,FRQ(I);
        IF INT(I/10) = I/10 THEN PRINT£1
        END IF
        NEXT I
        PRINT£1
2317    IF PF<>1 THEN PRINT£1,"Pressure :";P;"Pa"
2320    PRINT£1, "Reference temperature = ";TREF;"K"
        PRINT£1, "Electronic ground state degeneracy = ";EDEG
        IF ANH$="Y" THEN PRINT£1, "Anharmonicity Correction (xewe) = ";XEWE
2330    PRINT£1
        PRINT£1,"Temp      HT-H0      HT-Href   ";
        PRINT£1,"    Cp(T)       S(T)    -(GT-H0)/T  ";
        PRINT£1,"-(GT-Href)/T"
        PRINT£1,"  K       J/mol      J/mol     ";
        PRINT£1,"  J/mol/K     J/mol/K    J/mol/K     J/mol/K"
        PRINT£1
2340    FOR T=1 TO NT
        PRINT£1 USING FM$, T(T),H0(T),HREL(T),CP0(T),S0(T),frel0(T),frel(T)
        IF INT(T(T)/500) = T(T)/500 THEN PRINT£1
        END IF
2345    NEXT T
        PRINT£1,"<ff>"
2350    CLOSE£1
2360    RETURN

 SUMS:

2500    P=P*PF
        M=M/1000
2505    IF LIN$="L" THEN GOSUB ROTA_1 ELSE GOSUB ROTA_2

2509    REM     Temperature Ordering
2510    IF TF>TL THEN X=TF / TF=TL / TL=X
2520    NT=(TL-TF)/TI+1
        IF INT((TL-TF)/TI) <> (TL-TF)/TI THEN NT=NT+1
2530    FOR I=1 TO NT-1
        T(I)=(TF-TI)+(I*TI)
        NEXT I
2535    T(NT)=TL
2540    FOR J=1 TO NT
        IF T(J)<TREF THEN GOTO 2546
        ELSE IF T(J)=TREF THEN GOTO 2610
        ELSE IF T(J)>TREF THEN GOTO 2550
        END IF
2546    NEXT J
2550    NT=NT+1
        MJ=J
2560    FOR L=J+1 TO NT
        S(L)=T(L-1)
        NEXT L
2570    FOR L=(J+1)TO NT
        T(L)=S(L)
        NEXT L
2580    T(MJ)=TREF
2590    IF T(NT)<TREF THEN NT=NT+1
        T(NT)=TREF

2599    REM     Anharmonicity functions
```

```
2600    IF ANH$="N" THEN 2610
        END IF
        VIBO=FRQ(1)
        VIBE=VIBO+2*XEWE
        XE=XEWE/VIBE
        DE=4*B^3/VIBE^2
        GAMMA=0.5*SQR(DE/B)
        DELTA=6*SQR(GAMMA)*(SQR(XE)-SQR(GAMMA))

2610    REM     Calculate enthalpy functions
2620    TEMP=0
        T(TEMP)=TREF
        T=T(TEMP)
        GOSUB ANHARM
        GOSUB ENTHALPY
2630    FOR TEMP=1 TO NT
        T=T(TEMP)
2640    GOSUB ANHARM
        GOSUB ENTHALPY
        GOSUB HEAT_CAPACITY
        GOSUB ENTROPY
        GOSUB FREE_ENERGY
        NEXT TEMP
2660    RETURN

 ROTA_1:        (rotational constant - linear)

2700    IF LIN$="N" THEN GOTO 2720
2710    IF R1$="M" THEN B=FNROT1(BMIN)
2715    IF R1$="R" THEN B=BMIN
2720    RETURN

 ROTA_2:        (rotational constant - non linear)

2800    IF LIN$="L" THEN GOTO 2840
2810    IF R2$="S" THEN PR=A*B*C
2820    IF R1$="M" THEN ABC=FNROT2(PR)
2830    IF R1$="R" THEN ABC=PR
2840    RETURN

 SYMNO:

2900    C$=MID$(P$,1,1)
        N$=MID$(P$,2,1)
        IF N$="I" OR N$="S" OR N$="i" OR N$="s" THEN N$="1"
2910    N=VAL(N$)
        IF N=0 THEN LIN$="L" ELSE LIN$="N"
2915    IF N=0 THEN N=1
2920    IF C$="C" or C$="c" THEN SIGMA=N else
        IF C$="D" or C$="d" THEN SIGMA=N*2 else
        IF C$="S" or C$="s" THEN SIGMA=N/2 else
        IF C$="T" or C$="t" THEN SIGMA=12 else
        IF C$="O" or C$="o" THEN SIGMA=24
2930    RETURN

 FILE_READ:

3000    INPUT "Filename ";FILE$
3010    X=LEN(FILE$)-4
```

```
        Y$=MID$(FILE$,X,1)
        IF Y$="." THEN GOTO 3200
        ELSE FILE$=FILE$+".tdi"
3200    OPEN FILE$ FOR INPUT AS FILE£2
3220    INPUT£2,TITLE$
        INPUT£2; MOL$,M,P$
        GOSUB SYMNO
3230    IF LIN$="L" THEN INPUT£2; R1$,BMIN
        GOTO 3260
3240    IF LIN$="N" THEN INPUT£2; R1$,R2$
        IF R1$="r" THEN R1$="R" else
        IF R1$="m" THEN R1$="M" else
        IF R2$="s" THEN R2$="S" else
        IF R2$="p" THEN R2$="P"
3250    IF R2$="S" THEN INPUT£2; A,B,C
        ELSE INPUT£2; PR
3260    INPUT£2; NF
        FOR I=1 TO NF
        INPUT£2; FRQ(I)
        NEXT I
3270    IF NF=1 THEN INPUT£2; EDEG,TF,TL,TI,PF,TREF,XEWE
        ELSE INPUT£2; EDEG,TF,TL,TI,PF,TREF
3280    IF XEWE<>0 THEN ANH$="Y"
3300    CLOSE£2
3310    RETURN

 FORMATS:

4020    IF LIN$="N" THEN GOTO 4050
4030    IF R1$="M" THEN MINF$="I(B)              : £.£££^^^^ amu.nm^2"
        ELSE MINF$="B                 : £.£££^^^^ m"

4040    GOTO 4100
4050    IF R2$="S" THEN GOTO 4080
4060    IF R1$="M" THEN MINF$="I(A)*I(B)*I(C)    : £.£££^^^^ amu^3.nm^6"
        ELSE MINF$="A*B*C             : £.£££^^^^ m^3"
4070    GOTO 4100
4080    IF R1$="M" THEN MINFA$="I(A) : £.£££^^^^ amu.nm^2"
        MINFB$="I(B) : £.£££^^^^ amu.nm^2"
        MINFC$="I(C) : £.£££^^^^ amu.nm^2"
        MINF$=MINFA$+MINFB$+MINFC$
        GOTO 4100
4090    MINFA$="A : £.£££^^^^ m"
        MINFB$="B : £.£££^^^^ m"
        MINFC$="C : £.£££^^^^ m"
        MINF$=MINFA$+MINFB$+MINFC$
4100    RETURN
9999    END
```

```
10      rem INERTS  version 1.0  24 Feb 1988
        Program calculates product of moments of inertia
        from atomic masses and coordinates in amu,mn
100     rem   data read in from a file with extension .min
        data file format:
        run title
        mol$,no of atoms
          then for each atom:
        atom wt,x,y,z co-ordinates
          (co-ords can be relative to any origin)
200     gosub initialise
210     gosub read_file
220     gosub calc_1
230     gosub calc_2
240     gosub calc_3
250     gosub show
299     goto 9999

 initialise:

500     dim m(10),c(3,10),s1(3,3),s2(3)
        dim s3(3,3),i(3,3)
510     for i=1 to 3
        for j=1 to 3
        s1(i,j)=0
        s2(i)=0
        s3(i,j)=0
        next j
        next i
520     mass=0
530     return

 calc_1:

1000    for p=1 to 3
        for q=1 to 3
        if p>=q then 1020
1010    for i=1 to nat
        add1=(m(i)*(c(p,i)^2+c(q,i)^2))
        s1(p,q)=s1(p,q)+add1
        add2=(m(i)*c(p,i)*c(q,i))
        s3(p,q)=s3(p,q)+add2
        next i
1020    next q
1030    next p
1040    for p=1 to 3
        for i=1 to nat
        s2(p)=s2(p)+(m(i)*c(p,i))
        next i
        next p
1050    return

 calc_2:

1200    for i=1 to nat
        mass=mass+m(i)
        next i
1210    for p=1 to 3
        for q=1 to 3
```

```
        if p>=q then 1230
1220    i(p,q)=s3(p,q)-(s2(p)*s2(q))/mass
1230    next q
        next p
1240    for p=1 to 3
        q=(3*(p/3-int(p/3)))+1
        r=(3*((p+1)/3-int((p+1)/3)))+1
1250    if q>r then s1(q,r)=s1(r,q)
1260    i(p,p)=s1(q,r)-((s2(q)^2+s2(r)^2)/mass)
        next p
1270    return

 calc_3:

1400    t1=i(1,1)*i(2,2)*i(3,3)
        t2=-2*i(1,2)*i(1,3)*i(2,3)
        t3=-1*i(1,1)*i(2,3)^2
        t4=-1*i(2,2)*i(1,3)^2
        t5=-1*i(3,3)*i(1,2)^2
1410    prod=t1+t2+t3+t4+t5
1420    return

 read_file:

1600    input "Filename"; file$
1610    x=len(file$)-3
        y$=mid$(file$,x,1)
        if y$="." then goto 1620
        else file$=file$+".min"
1620    open file$ for input as file£1
1630    input£1, title$
        input£1, mol$,nat
1640    for i=1 to nat
        input£1,m(i),c(1,i),c(2,i),c(3,i)
        next i
1645    close£1
1650    return

 show:

1800    print "I(A)*I(B)*I(C) = ";prod;"amu^3.nm^6"
1810    input"Print out ";r$
1820    if r$="n" or r$="N" then 1880
1830    open "TT1:" for output as file£1
1840    print£1,title$
        print£1
        print£1,"Data read from ";file$
        print£1,mol$
        print£1,"     mass      x/nm      y/nm      z/nm"
        form$=  " ££   £££    ££.£££   ££.£££   ££.£££"
1850    for i=1 to nat
        print£1 using form$,i,m(i),c(1,i),c(2,i),c(3,i)
        next i
1860    print£1
        print£1,"I(A)*I(B)*I(C) = ";prod;"amu^3.nm^6"
1870    close£1
1880    return

9999    end
```

APPENDIX 2

F-G ANALYSIS OF A PLANAR M_2X_2 MOLECULE

F-G ANALYSIS OF A PLANAR M_2X_2 MOLECULE

1. DEFINITION OF INTERNAL COORDINATES

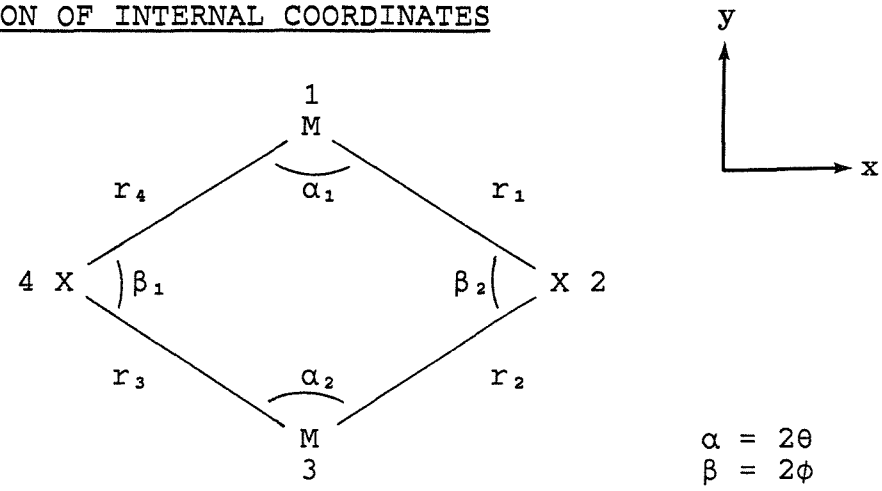

$\alpha = 2\theta$
$\beta = 2\phi$

$\underline{R}$ is the column matrix of internal coordinates

$$\underline{R} = \begin{bmatrix} \Delta r_1 \\ \Delta r_2 \\ \Delta r_3 \\ \Delta r_4 \\ \Delta\alpha_1 \\ \Delta\alpha_2 \\ \Delta\beta_1 \\ \Delta\beta_2 \end{bmatrix}$$

and $\tilde{\underline{R}}$ is its transpose:

$$\tilde{\underline{R}} = [\Delta r_1 \ \Delta r_2 \ \Delta r_3 \ \Delta r_4 \ \Delta\alpha_1 \ \Delta\alpha_2 \ \Delta\beta_1 \ \Delta\beta_2]$$

In terms of these internal coordinates, the potential and kinetic energies are

$$2V = \tilde{\underline{R}} \ \underline{F} \ \underline{R}$$

and $$2T = \dot{\tilde{\underline{R}}} \ \underline{G}^{-1} \ \dot{\underline{R}}$$

where $\underline{F}$ is the matrix of force constants, and $\underline{G}^{-1}$ is the reciprocal of the $\underline{G}$ matrix.

These matrices are related to the vibration frequencies $\bar{\nu}$ by the secular equation

$$\left| \underline{G}\,\underline{F} - \underline{E}\,\lambda \right| = 0 \qquad [1]$$

where $\lambda = 4\pi^2 c^2 \bar{\nu}^2$, and $\underline{E}$ is the unit matrix.

2. DEFINITION OF SYMMETRY COORDINATES

Solution of the secular equation is greatly simplified if symmetrised $\underline{G}$ and $\underline{F}$ matrices are used. The matrix of symmetry coordinates, $\underline{S}$, is formed by multiplying $\underline{R}$ by an orthogonal matrix $\underline{U}$, ie

$$\underline{S} = \underline{U}\,\underline{R} \qquad [2]$$

and then

$$\underline{F}_S = \underline{U}\,\underline{R}\,\tilde{\underline{U}} \quad \text{and} \quad \underline{G}_S = \underline{U}\,\underline{G}\,\tilde{\underline{U}} \qquad [3]$$

It can be shown that the secular equation

$$\left| \underline{G}_S\,\underline{F}_S - \underline{E}\,\lambda \right|$$

gives identical solutions to those obtained from the original $\underline{F}$ and $\underline{G}$ matrices.

Each symmetry coordinate belongs to one of the symmetry species of the molecular point group, and is formed using the equation:

$$S_i = N \sum_L \chi_i(L).L(R)$$

where N is a normalising factor, L is a symmetry operation and $\chi_i(L)$ is the character of L in the representation to which S belongs. L(R) is the internal coordinate into which the generator coordinate R is transformed by the operation L.

For the D_{2h} M_2X_2, molecule, using Δr_2, Δr_1 and $\Delta\beta_1$ as generators, the following symmetry coordinates are obtained:

$S_1 = \frac{1}{2}(\Delta r_1 + \Delta r_2 + \Delta r_3 + \Delta r_4)$
$S_2 = \sqrt{\frac{1}{2}}(\Delta\alpha_1 + \Delta\alpha_2)$ A_g species
$S_3 = \sqrt{\frac{1}{2}}(\Delta\beta_1 + \Delta\beta_2)$

$S_4 = \frac{1}{2}(\Delta r_1 - \Delta r_2 + \Delta r_3 - \Delta r_4)$ B_{1g} species

$S_5 = \frac{1}{2}(\Delta r_1 - \Delta r_2 - \Delta r_3 + \Delta r_4)$ B_{2u} species
$S_6 = \sqrt{\frac{1}{2}}(\Delta\alpha_1 - \Delta\alpha_2)$

$S_7 = \frac{1}{2}(\Delta r_1 + \Delta r_2 - \Delta r_3 - \Delta r_4)$ B_{3u} species
$S_8 = \sqrt{\frac{1}{2}}(\Delta\beta_1 - \Delta\beta_2)$

The $\underline{U}$ matrix is therefore

$$\underline{U} = \begin{bmatrix} \frac{1}{2} & \frac{1}{2} & \frac{1}{2} & \frac{1}{2} & 0 & 0 & 0 & 0 \\ 0 & 0 & 0 & 0 & \sqrt{\frac{1}{2}} & \sqrt{\frac{1}{2}} & 0 & 0 \\ 0 & 0 & 0 & 0 & 0 & 0 & \sqrt{\frac{1}{2}} & \sqrt{\frac{1}{2}} \\ \frac{1}{2} & -\frac{1}{2} & \frac{1}{2} & -\frac{1}{2} & 0 & 0 & 0 & 0 \\ \frac{1}{2} & -\frac{1}{2} & -\frac{1}{2} & \frac{1}{2} & 0 & 0 & 0 & 0 \\ 0 & 0 & 0 & 0 & \sqrt{\frac{1}{2}} & -\sqrt{\frac{1}{2}} & 0 & 0 \\ \frac{1}{2} & \frac{1}{2} & -\frac{1}{2} & -\frac{1}{2} & 0 & 0 & 0 & 0 \\ 0 & 0 & 0 & 0 & 0 & 0 & \sqrt{\frac{1}{2}} & -\sqrt{\frac{1}{2}} \end{bmatrix}$$

3. DEFINITION OF THE G MATRIX

The $\underline{G}$ matrix is defined by

$$\underline{G} = \underline{B}\ \underline{M}\ \tilde{\underline{B}} \qquad [4]$$

where $\underline{M}$ is a diagonal matrix whose elements are the reciprocal masses of the atoms, and $\underline{B}$ is the matrix which transforms cartesian to internal coordinates:

$$\underline{R} = \underline{B}\,\underline{X} \qquad [5]$$

where $\underline{X}$ is a column matrix whose components are the cartesian displacement coordinates.

$\underline{G}$ matrix elements for many types of coordinates have been tabulated, and it is possible to construct the $\underline{G}$ matrix from these and obtain the symmetrised form by the transformation given in [3]. However, it is more convenient to construct the symmetrised $\underline{G}_S$ matrix directly.

Combining [3] and [4]

$$\underline{G}_S = \underline{V}\,\underline{M}\,\tilde{\underline{V}} \quad \text{where} \quad \underline{V} = \underline{U}\,\underline{B}$$

The $\underline{U}$ matrix has already been defined; the $\underline{B}$ matrix is constructed by considering how each cartesian coordinate influences each internal coordinate. For the coordinate system used in the above diagram, the $\underline{B}$ matrix is given by:

$$\begin{bmatrix} \Delta r_1 \\ \Delta r_2 \\ \Delta r_3 \\ \Delta r_4 \\ \Delta \alpha_1 \\ \Delta \alpha_2 \\ \Delta \beta_1 \\ \Delta \beta_2 \end{bmatrix} = \begin{bmatrix} -S & C & S & -C & 0 & 0 & 0 & 0 \\ 0 & 0 & S & C & -S & -C & 0 & 0 \\ 0 & 0 & 0 & 0 & S & -C & -S & C \\ S & C & 0 & 0 & 0 & 0 & -S & -C \\ 0 & -2\rho S & \rho C & \rho S & 0 & 0 & -\rho C & \rho S \\ 0 & 0 & \rho C & -\rho S & 0 & 2\rho S & -\rho C & -\rho S \\ -\rho C & \rho S & 0 & 0 & -\rho C & -\rho S & 2\rho C & 0 \\ \rho C & \rho S & -2\rho C & 0 & \rho C & -\rho S & 0 & 0 \end{bmatrix} \begin{bmatrix} \Delta x_1 \\ \Delta y_1 \\ \Delta x_2 \\ \Delta y_2 \\ \Delta x_3 \\ \Delta y_3 \\ \Delta x_4 \\ \Delta y_4 \end{bmatrix}$$

$\underline{R}$ $\underline{B}$ $\underline{X}$

where S = sin θ, C = cos θ, and ρ is the reciprocal of the equilibrium M-X bond length. This gives

$$\underline{V} = \underline{U}\,\underline{B} = \begin{bmatrix} 0 & C & S & 0 & 0 & -C & -S & 0 \\ 0 & -\sqrt{2}\rho S & \sqrt{2}\rho C & 0 & 0 & \sqrt{2}\rho S & -\sqrt{2}\rho C & 0 \\ 0 & \sqrt{2}\rho S & -\sqrt{2}\rho C & 0 & 0 & -\sqrt{2}\rho S & \sqrt{2}\rho C & 0 \\ -S & 0 & 0 & -C & S & 0 & 0 & C \\ 0 & C & 0 & -C & 0 & C & 0 & -C \\ 0 & -\sqrt{2}\rho S & 0 & \sqrt{2}\rho S & 0 & -\sqrt{2}\rho S & 0 & \sqrt{2}\rho S \\ -S & 0 & S & 0 & -S & 0 & S & 0 \\ -\sqrt{2}\rho C & 0 & \sqrt{2}\rho C & 0 & -\sqrt{2}\rho C & 0 & \sqrt{2}\rho C & 0 \end{bmatrix}$$

$\underline{G}_S = \underline{V}\,\underline{M}\,\tilde{\underline{V}}$, where

$$\underline{M} = \begin{bmatrix} \mu_m & & & & & & & \\ & \mu_m & & & & & 0 & \\ & & \mu_x & & & & & \\ & & & \mu_x & & & & \\ & & & & \mu_m & & & \\ & 0 & & & & \mu_m & & \\ & & & & & & \mu_x & \\ & & & & & & & \mu_x \end{bmatrix}$$

The resulting G_S matrix has the structure:

$$\begin{bmatrix} G_{11} & G_{12} & G_{13} & & & & & \\ G_{12} & G_{22} & G_{23} & & & & 0 & \\ G_{13} & G_{23} & G_{33} & & & & & \\ & & & G_{44} & & & & \\ & & & & G_{55} & G_{56} & & \\ & & & & G_{56} & G_{66} & & \\ & 0 & & & & & G_{77} & G_{78} \\ & & & & & & G_{78} & G_{88} \end{bmatrix}$$

The four sub-matrices correspond to the different symmetry species:

$$\underline{G}_{A_1} = \begin{bmatrix} 2(C^2\mu_m+S^2\mu_x) & 2\sqrt{2}\rho SC(\mu_x-\mu_m) & 2\sqrt{2}\rho SC(\mu_m-\mu_x) \\ 2\sqrt{2}\rho SC(\mu_x-\mu_m) & 4\rho^2(S^2\mu_m+C^2\mu_x) & -4\rho^2(S^2\mu_m+C^2\mu_x) \\ 2\sqrt{2}\rho SC(\mu_m-\mu_x) & -4\rho^2(S^2\mu_m+C^2\mu_x) & 4\rho^2(S^2\mu_m+C^2\mu_x) \end{bmatrix}$$

$$\underline{G}_{B_{1g}} = \begin{bmatrix} 2(S^2\mu_m+C^2\mu_x) \end{bmatrix}$$

$$\underline{G}_{B_{2u}} = \begin{bmatrix} 2C^2(\mu_m+\mu_x) & -2\sqrt{2}\rho SC(\mu_m+\mu_x) \\ -2\sqrt{2}\rho SC(\mu_m+\mu_x) & 4\rho^2S^2(\mu_m+\mu_x) \end{bmatrix}$$

$$\underline{G}_{B_{3u}} = \begin{bmatrix} 2S^2(\mu_m+\mu_x) & 2\sqrt{2}\rho SC(\mu_m+\mu_x) \\ 2\sqrt{2}\rho SC(\mu_m+\mu_x) & 4\rho^2C^2(\mu_m+\mu_x) \end{bmatrix}$$

4. DEFINITION OF THE F MATRIX

The complete $\underline{F}$ matrix for this molecule contains thirteen independent terms: the principal stretching force constant F_r, two principal bending force constants F_α and F_β, and ten interaction terms (three stretch-stretch, three bend-bend and four stretch-bend). These terms cannot all be uniquely determined from the observed frequency data, and so a simplified $\underline{F}$ matrix is used in which all the non-diagonal (interaction) terms are set to zero. This can be written as:

$$\underline{F} = \begin{bmatrix} F_r & & & & & & 0 & \\ & F_r & & & & & & \\ & & F_r & & & & & \\ & & & F_r & & & & \\ & & & & r_O^2F_\alpha & & & \\ & & & & & r_O^2F_\alpha & & \\ & 0 & & & & & r_O^2F_\beta & \\ & & & & & & & r_O^2F_\beta \end{bmatrix}$$

where r_o is the equilibrium bond length. The bending force constants are multiplied by r_o^2 to make the dimensions of all the $\underline{F}$-matrix elements the same.

The symmetrised $\underline{F}$ matrix, obtained by applying

$$\underline{F}_S = \underline{U}\ \underline{F}\ \tilde{\underline{U}}$$

has the same structure as the $\underline{G}_S$ matrix shown above, and the four sub-matrices are:

$$\underline{F}_{A_1} = \begin{bmatrix} F_r & 0 & 0 \\ 0 & r_o^2 F_\alpha & 0 \\ 0 & 0 & r_o^2 F_\beta \end{bmatrix}$$

$$\underline{F}_{B_{1g}} = \begin{bmatrix} F_r \end{bmatrix}$$

$$\underline{F}_{B_{2u}} = \begin{bmatrix} F_r & 0 \\ 0 & r_o^2 F_\beta \end{bmatrix}$$

$$\underline{F}_{B_{3u}} = \begin{bmatrix} F_r & 0 \\ 0 & r_o^2 F_\beta \end{bmatrix}$$

5. SOLUTION OF THE SECULAR EQUATION

The secular equation,

$$\left|\underline{G}_S\underline{F}_S - \underline{E}\lambda\right| = 0$$

can be solved for each of the symmetry species. For the A_1 species

$$\left|\underline{GF} - \underline{E}\lambda\right| = \begin{vmatrix} G_{11}F_r - \lambda & G_{12}r_o^2F_\alpha & G_{13}r_o^2F_\beta \\ G_{12}F_r & G_{22}r_o^2F_\alpha - \lambda & G_{23}r_o^2F_\beta \\ G_{13}F_r & G_{23}r_o^2F_\alpha & G_{33}r_o^2F_\beta - \lambda \end{vmatrix} = 0$$

This expands to

$$(G_{11}F_r-\lambda)\{(G_{22}r_o^2F_\alpha-\lambda)(G_{33}r_o^2F_\beta-\lambda) - (G_{23}r_o^2F_\alpha)(G_{23}r_o^2F_\beta)\}$$

$$- (G_{12}r_o^2F_\alpha)\{(G_{12}F_r)(G_{33}r_o^2F_\beta-\lambda) - (G_{13}F_r)(G_{23}r_o^2F_\beta)\}$$

$$+ (G_{13}r_o^2F_\beta)\{(G_{12}F_r)(G_{23}r_o^2F_\alpha) - (G_{13}F_r)(G_{22}r_o^2F_\alpha-\lambda)\} = 0$$

$$\longrightarrow \quad - \lambda^3 + (G_{11}F_r + G_{22}r_o^2F_\alpha + G_{33}r_o^2F_\beta)\lambda^2$$

$$- \{(G_{11}G_{22} - G_{12}^2)F_r r_o^2F_\alpha + (G_{11}G_{33} - G_{13}^2)F_r r_o^2F_\beta +$$

$$(G_{22}G_{33} - G_{23}^2)r_o^4F_\alpha F_\beta\}\lambda$$

$$+ \{G_{11}G_{22}G_{33} + 2G_{12}G_{23}G_{13} - G_{11}G_{23}^2 - G_{22}G_{13}^2$$

$$- G_{33}G_{12}^2\}(F_r r_o^4F_\alpha F_\beta) = 0$$

Substituting the appropriate $\underline{G}$ matrix elements gives:

$$- \lambda [\lambda^2 - \{(2C^2\mu_m + S^2\mu_x)F_r + 4(S^2\mu_m + C^2\mu_x)(F_\alpha + F_\beta)\}\lambda$$

$$+ 8\mu_m\mu_xF_r(F_\alpha + F_\beta)] = 0$$

One of the roots of this equation is obviously zero; the sum and product of the two non-zero roots are given by

$$\lambda_1 + \lambda_2 = (2C^2\mu_m + S^2\mu_x)F_r + 4(s^2\mu_m + C^2\mu_x)(F_\alpha + F_\beta)$$

$$\lambda_1 \lambda_2 = 8\mu_m\mu_xF_r(F_\alpha + F_\beta)$$

For the B_{1g} mode, the secular equation is simply

$$(G_{44}F_r - \lambda) = 0$$

and therefore

$$\lambda_3 = G_{44}F_r = 2(S^2\mu_m + C^2\mu_x)$$

The secular equation for the B_{2u} species expands to

$$(G_{55}F_r-\lambda)(G_{66}r_o^2F_\alpha-\lambda) - (G_{56}^2F_r r_o^2F_\alpha) = 0$$

$$\lambda^2 - (G_{55}F_r + G_{66}r_o^2F_\alpha)\lambda + (G_{55}G_{66} - G_{56}^2)F_r r_o^2F_\alpha = 0$$

Substituting the appropriate $\underline{G}$ matrix elements gives

$$\lambda[\lambda - 2(\mu_m + \mu_x)(C^2F_r + 2S^2F_\alpha)] = 0$$

and similarly for the B_{3u} species

$$\lambda[\lambda - 2(\mu_m + \mu_x)(S^2F_r + 2C^2F_\beta)] = 0$$

Both of these equations have one zero root;
the non-zero roots are

$$\lambda_4 = 2(\mu_m + \mu_x)(C^2F_r + 2S^2F_\alpha) \quad (B_{2u})$$

$$\lambda_5 = 2(\mu_m + \mu_x)(S^2F_r + 2C^2F_\beta) \quad (B_{3u})$$

APPENDIX 3

TABULATED THERMODYNAMIC FUNCTIONS

SnTe
26-Oct-89 01:14 PM

Input data read from snte.tdi:

SnTe
molecular weight : .2463 kg.mol^-1
point group : C0
I(B) : 3.940E+00 amu.nm^2

vibration frequencies (cm-1)
258
Reference temperature = 298 K
Electronic ground state degeneracy = 1

Temp K	HT-H0 J/mol	HT-Href J/mol	Cp(T) J/mol/K	S(T) J/mol/K	-(GT-H0)/T J/mol/K	-(GT-Href)/T J/mol/K
100	2987.3	-6931.4	32.04	225.47	195.60	294.78
200	6391.7	-3527.0	35.39	248.93	216.98	266.57
298	9918.7	0.0	36.42	263.27	229.99	263.27
300	9991.5	72.8	36.43	263.52	230.21	263.27
400	13657.9	3739.2	36.84	274.06	239.92	264.71
500	17353.2	7434.5	37.04	282.31	247.60	267.44
600	21063.5	11144.9	37.15	289.07	253.96	270.49
700	24782.6	14863.9	37.22	294.80	259.40	273.57
800	28507.2	18588.5	37.27	299.78	264.14	276.54
900	32235.5	22316.8	37.30	304.17	268.35	279.37
1000	35966.4	26047.7	37.32	308.10	272.13	282.05
1100	39699.2	29780.5	37.34	311.66	275.57	284.58
1200	43433.4	33514.8	37.35	314.90	278.71	286.98
1300	47168.8	37250.1	37.36	317.89	281.61	289.24
1400	50905.0	40986.3	37.37	320.66	284.30	291.39
1500	54641.9	44723.2	37.37	323.24	286.81	293.43
1600	58379.4	48460.7	37.38	325.65	289.17	295.37
1700	62117.3	52198.6	37.38	327.92	291.38	297.22
1800	65855.6	55936.9	37.38	330.06	293.47	298.98
1900	69594.3	59675.6	37.39	332.08	295.45	300.67
2000	73333.2	63414.5	37.39	334.00	297.33	302.29
2100	77072.4	67153.7	37.39	335.82	299.12	303.84
2200	80811.7	70893.1	37.39	337.56	300.83	305.34
2300	84551.3	74632.6	37.40	339.22	302.46	306.77
2400	88291.0	78372.3	37.40	340.81	304.03	308.16
2500	92030.9	82112.2	37.40	342.34	305.53	309.50

SnTe dimer
26-Oct-89 01:24 PM

Input data read from sn2te2.tdi:

Sn2Te2
molecular weight : .4926 kg.mol^-1
point group : D2h
I(A)*I(B)*I(C) : 1.655E+03 amu^3.nm^6

vibration frequencies (cm-1)
178 57 177 191 172 20
Reference temperature = 298 K
Electronic ground state degeneracy = 1

Temp K	HT-H0 J/mol	HT-Href J/mol	Cp(T) J/mol/K	S(T) J/mol/K	-(GT-H0)/T J/mol/K	-(GT-Href)/T J/mol/K
100	5283.5	-15369.0	69.00	313.53	260.69	467.22
200	12800.3	-7852.2	78.75	365.25	301.25	404.51
298	20652.5	0.0	81.08	397.17	327.86	397.17
300	20814.7	162.2	81.10	397.71	328.33	397.17
400	28974.7	8322.2	81.98	421.18	348.74	400.37
500	37195.4	16542.9	82.39	439.52	365.13	406.44
600	45446.9	24794.4	82.62	454.57	378.82	413.24
700	53716.2	33063.7	82.76	467.31	390.57	420.08
800	61996.7	41344.2	82.85	478.37	400.87	426.69
900	70284.7	49632.2	82.91	488.13	410.04	432.98
1000	78578.0	57925.5	82.95	496.87	418.29	438.94
1100	86875.0	66222.5	82.99	504.78	425.80	444.57
1200	95174.9	74522.4	83.01	512.00	432.69	449.90
1300	103477.0	82824.6	83.03	518.64	439.05	454.93
1400	111781.0	91128.4	83.05	524.80	444.95	459.71
1500	120086.0	99433.7	83.06	530.53	450.47	464.24
1600	128393.0	107740.0	83.07	535.89	455.64	468.55
1700	136700.0	116047.0	83.08	540.92	460.51	472.66
1800	145008.0	124355.0	83.08	545.67	465.11	476.59
1900	153317.0	132664.0	83.09	550.17	469.47	480.34
2000	161626.0	140974.0	83.10	554.43	473.61	483.94
2100	169936.0	149283.0	83.10	558.48	477.56	487.39
2200	178246.0	157593.0	83.10	562.35	481.33	490.71
2300	186556.0	165904.0	83.11	566.04	484.93	493.91
2400	194868.0	174215.0	83.11	569.58	488.38	496.99
2500	203179.0	182526.0	83.11	572.97	491.70	499.96

PbSe
26-Oct-89 01:10 PM

Input data read from pbse.tdi:

PbSe
molecular weight : .2862 kg.mol^-1
point group : C0
I(B) : 3.380E+00 amu.nm^2

vibration frequencies (cm-1)
276
Reference temperature = 298 K
Electronic ground state degeneracy = 1

Temp K	HT-H0 J/mol	HT-Href J/mol	Cp(T) J/mol/K	S(T) J/mol/K	-(GT-H0)/T J/mol/K	-(GT-Href)/T J/mol/K
100	2973.4	-6881.4	31.67	225.88	196.15	294.70
200	6345.5	-3509.4	35.15	249.12	217.39	266.66
298	9854.8	0.0	36.29	263.38	230.31	263.38
300	9927.4	72.6	36.30	263.62	230.53	263.38
400	13583.6	3728.8	36.76	274.14	240.18	264.82
500	17272.6	7417.7	36.99	282.37	247.82	267.53
600	20978.5	11123.7	37.12	289.13	254.16	270.59
700	24694.4	14839.6	37.19	294.85	259.58	273.65
800	28416.6	18561.8	37.25	299.82	264.30	276.62
900	32143.1	22288.2	37.28	304.21	268.50	279.45
1000	35872.4	26017.6	37.31	308.14	272.27	282.12
1100	39604.0	29749.2	37.32	311.70	275.69	284.65
1200	43337.2	33482.4	37.34	314.95	278.83	287.04
1300	47071.7	37216.9	37.35	317.94	281.73	289.31
1400	50807.2	40952.3	37.36	320.70	284.41	291.45
1500	54543.4	44688.6	37.37	323.28	286.92	293.49
1600	58280.3	48425.5	37.37	325.69	289.27	295.43
1700	62017.7	52162.9	37.38	327.96	291.48	297.28
1800	65755.6	55900.8	37.38	330.10	293.57	299.04
1900	69493.9	59639.0	37.38	332.12	295.54	300.73
2000	73232.4	63377.6	37.39	334.03	297.42	302.35
2100	76971.3	67116.4	37.39	335.86	299.21	303.90
2200	80710.3	70855.5	37.39	337.60	300.91	305.39
2300	84449.6	74594.8	37.39	339.26	302.54	306.83
2400	88189.1	78334.2	37.40	340.85	304.11	308.21
2500	91928.7	82073.8	37.40	342.38	305.61	309.55

PbSe dimer
26-Oct-89 01:25 PM

Input data read from pb2se2.tdi:

Pb2Se2
molecular weight : .5724 kg.mol^-1
point group : D2h
I(A)*I(B)*I(C) : 1.537E+03 amu^3.nm^6

vibration frequencies (cm-1)
191 56 194 202 191 20
Reference temperature = 298 K
Electronic ground state degeneracy = 1

Temp K	HT-H0 J/mol	HT-Href J/mol	Cp(T) J/mol/K	S(T) J/mol/K	-(GT-H0)/T J/mol/K	-(GT-Href)/T J/mol/K
100	5188.3	-15215.4	67.38	313.70	261.82	465.85
200	12597.6	-7806.1	78.08	364.64	301.65	403.67
298	20403.7	0.0	80.75	396.37	327.90	396.37
300	20565.2	161.5	80.78	396.91	328.36	396.37
400	28700.3	8296.6	81.79	420.30	348.55	399.56
500	36905.6	16501.9	82.27	438.61	364.80	405.61
600	45146.7	24743.1	82.53	453.64	378.39	412.40
700	53408.6	33004.9	82.69	466.37	390.07	419.22
800	61683.5	41279.8	82.80	477.42	400.32	425.82
900	69967.1	49563.4	82.87	487.18	409.44	432.11
1000	78256.8	57853.1	82.92	495.91	417.65	438.06
1100	86551.0	66147.3	82.96	503.82	425.13	443.68
1200	94848.5	74444.8	82.99	511.04	432.00	449.00
1300	103149.0	82744.9	83.01	517.68	438.33	454.03
1400	111451.0	91047.1	83.03	523.83	444.22	458.80
1500	119754.0	99350.8	83.04	529.56	449.73	463.33
1600	128060.0	107656.0	83.06	534.92	454.88	467.64
1700	136366.0	115962.0	83.07	539.96	459.74	471.74
1800	144673.0	124269.0	83.07	544.71	464.33	475.67
1900	152981.0	132577.0	83.08	549.20	468.68	479.42
2000	161289.0	140885.0	83.09	553.46	472.81	483.02
2100	169598.0	149194.0	83.09	557.51	476.75	486.47
2200	177908.0	157504.0	83.10	561.38	480.51	489.79
2300	186217.0	165814.0	83.10	565.07	484.11	492.98
2400	194528.0	174124.0	83.10	568.61	487.56	496.06
2500	202838.0	182435.0	83.11	572.00	490.87	499.03

PbTe
26-Oct-89 01:22 PM

Input data read from pbte.tdi:

PbTe
molecular weight : .3348 kg.mol^-1
point group : C0
I(B) : 5.500E+00 amu.nm^2

vibration frequencies (cm-1)
213
Reference temperature = 298 K
Electronic ground state degeneracy = 1

Temp K	HT-H0 J/mol	HT-Href J/mol	Cp(T) J/mol/K	S(T) J/mol/K	-(GT-H0)/T J/mol/K	-(GT-Href)/T J/mol/K
100	3034.7	-7055.3	33.11	232.74	202.39	303.29
200	6522.1	-3567.9	35.96	256.80	224.19	274.64
298	10090.1	0.0	36.72	271.31	237.45	271.31
300	10163.5	73.4	36.73	271.55	237.67	271.31
400	13852.8	3762.8	37.02	282.16	247.53	272.76
500	17562.5	7472.4	37.16	290.44	255.32	275.50
600	21282.6	11192.5	37.24	297.22	261.75	278.57
700	25008.7	14918.6	37.28	302.97	267.24	281.65
800	28738.6	18648.5	37.31	307.95	272.02	284.64
900	32471.0	22381.0	37.33	312.34	276.27	287.48
1000	36205.3	26115.2	37.35	316.28	280.07	290.16
1100	39940.8	29850.8	37.36	319.84	283.53	292.70
1200	43677.3	33587.3	37.37	323.09	286.69	295.10
1300	47414.6	37324.6	37.38	326.08	289.61	297.37
1400	51152.5	41062.4	37.38	328.85	292.31	299.52
1500	54890.8	44800.8	37.39	331.43	294.84	301.56
1600	58629.6	48539.5	37.39	333.84	297.20	303.51
1700	62368.6	52278.6	37.39	336.11	299.42	305.36
1800	66107.9	56017.9	37.39	338.25	301.52	307.13
1900	69847.5	59757.4	37.40	340.27	303.51	308.82
2000	73587.2	63497.1	37.40	342.19	305.39	310.44
2100	77327.1	67237.0	37.40	344.01	307.19	311.99
2200	81067.1	70977.0	37.40	345.75	308.90	313.49
2300	84807.3	74717.2	37.40	347.41	310.54	314.93
2400	88547.5	78457.5	37.40	349.01	312.11	316.32
2500	92287.9	82197.8	37.40	350.53	313.62	317.65

PbTe dimer
26-Oct-89 01:27 PM

Input data read from pb2te2.tdi:

Pb2Te2
molecular weight : .6696 kg.mol^-1
point group : D2h
I(A)*I(B)*I(C) : 4.365E+03 amu^3.nm^6

vibration frequencies (cm-1)
147 48 151 161 144 20
Reference temperature = 298 K
Electronic ground state degeneracy = 1

Temp K	HT-H0 J/mol	HT-Href J/mol	Cp(T) J/mol/K	S(T) J/mol/K	-(GT-H0)/T J/mol/K	-(GT-Href)/T J/mol/K
100	5552.7	-15657.9	72.30	326.46	270.94	483.04
200	13275.0	-7935.6	79.97	379.69	313.32	419.37
298	21210.6	0.0	81.67	411.96	340.79	411.96
300	21373.9	163.4	81.69	412.51	341.26	411.96
400	29578.3	8367.8	82.31	436.11	362.16	415.19
500	37826.1	16615.6	82.61	454.51	378.86	421.28
600	46096.0	24885.4	82.77	469.59	392.76	428.11
700	54378.4	33167.8	82.87	482.35	404.67	434.97
800	62668.8	41458.3	82.93	493.42	415.09	441.60
900	70964.5	49753.9	82.98	503.20	424.35	447.91
1000	79263.9	58053.3	83.01	511.94	432.68	453.89
1100	87565.9	66355.4	83.03	519.85	440.25	459.53
1200	95870.1	74659.6	83.05	527.08	447.19	464.86
1300	104176.0	82965.3	83.06	533.73	453.59	469.91
1400	112483.0	91272.2	83.07	539.88	459.54	474.69
1500	120791.0	99580.1	83.08	545.61	465.09	479.23
1600	129099.0	107889.0	83.09	550.98	470.29	483.55
1700	137409.0	116198.0	83.10	556.01	475.19	487.66
1800	145719.0	124508.0	83.10	560.76	479.81	491.59
1900	154029.0	132818.0	83.11	565.26	484.19	495.35
2000	162340.0	141129.0	83.11	569.52	488.35	498.96
2100	170651.0	149440.0	83.11	573.57	492.31	502.41
2200	178962.0	157752.0	83.12	577.44	496.09	505.74
2300	187274.0	166063.0	83.12	581.14	499.71	508.93
2400	195586.0	174375.0	83.12	584.67	503.18	512.02
2500	203898.0	182687.0	83.12	588.07	506.51	514.99

Ga2Se
10-Nov-89 09:46 AM

Input data read from ga2se.tdi:

Ga2Se
molecular weight : .2184 kg.mol^-1
point group : C2v
I(A)*I(B)*I(C) : 1.100E+01 amu^3.nm^6

vibration frequencies (cm-1)
164 107 244
Reference temperature = 298 K
Electronic ground state degeneracy = 1

Temp K	HT-H0 J/mol	HT-Href J/mol	Cp(T) J/mol/K	S(T) J/mol/K	-(GT-H0)/T J/mol/K	-(GT-Href)/T J/mol/K
100	3969.7	-10756.6	48.69	259.27	219.57	366.84
200	9236.0	-5490.3	55.06	295.52	249.34	322.97
298	14726.3	0.0	56.70	317.84	268.43	317.84
300	14839.7	113.4	56.72	318.22	268.76	317.84
400	20547.2	5820.9	57.35	334.64	283.27	320.08
500	26298.7	11572.4	57.65	347.47	294.87	324.33
600	32072.6	17346.3	57.82	358.00	304.54	329.09
700	37859.6	23133.2	57.92	366.92	312.83	333.87
800	43654.7	28928.4	57.98	374.66	320.09	338.49
900	49455.3	34729.0	58.03	381.49	326.54	342.90
1000	55259.8	40533.5	58.06	387.60	332.34	347.07
1100	61067.1	46340.8	58.08	393.14	337.62	351.01
1200	66876.6	52150.2	58.10	398.19	342.46	354.73
1300	72687.6	57961.3	58.12	402.84	346.93	358.26
1400	78499.9	63773.6	58.13	407.15	351.08	361.60
1500	84313.3	69586.9	58.14	411.16	354.95	364.77
1600	90127.4	75401.1	58.15	414.91	358.58	367.79
1700	95942.3	81215.9	58.15	418.44	362.00	370.67
1800	101758.0	87031.4	58.16	421.76	365.23	373.41
1900	107574.0	92847.3	58.16	424.91	368.29	376.04
2000	113390.0	98663.6	58.17	427.89	371.20	378.56
2100	119207.0	104480.0	58.17	430.73	373.96	380.98
2200	125024.0	110297.0	58.17	433.44	376.61	383.30
2300	130841.0	116115.0	58.17	436.02	379.13	385.54
2400	136658.0	121932.0	58.18	438.50	381.56	387.69
2500	142476.0	127750.0	58.18	440.87	383.88	389.77

In2Se
04-Dec-89 09:43 AM

Input data read from in2se.tdi:

In2Se
molecular weight : .3086 kg.mol^-1
point group : C2v
I(A)*I(B)*I(C) : 2.030E+02 amu^3.nm^6

symmetry number : 2

vibration frequencies (cm-1)
211 77 222
Reference temperature = 298 K
Electronic ground state degeneracy = 1

Temp K	HT-H0 J/mol	HT-Href J/mol	Cp(T) J/mol/K	S(T) J/mol/K	-(GT-H0)/T J/mol/K	-(GT-Href)/T J/mol/K
100	4020.8	-10744.2	48.61	277.22	237.01	384.66
200	9278.8	-5486.3	55.00	313.41	267.02	340.84
298	14765.0	0.0	56.67	335.71	286.17	335.71
300	14878.4	113.4	56.69	336.09	286.50	335.72
400	20583.8	5818.7	57.33	352.50	301.04	337.96
500	26333.9	11568.8	57.64	365.33	312.66	342.19
600	32106.9	17341.9	57.81	375.86	322.35	346.95
700	37893.3	23128.2	57.91	384.78	330.64	351.74
800	43687.9	28922.9	57.98	392.51	337.90	356.36
900	49488.2	34723.2	58.02	399.35	344.36	360.76
1000	55292.4	40527.4	58.06	405.46	350.17	364.93
1100	61099.5	46334.4	58.08	411.00	355.45	368.87
1200	66908.7	52143.6	58.10	416.05	360.29	372.60
1300	72719.5	57954.5	58.12	420.70	364.76	376.12
1400	78531.7	63766.7	58.13	425.01	368.92	379.46
1500	84344.9	69579.9	58.14	429.02	372.79	382.63
1600	90159.0	75394.0	58.14	432.77	376.42	385.65
1700	95973.8	81208.7	58.15	436.30	379.84	388.53
1800	101789.0	87024.0	58.16	439.62	383.07	391.27
1900	107605.0	92839.9	58.16	442.77	386.13	393.90
2000	113421.0	98656.1	58.16	445.75	389.04	396.42
2100	119238.0	104473.0	58.17	448.59	391.81	398.84
2200	125055.0	110290.0	58.17	451.29	394.45	401.16
2300	130872.0	116107.0	58.17	453.88	396.98	403.40
2400	136689.0	121924.0	58.18	456.35	399.40	405.55
2500	142507.0	127742.0	58.18	458.73	401.73	407.63

Ga2Te
10-Nov-89 09:47 AM

Input data read from ga2te.tdi:

Ga2Te
molecular weight : .27604 kg.mol^-1
point group : C2v
I(A)*I(B)*I(C) : 7.400E+01 amu^3.nm^6

vibration frequencies (cm-1)
199 81 193
Reference temperature = 298 K
Electronic ground state degeneracy = 1

Temp K	HT-H0 J/mol	HT-Href J/mol	Cp(T) J/mol/K	S(T) J/mol/K	-(GT-H0)/T J/mol/K	-(GT-Href)/T J/mol/K
100	4062.0	-10848.4	49.60	272.08	231.46	380.57
200	9391.3	-5519.1	55.47	308.79	261.84	336.39
298	14910.4	0.0	56.91	331.23	281.20	331.23
300	15024.2	113.8	56.92	331.61	281.53	331.23
400	20747.6	5837.2	57.47	348.08	296.21	333.48
500	26508.9	11598.5	57.73	360.93	307.91	337.73
600	32289.6	17379.2	57.87	371.47	317.65	342.50
700	38081.3	23170.9	57.96	380.40	326.00	347.30
800	43880.1	28969.7	58.01	388.14	333.29	351.93
900	49683.6	34773.2	58.05	394.98	339.77	356.34
1000	55490.4	40580.0	58.08	401.09	345.60	360.51
1100	61299.6	46389.2	58.10	406.63	350.90	364.46
1200	67110.5	52200.1	58.12	411.69	355.76	368.19
1300	72922.9	58012.5	58.13	416.34	360.24	371.71
1400	78736.3	63825.9	58.14	420.65	364.41	375.06
1500	84550.7	69640.3	58.15	424.66	368.29	378.23
1600	90365.7	75455.3	58.15	428.41	371.93	381.25
1700	96181.3	81270.9	58.16	431.94	375.36	384.13
1800	101997.0	87087.0	58.16	435.26	378.60	386.88
1900	107814.0	92903.5	58.17	438.41	381.66	389.51
2000	113631.0	98720.4	58.17	441.39	384.57	392.03
2100	119448.0	104538.0	58.17	444.23	387.35	394.45
2200	125265.0	110355.0	58.18	446.93	390.00	396.77
2300	131083.0	116173.0	58.18	449.52	392.53	399.01
2400	136901.0	121991.0	58.18	452.00	394.95	401.17
2500	142719.0	127809.0	58.18	454.37	397.28	403.25

In2Te
04-Dec-89 09:46 AM

Input data read from in2te.tdi:

In2Te
molecular weight : .3572 kg.mol^-1
point group : C2v
I(A)*I(B)*I(C) : 1.540E+02 amu^3.nm^6

symmetry number : 2

vibration frequencies (cm-1)
110 70 166
Reference temperature = 298 K
Electronic ground state degeneracy = 1

Temp K	HT-H0 J/mol	HT-Href J/mol	Cp(T) J/mol/K	S(T) J/mol/K	-(GT-H0)/T J/mol/K	-(GT-Href)/T J/mol/K
100	4348.4	-11138.4	52.96	283.57	240.09	394.95
200	9884.4	-5602.4	56.68	321.80	272.38	349.81
298	15486.8	0.0	57.50	344.59	292.62	344.59
300	15601.8	115.0	57.51	344.97	292.96	344.59
400	21369.5	5882.7	57.81	361.56	308.14	346.85
500	27157.9	11671.1	57.95	374.48	320.16	351.13
600	32956.8	17470.0	58.02	385.05	330.12	355.93
700	38761.7	23274.9	58.07	394.00	338.62	360.75
800	44570.3	29083.5	58.10	401.75	346.04	365.40
900	50381.5	34894.7	58.12	408.60	352.62	369.83
1000	56194.4	40707.6	58.14	414.72	358.53	374.01
1100	62008.6	46521.8	58.15	420.26	363.89	377.97
1200	67823.8	52337.0	58.16	425.32	368.80	381.71
1300	73639.7	58152.9	58.16	429.98	373.33	385.25
1400	79456.2	63969.4	58.17	434.29	377.54	388.60
1500	85273.2	69786.4	58.17	438.30	381.45	391.78
1600	91090.5	75603.8	58.18	442.06	385.13	394.81
1700	96908.2	81421.4	58.18	445.58	388.58	397.69
1800	102726.0	87239.3	58.18	448.91	391.84	400.44
1900	108544.0	93057.5	58.18	452.06	394.93	403.08
2000	114363.0	98875.8	58.18	455.04	397.86	405.60
2100	120181.0	104694.0	58.19	457.88	400.65	408.02
2200	126000.0	110513.0	58.19	460.59	403.31	410.35
2300	131819.0	116332.0	58.19	463.17	405.86	412.59
2400	137637.0	122151.0	58.19	465.65	408.30	414.75
2500	143456.0	127969.0	58.19	468.02	410.64	416.84

Caesium Molybdate - SOTONVIB frequencies
28-Nov-89 03:56 PM

Input data read from csmo.tdi:

Cs2MoO4
molecular weight : .42576 kg.mol^-1
point group : D2d
I(A)*I(B)*I(C) : 1.578E+03 amu^3.nm^6

symmetry number : 4

vibration frequencies (cm-1)
891 369 124 278 837 369 163 828 828 315
315 143 143 30 30
Reference temperature = 298 K
Electronic ground state degeneracy = 1

Temp K	HT-H0 J/mol	HT-Href J/mol	Cp(T) J/mol/K	S(T) J/mol/K	-(GT-H0)/T J/mol/K	-(GT-Href)/T J/mol/K
100	5850.8	-21310.3	81.88	320.69	262.18	533.79
200	15592.4	-11568.7	109.68	387.11	309.14	444.95
298	27161.1	0.0	125.27	433.97	342.83	433.97
300	27411.9	250.8	125.52	434.81	343.44	433.98
400	40505.9	13344.9	135.60	472.41	371.15	439.05
500	54408.8	27247.7	141.99	503.41	394.59	448.91
600	68828.8	41667.7	146.13	529.69	414.97	460.24
700	83589.2	56428.1	148.91	552.44	433.02	471.83
800	98581.9	71420.8	150.84	572.45	449.23	483.18
900	113739.0	86577.6	152.23	590.30	463.93	494.11
1000	129015.0	101854.0	153.25	606.40	477.38	504.55
1100	144381.0	117220.0	154.03	621.04	489.79	514.48
1200	159815.0	132654.0	154.63	634.47	501.29	523.93
1300	175303.0	148142.0	155.11	646.87	512.02	532.91
1400	190834.0	163673.0	155.49	658.38	522.07	541.47
1500	206399.0	179238.0	155.80	669.12	531.52	549.63
1600	221993.0	194832.0	156.06	679.18	540.44	557.41
1700	237610.0	210449.0	156.27	688.65	548.88	564.86
1800	253246.0	226085.0	156.45	697.59	556.89	571.98
1900	268899.0	241738.0	156.61	706.05	564.52	578.82
2000	284567.0	257405.0	156.74	714.09	571.80	585.38
2100	300246.0	273085.0	156.85	721.74	578.76	591.70
2200	315936.0	288775.0	156.95	729.04	585.43	597.77
2300	331635.0	304474.0	157.03	736.01	591.82	603.63
2400	347343.0	320181.0	157.11	742.70	597.97	609.29
2500	363057.0	335896.0	157.18	749.11	603.89	614.76

InI3 dimer
29-Nov-89 04:00 PM

Input data read from in2i6.tdi:

In2I6
molecular weight : .992 kg.mol^-1
point group : D2h
I(A)*I(B)*I(C) : 2.381E+05 amu^3.nm^6

symmetry number : 4

vibration frequencies (cm-1)
187 134 69 40 35 114 55 228 54 232
49 158 49 44 178 125 59 15
Reference temperature = 298 K
Electronic ground state degeneracy = 1

Temp K	HT-H0 J/mol	HT-Href J/mol	Cp(T) J/mol/K	S(T) J/mol/K	-(GT-H0)/T J/mol/K	-(GT-Href)/T J/mol/K
100	10839.3	-34026.0	154.60	451.34	342.94	791.60
200	27534.3	-17331.1	174.09	566.30	428.63	652.95
298	44865.4	0.0	178.75	636.76	486.20	636.76
300	45222.9	357.6	178.81	637.96	487.21	636.76
400	63203.6	18338.2	180.56	689.67	531.66	643.82
500	81306.3	36441.0	181.40	730.06	567.45	657.18
600	99471.2	54605.8	181.86	763.18	597.39	672.17
700	117672.0	72806.5	182.14	791.24	623.13	687.23
800	135895.0	91029.8	182.32	815.57	645.70	701.78
900	154134.0	109268.0	182.44	837.05	665.79	715.64
1000	172382.0	127517.0	182.53	856.28	683.89	728.76
1100	190639.0	145774.0	182.60	873.68	700.37	741.16
1200	208902.0	164036.0	182.65	889.57	715.48	752.87
1300	227168.0	182303.0	182.69	904.19	729.44	763.96
1400	245439.0	200574.0	182.72	917.73	742.42	774.46
1500	263712.0	218847.0	182.74	930.34	754.53	784.44
1600	281988.0	237122.0	182.77	942.13	765.89	793.93
1700	300265.0	255400.0	182.78	953.21	776.59	802.98
1800	318544.0	273679.0	182.80	963.66	786.69	811.62
1900	336824.0	291959.0	182.81	973.54	796.27	819.88
2000	355106.0	310240.0	182.82	982.92	805.37	827.80
2100	373388.0	328523.0	182.83	991.84	814.04	835.40
2200	391671.0	346806.0	182.84	1000.35	822.31	842.71
2300	409955.0	365090.0	182.84	1008.47	830.23	849.74
2400	428240.0	383374.0	182.85	1016.26	837.82	856.52
2500	446525.0	401659.0	182.85	1023.72	845.11	863.06

InI3
28-Nov-89 03:58 PM

Input data read from ini3.tdi:

InI3
molecular weight : .496 kg.mol^-1
point group : D3h
I(A)*I(B)*I(C) : 4.704E+03 amu^3.nm^6

symmetry number : 6

vibration frequencies (cm-1)
236 236 151 56 44 44
Reference temperature = 298 K
Electronic ground state degeneracy = 1

Temp K	HT-H0 J/mol	HT-Href J/mol	Cp(T) J/mol/K	S(T) J/mol/K	-(GT-H0)/T J/mol/K	-(GT-Href)/T J/mol/K
100	5486.3	-15369.9	69.79	316.72	261.85	470.41
200	13014.4	-7841.9	78.64	368.55	303.47	407.76
298	20856.3	0.0	80.98	400.43	330.44	400.43
300	21018.2	162.0	81.01	400.97	330.91	400.43
400	29170.6	8314.4	81.92	424.41	351.49	403.63
500	37386.2	16529.9	82.35	442.75	367.97	409.69
600	45634.1	24777.8	82.59	457.78	381.73	416.49
700	53900.7	33044.5	82.73	470.52	393.52	423.32
800	62179.2	41322.9	82.83	481.58	403.86	429.93
900	70465.5	49609.3	82.89	491.34	413.04	436.22
1000	78757.4	57901.2	82.94	500.08	421.32	442.17
1100	87053.5	66197.2	82.98	507.98	428.84	447.80
1200	95352.5	74496.2	83.00	515.20	435.74	453.12
1300	103654.0	82797.5	83.02	521.85	442.11	458.16
1400	111957.0	91100.8	83.04	528.00	448.03	462.93
1500	120262.0	99405.4	83.05	533.73	453.56	467.46
1600	128568.0	107711.0	83.06	539.09	458.74	471.77
1700	136874.0	116018.0	83.07	544.13	463.61	475.88
1800	145182.0	124326.0	83.08	548.88	468.22	479.81
1900	153491.0	132634.0	83.09	553.37	472.58	483.56
2000	161800.0	140943.0	83.09	557.63	476.73	487.16
2100	170109.0	149253.0	83.10	561.68	480.68	490.61
2200	178419.0	157563.0	83.10	565.55	484.45	493.93
2300	186729.0	165873.0	83.10	569.24	488.06	497.13
2400	195040.0	174184.0	83.11	572.78	491.51	500.20
2500	203351.0	182495.0	83.11	576.17	494.83	503.18

InI
28-Nov-89 03:57 PM

Input data read from ini.tdi:

InI
molecular weight : .242 kg.mol^-1
point group : C0
I(B) : 4.564E+00 amu.nm^2

symmetry number : 1

vibration frequencies (cm-1)
177
Reference temperature = 298 K
Electronic ground state degeneracy = 1

Temp K	HT-H0 J/mol	HT-Href J/mol	Cp(T) J/mol/K	S(T) J/mol/K	-(GT-H0)/T J/mol/K	-(GT-Href)/T J/mol/K
100	3090.0	-7149.8	34.07	227.97	197.07	299.47
200	6643.0	-3596.8	36.38	252.51	219.29	270.49
298	10239.8	0.0	36.93	267.14	232.78	267.14
300	10313.6	73.9	36.93	267.39	233.01	267.14
400	14018.6	3778.9	37.14	278.04	243.00	268.60
500	17737.9	7498.2	37.24	286.34	250.87	271.35
600	21464.6	11224.8	37.29	293.14	257.36	274.43
700	25195.4	14955.6	37.32	298.89	262.89	277.52
800	28928.8	18689.1	37.34	303.87	267.71	280.51
900	32664.1	22424.3	37.36	308.27	271.98	283.36
1000	36400.5	26160.8	37.37	312.21	275.81	286.05
1100	40137.9	29898.1	37.38	315.77	279.28	288.59
1200	43875.9	33636.2	37.38	319.02	282.46	290.99
1300	47614.5	37374.7	37.39	322.02	285.39	293.27
1400	51353.5	41113.7	37.39	324.79	288.11	295.42
1500	55092.8	44853.0	37.39	327.37	290.64	297.46
1600	58832.3	48592.6	37.40	329.78	293.01	299.41
1700	62572.1	52332.3	37.40	332.05	295.24	301.26
1800	66312.1	56072.3	37.40	334.18	297.34	303.03
1900	70052.2	59812.4	37.40	336.21	299.34	304.73
2000	73792.5	63552.7	37.40	338.13	301.23	306.35
2100	77532.8	67293.1	37.40	339.95	303.03	307.91
2200	81273.3	71033.5	37.41	341.69	304.75	309.40
2300	85013.8	74774.1	37.41	343.35	306.39	310.84
2400	88754.5	78514.7	37.41	344.95	307.96	312.23
2500	92495.1	82255.4	37.41	346.47	309.47	313.57